Encoding and recall of memory for reward location in the mouse hippocampus

Przemysław Jarzębowski

This thesis is submitted for
the degree of Doctor of Philosophy

University of Cambridge
Dept. of Physiology, Development & Neuroscience
St Edmund's College

December 2021

Declaration

This thesis is the result of my own work and includes nothing which is the outcome of work done in collaboration except as declared in the Introduction and specified in the text. I further state that no substantial part of my thesis has already been submitted, or, is being concurrently submitted for any such degree, diploma or other qualification at the University of Cambridge or any other University or similar institution. It does not exceed the prescribed word limit for the relevant Degree Committee.

Encoding and recall of memory for reward location in the mouse hippocampus

Przemysław Jarzębowski

Summary

The memory of where to find food can be crucial for an animal's survival. Encoding and recall of these spatial memories involves the hippocampus, but whether and how hippocampal activity integrates memories of spatial relationships and locations is poorly understood. This thesis investigates how hippocampal activity facilitates the encoding of reward memories and how this encoding shapes hippocampal activity during memory recall in mice learning reward locations.

Encoding of memory happens in stages that depend on the hippocampal state. The thesis interrogated how two different hippocampal states, one during movement and the other during reward consumption, are affected by acetylcholine – a neuromodulator released predominantly during movement and exploration. The findings highlight how acetylcholine modulates hippocampal state and how, when experimentally altered, it can impede memory encoding.

Hippocampal activity facilitates navigation towards the learned reward locations. Individual neurons fire at specific locations of the environment, and, collectively, they cover the environment forming its cognitive map. To answer how the hippocampal activity could encode a memory of reward location, the thesis investigated how these spatial representations and the population activity change after learning. I found that the reward memory shapes the activity in the dorsal CA1 of the hippocampus by modulating its overall population activity and in the intermediate CA1 by modulating the activity of a reward-specific cell population.

Together, these results suggest how hippocampal activity could facilitate encoding and recall of memory for reward locations.

Acknowledgments

First, I would like to thank my supervisor Professor Ole Paulsen who was a patient mentor and teacher, and guided me in my scientific explorations. I appreciate the insights, commitment and time he has given me.

I also thank Dr Audrey Hay, who trained me, offered advice and guidance on countless occasions. I am grateful to her and Dr Clara Tang for involving me in their work. In addition, I would like to thank them and Drs Tanja Fuchsberger and Benjamin Phillips for making the laboratory a friendly and supportive place. I want to thank Dr Susanna Mierau for her guidance and support before the start of the PhD. I also thank the current and past members of the Neuronal Oscillations group for great company.

I would also like to dearly thank Agata, who was great support and made these years so much better.

Lastly, I am grateful to Biotechnology and Biological Sciences Research Council for providing the funding for my PhD and to St Edmund's College for the support throughout.

Table of contents

List of Figures

List of Abbreviations

ACh	acetylcholine
CA	*cornu ammonis*
CDF	cumulative distribution function
ChR2	*channelrhodopsin-2*
dCA1	dorsal CA1
DG	dentate gyrus
EC	entorhinal cortex
EMG	electromyography
iCA1	intermediate CA1
LFP	local field potential
LTD	long-term depression
LTP	long-term potentiation
MS	medial septum
MTL	medial temporal lobe
NMDA	N-methyl-D-aspartate
NREM	non-rapid-eye movement
pp	percentage points
PSD	power spectral density
REM	rapid-eye movement
ROI	region of interest
STDP	spike-timing-dependent plasticity
SWRs	sharp wave ripples
vCA1	ventral CA1

Chapter 1

Introduction

A single, brief experience can leave a long-lasting memory. The experience leaves a mark in the physical substrate of the brain, creating the initial memory encoding. Later, the encoding is updated and maintained by a process of consolidation. The memory persists in a latent state until the time of memory recall when the encoded neural pattern of activity resurfaces. All three stages of memory formation: initial encoding, consolidation and recall can depend on the hippocampus. Spatial memory is one of the memory types, for which the neural activity in the hippocampus is critical. This thesis asks how the hippocampus encodes memories of reward locations and what neural activity leads to their recall. I approach these questions by studying hippocampal activity in mice learning and navigating towards reward locations.

The process of memory encoding is thought to happen in the hippocampus in stages that depend on the region-wide state of the neural activity. Hippocampal neurons temporally coordinate their activity, leading to regular oscillations in the local field potential (LFP). These oscillations delineate the hippocampal states corresponding to different behaviours. In Chapter 3, I interrogate how the hippocampal states and the learning are affected by experimentally stimulating release of acetylcholine (ACh) – a neuromodulator released predominantly during movement and exploration.

After the memory for reward locations is encoded, hippocampus is thought to facilitate navigation towards the learned locations. During the animal's navigation, hippocampal neurons called place cells restrict their firing to spatially defined parts of the environment. To study how the hippocampal activity encodes memory of reward

location, in Chapter 4, I interrogate how the hippocampal cells and population activity change after learning as mice approach the reward. In particular, I investigate how cells are recruited to the encoding of reward memory: if the same cells encode experience of different reward locations or different, stochastically selected cells are recruited each time.

The introduction that follows reviews the role of the hippocampus in memory, the neural processes that could support it, and characterises hippocampal activity during spatial navigation. Results reported in Chapter 3 of this thesis were published in Jarzebowski et al. (2021b) and results reported in Chapter 4 were published in Jarzebowski et al. (2021a).

1.1 Hippocampal neuroanatomy

Hippocampus has a unique neuroanatomy, which may be critical in facilitating memory and, which has motivated numerous studies on the general principles of neuronal function. The hippocampal formation is composed of four anatomical regions: hippocampus proper, dentate gyrus (DG), subicular complex and entorhinal cortex (EC) (as defined by Amaral and Witter, 1989). Hippocampus proper is further divided into *cornu ammonis* (CA) fields 1 to 4 (Lorente de Nó, 1934), where CA4 is not present in rodents (Amaral and Witter, 1989).

1.1.1 Hippocampal circuit

The first unique feature of hippocampal anatomy is its internal circuitry that largely consists of unidirectional excitatory connections (Figure 1.1; Andersen et al., 1966; Amaral and Witter, 1989; Witter and Amaral, 2004). They constitute only a part of all of the hippocampal connections but this part forms the backbone of a trisynaptic circuit, first described by Ramón Y Cajal (1911). The circuit's first synapse from EC to the DG provides much of the cortical input to the hippocampus proper via perforant path. From there, the second synapse connects DG granule cells via mossy fibres axons to CA3 pyramidal cells. These, in turn, synapse onto CA1 pyramidal cells via Schaffer

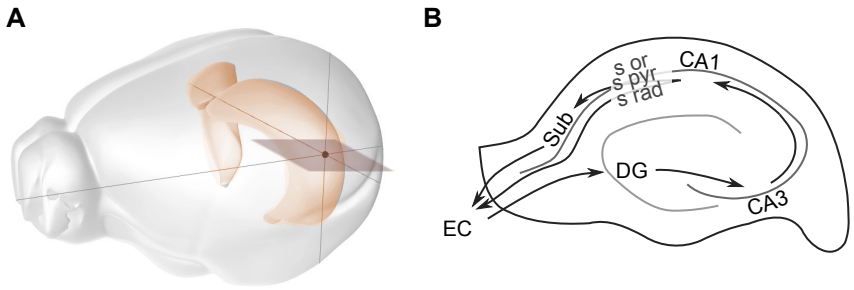

Figure 1.1: Hippocampal anatomy. **(A)** Location of the hippocampus proper in the mouse brain. The horizontal plane shows a transverse section through the hippocampus. **(B)** Illustration of the transverse section of the hippocampus showing its main subdivisions and its mainly unidirectional circuit. EC, entorhinal cortex; DG, dentate gyrus; Sub, subiculum; s or, *stratum oriens*; s pyr, pyramidal cell layer; s rad, *stratum radiatum*.

collateral axons (Amaral and Witter, 1989; Swanson et al., 1978). Last, CA1 connects back to EC either directly or through subiculum, completing the mainly unidirectional circuit (Amaral and Witter, 1989).

The second unique feature of hippocampal anatomy relates to a layered organisation of cell types and their axonal projections (reviewed by Witter and Amaral, 2004). The most striking is the pyramidal cell layer which aggregates cell bodies of pyramidal cells and several interneuron classes. In CA1 and CA3, the pyramidal cell layer is placed between relatively cell-free *stratum oriens* (deep of the pyramidal cell layer), and *stratum radiatum* (superficial of the pyramidal cell layer). *Stratum radiatum* contains cell bodies of interneurons and afferents from CA3. In CA3, the afferents arriving in *stratum radiatum* include recurrent local connections, while in CA1 these are the CA3 inputs arriving via Schaffer collateral fibres. The most superficial layer is *loconosum moleculare* where EC inputs to CA1 pyramidal cells arrive via perforant path, and where inhibitory cell bodies are located.

The third feature of hippocampal anatomy relates to diverging, fan-out connections from EC to DG and the recurrent connections in CA3 (Witter and Amaral, 2004). This feature is thought to facilitate pattern separation and completion. In this model for the flow of information through the hippocampus initially proposed by Marr and Brindley (1971), the incoming signals are first separated so that similar inputs from EC activate different sets of DG cells. Next, the pattern-separated signal arrives in CA3 where the previously learned patterns are recalled. The recurrent activity in

CA3 helps to recover a stored pattern from its fragment, providing pattern completion of the input. Experimental evidence supports the presence of pattern separation and completion in the hippocampus (reviewed by Knierim and Neunuebel, 2016) and these two transformations could be fundamental computations performed during memory recall.

1.1.2 Dorso-ventral axis

While the features described above are preserved, other genetic and anatomical features differ between the posterior and anterior hippocampus and their homologues, the dorsal and ventral hippocampus, in rodents (Fanselow and Dong, 2010; Dong et al., 2009; Thompson et al., 2008). The further description of the anatomy focuses on rodents, however, similar anatomy is found in primates (Fanselow and Dong, 2010).

Based on differing genetic expression in CA1, Dong et al. (2009) proposed its division into three domains: dorsal, intermediate and ventral. The domains differ in gene markers (Dong et al., 2009), morphological and electrophysiologial properies (Malik et al., 2016), and in connectivity patterns (Amaral and Witter, 1989). Despite clear differences, there are no clear boundaries between the domains, and others emphasised the presence of gradient-like transitions (Strange et al., 2014; Malik et al., 2016; Cembrowski et al., 2016). Historically, some studies referred to intermediate-to-ventral hippocampus as ventral. Throughout this thesis, I make a distinction between these two domains when citing these studies.

The gradual changes in gene expression from dorsal to ventral CA1 overlap with the gradual changes in the connectivity. The trisynaptic circuit is preserved across the dorso-ventral axis, but both the inputs and outputs differ (Swanson et al., 1978; Cenquizca and Swanson, 2007). For example, the intermediate-to-ventral CA1 but not the dorsal CA1 (dCA1) projects to amygdala (Pitkänen et al., 2006) and medial prefrontal cortex (Hoover and Vertes, 2007). These input-output differences correlate with functional differences (Moser and Moser, 1998; Fanselow and Dong, 2010), which are further described in the later sections.

1.2 Hippocampal role in memory

1.2.1 Early evidence from human studies

The most striking evidence for a role of the hippocampal formation in memory comes from human patients with hippocampal damage, among whom patient H.M. is the most famous (Scoville and Milner, 1957). His memory impairment was prominent: H.M. could recall few episodes after a surgery removing his hippocampal formation (anterograde amnesia) without losing his ability to learn new motor skills. Patient H.M. could remember episodes for a short time, but if distracted, he immediately forgot (Scoville and Milner, 1957). His memory for events before the surgery was also affected, but the impairment was most severe for events soon before the surgery (graded retrograde amnesia) and was mostly restricted to personal events. H.M.'s memory impairment is mostly attributed to the near-complete removal of the hippocampal formation; however, some adjacent brain tissue was also removed (Annese et al., 2014).

The distinction between the memories affected by hippocampal and other brain lesions gave anatomical evidence for the taxonomy of memory systems proposed by Tulving (1972). The taxonomy distinguishes between the system for declarative memory, which is the memory for facts (semantic) or events (episodic), and non-declarative memory, a collection of memory faculties that includes procedural and perceptual learning. Only declarative memory is affected by hippocampal lesions (Squire, 2004). Tulving (1972) defined declarative memory as a model of the external world that allows comparison of relationships between objects, facts and events. The memory's episodic and semantic components are hard to experimentally test in animals. Therefore, it is unanswered how this taxonomy of memory systems translates to non-human animals. Nevertheless, the evidence presented in the sections below suggests that specialized memory systems that differently depend on the hippocampus are present across species.

1.2.2 Spatial memory

Studies in rodents revealed that hippocampus is critical for spatial memory – the ability to recall locations and their relative positions in space in order to navigate between them. Rats after removal of the hippocampus can learn simple rules to turn left or right but perform badly when navigating on multiple-choice mazes (Kaada et al., 1961; Kveim et al., 1964).

Later studies improved the hippocampal lesions to ablate hippocampal cells without causing damage to the passing neural fibres and refined spatial memory tests. Rats after the lesion perform worse in learning the location of an escape platform hidden below water surface (water maze task, Morris et al., 1982, 1990). The distance and time it takes them to find the platform after multiple learning trials is longer than in control rats. The rats after the lesion are not impaired when the platform is visible above the water surface, showing that the longer time and distance are not caused by some motor, motivational or reinforcing changes (Morris et al., 1982). Consistent with spatial memory impairment in rodents, human patients with hippocampal lesions are impaired in creating object-location associations (Smith, 1988) and in tests referring to acquired topographical knowledge of novel environments (Maguire et al., 1996).

Partial lesions of the hippocampus highlight the different involvement of the dorsal, intermediate and ventral hippocampus in spatial memory. Lesions of the dorsal hippocampus cause spatial memory impairment in rats learning the location of the escape platform in the water maze task for several trials, while lesions of the intermediate-to-ventral hippocampus do not cause the impairment (Moser et al., 1993, 1995; Bannerman et al., 1999). However, later experimental evidence suggests that intermediate and ventral hippocampus are required for spatial memory during the early phases of spatial learning. Intermediate hippocampus is required for learning when a rat is given only one trial to learn the location of the escape platform (Bast et al., 2009), and the ventral hippocampus supports navigation during the early phase of spatial learning (Ruediger et al., 2012). Similarily, navigation in complex mazes requires both the dorsal and ventral hippocampus. Lesions of either impair spatial navigation when the rat needs to navigate around obstacles to a learned reward location (Contr-

eras et al., 2018). It is important to note that the impairment in spatial memory caused by lesions could be due to the lesioned part mediating some aspects of behavioural performance that is necessary for spatial navigation but is independent of spatial memory (Bast et al., 2009) – two aspects that are difficult to disentangle by behavioural studies.

Connectivity differences also suggest that the hippocampal domains are differently involved in spatial memory. The cortical inputs to the dorsal and ventral hippocampus come from non-overlapping parts of EC (Witter and Amaral, 2004), whose intrinsic connections are segregated (Dolorfo and Amaral, 1998b,a). As a result, the EC signal is processed by largely parallel hippocampal pathways (Moser and Moser, 1998). Dorsal hippocampus projects to several areas involved in spatial navigation, while such projections from the ventral hippocampus are fewer. dCA1 and subiculum target retrosplenial cortex (Cenquizca and Swanson, 2007) which is required for spatial navigation (Vann et al., 2009). Additionally, the dorsal subiculum sends projections to the medial and lateral mammillary nuclei and the anterior thalamic complex (Swanson and Cowan, 1975) – two structures whose neuronal subpopulations tune activity to particular head directions (Taube, 2007).

1.2.3 Affective behaviours and memory

Apart from spatial memory, the hippocampus is implicated in other aspects of behaviour. For instance, lesion studies show its involvement in locomotion (Kimble and Pribram, 1963; Nadel, 1968), feeding (reviewed in Kanoski and Grill, 2017), stress response (Jacobson and Sapolsky, 1991) and fear expression (Kjelstrup et al., 2002; Fanselow and Dong, 2010). The affected behavioural aspects change along the dorsoventral axis (Fanselow and Dong, 2010; Strange et al., 2014; Bannerman et al., 2004). The affective functions are attributed to the ventral hippocampus (Fanselow and Dong, 2010; Bannerman et al., 2004; Moser and Moser, 1998). Many of these functions correlate with particular efferent connections from CA1 and subiculum, which are more ample and diverse in intermediate and ventral than in dorsal hippocampus (Witter and Amaral, 2004). Studies of these connections revealed that particular neuronal populations have unique roles in controlling specific behaviours and in specific memory types.

Connections to the amygdala have received a particular interest because of the amygdala's role in unconditioned and learned fear (LeDoux, 2000). Projections to the amygdala are much stronger from the intermediate and ventral CA1 and subiculum than from their dorsal counterparts (Pitkänen et al., 2006). Accordingly, the dorsal and ventral hippocampus are differently involved in fear memory (Hunsaker and Kesner, 2008). The difference was revealed by a paradigm testing contextual fear memory (Hunsaker and Kesner, 2008). During contextual fear learning, the animal associates an electric shock with the preceding tone cue and the chamber where the shock was delivered. Afterwards, upon hearing the tone cue in the same chamber the animal freezes, which is interpreted as a fear response. When the animal hears the tone in a sufficiently different chamber, it does not express the fear response. The performance of this task depends on the intact amygdala (Phillips and LeDoux, 1992) and the hippocampus (Kim and Fanselow, 1992). Lesions of the dorsal hippocampus impair learning and retrieval of contextual fear memories (Kim and Fanselow, 1992; Hunsaker and Kesner, 2008), while lesions of the ventral hippocampus only impair the memory retrieval (Hunsaker and Kesner, 2008), which depends on specific projections from the ventral CA1 (vCA1) and subiculum to the amygdala (Xu et al., 2016; Jimenez et al., 2018).

Intermediate and ventral hippocampus modulate two contrasting behaviours: avoidance and approach. In rodents, avoidance is exemplified by the animals avoiding open, exposed spaces. This behaviour decreases as result of ventral hippocampus lesions (Kjelstrup et al., 2002). Avoidance is modulated by vCA1 projections to the medial prefrontal cortex, which promote the avoidance (Padilla-Coreano et al., 2019), and by projections to the lateral hypothalamus, which signal anxiolytic stimuli (Jimenez et al., 2018).

Approach is regulated by both the intermediate and ventral hippocampus. Activation of either inhibits approach to a conditioned stimulus (Ito et al., 2008; Britt et al., 2012; LeGates et al., 2018; Zhou et al., 2019; Davis et al., 2020; Shpokayte et al., 2020), while an increased approach correlates with strengthened excitatory synapses from the intermediate CA1 (iCA1) (LeGates et al., 2018) and vCA1 (Zhou et al., 2019) onto the nucleus accumbens shell. The nucleus accumbens shell was proposed

to coordinate selection of reward-directed behaviours (Nic, 2007; Floresco, 2015), and therefore could provide a pathway for iCA1 and vCA1 to invoke approach to learned reward locations. The projections to the nucleus accumbens shell are not the only ones involved in conditioned approach. Activity of the neurons projecting from the vCA1 to the lateral septum also controls approach to learned reward locations (Davis et al., 2020; Kosugi et al., 2021). A synchronous activity of the lateral septum neurons that project to the lateral hypothalamus promotes food intake (Car, 2017). As a result, interactions between these two areas and the intermediate and ventral hippocampus can lead to the appetitive behaviour in the presence of food-associated cues (Car, 2017).

The fact that both the approach and avoidance depend on the ventral hippocampus indicates that the ventral hippocampus could balance these two behaviours. Evidence in favour of this interpretation comes from experiments where the animal was first conditioned to approach one and avoid another cue in a particular context. Later, when tested on a combination of the two cues, the inactivation of the ventral hippocampus skewed the animal's choices towards the conflicting cue (Schumacher et al., 2016; Riaz et al., 2017).

The description so far gives a view of the hippocampus as functionally segregated along the dorso-ventral axis, in a way that follows changes in the hippocampal input and output connectivity. While the evidence suggests a level of functional specialisation by the hippocampal domains, some authors emphasise the integral view of the hippocampal function as the general memory network (Rolls, 1996; Eichenbaum and Cohen, 2014). The conserved trisynaptic circuit throughout the hippocampus gives a computational framework for learning spatial and non-spatial relationships and associations (Rolls, 1996; Marr and Brindley, 1971; Whittington et al., 2020).

1.3 Memory encoding

1.3.1 Neural mechanisms for memory

Co-active neuronal assemblies

In a proposal that dominates the current understanding of the cellular mechanisms for memory, Hebb (1949) suggested that synaptic connections between cells strengthen to bind them into co-active assemblies encoding information. A synapse would strengthen if the two neurons it connects are active at the same time (Hebbian learning). The resulting synaptic changes would have implications for the assembly reactivation, as the activity in a fraction of the assembly cells could recall the encoded memory by reactivating the entire assembly.

Synaptic plasticity

Experimental evidence confirms Hebb's proposal that synapses are plastic. They can strengthen or weaken the efficacy with which they excite or inhibit the postsynaptic neuron. Synaptic transmission recorded in a neuron is strengthened by a brief, high-frequency stimulation of the neuron's excitatory inputs (Bliss and Lømo, 1973). The increased synaptic transmission persists over several hours *in vitro* or over days when induced in freely moving animals and is termed long-term potentiation (LTP) (Bliss and Collingridge, 1993). The synapses that undergo potentiation are those which were active at the time when the dendritic region where they terminate was depolarised (Andersen et al., 1977). The lasting effects and specificity of LTP make it a suitable substrate for memory encoding.

The induction of LTP relies on the detection of coincidental activity in the pre- and postsynaptic neurons (Bliss and Collingridge, 1993). Such role was ascribed to the N-methyl-D-aspartate (NMDA) receptor (Bliss and Collingridge, 1993). For its channel to open, glutamate has to bind to its receptors at the same time as the channel's membrane potential is sufficiently depolarised. The NMDA channel is permeable to Ca^{2+}, which on entry initiates a molecular cascade that modifies the synaptic strength

(Bliss and Collingridge, 1993; Yan-You Huang et al., 1996). The molecular changes could take place in the pre- and postsynaptic neurons, and provide a physical substrate that underpins encoding of neuronal assemblies envisioned by Hebb (1949).

The direction of the synaptic plasticity is affected by the timing of the neuronal firing. A synapse whose pre- and postsynaptic neuron spiked in that order undergoes LTP, while a synapse whose neurons spiked in reverse undergoes long-term depression (LTD) (Markram et al., 1997; Bi and Poo, 1998). These two rules for changes in synapses are known as spike-timing-dependent plasticity (STDP). STDP can be induced by repeated pairings of precisely-timed single action potentials in the pre- and postsynaptic neurons (Bi and Poo, 1998). Such neuronal activation is considered more biologically plausible than high-frequency stimulation because it could conceivably occur during an animal's behaviour.

Dependence of the synaptic plasticity on the directional activation of neurons allows the creation of long, sequential neuronal patterns, which extend in duration the assemblies consisting only of co-activated neurons proposed by Hebb (Paulsen and Sejnowski, 2000). Additionally, the sequential firing patterns created by potentiation could be stabilised by balanced LTD through recurrent connections (Paulsen and Sejnowski, 2000). This way, the spike-timing-dependent plasticity of synapses allows storing complex temporal patterns of neuronal activity.

Memory engram

Experimental evidence indicates that cells active during an experience are later reactivated during its recall (Reijmers et al., 2007; Liu et al., 2012; Ramirez et al., 2013). The reactivated cell assembly was proposed to form a memory trace or engram, which means their synapses underwent synaptic plasticity and their reactivation reinstates the memory (Tonegawa et al., 2015; Josselyn and Tonegawa, 2020). Contextual fear learning experiments localised sets of neurons whose experimental reactivation controls the expression of conditioned fear. Activation of fear-memory engram cells formed in DG leads to increased freezing, suggesting that the activation of these cells is sufficient to recall memory (Liu et al., 2012; Ramirez et al., 2013); while inhibition of the DG, CA1 or CA3 engram cells blocks the expression of freezing in the learned context,

suggesting impaired memory recall (Tanaka et al., 2014; Denny et al., 2014). The sufficiency and necessity of these cells for memory recall gives strong evidence for their role in selective gating of the memory expression. Compared with the non-reactivated cells, the DG memory engram cells have increased dendritic spine density (Ryan et al., 2015). They also have increased synaptic transmission upon stimulation of the perforant path (Ryan et al., 2015), in-line with the hypothesis that these cells underwent a form of LTP.

1.3.2 Systems consolidation

The initial encoding of memories is not permanent and their representations reorganise across the brain in a process of memory consolidation. The consolidation continuously modifies the memory encoding rendering it less liable to being forgotten (Dudai, 2012).

The idea for memory consolidation originates from the observations that the medial temporal lobe (MTL), which encompasses the hippocampal formation, is involved in declarative memories, but its necessity appears only temporary (Alvarez and Squire, 1994; Squire, 2004). Human patients with MTL damage remember events tens of years prior to the damage better than events one year prior (temporally graded retrograde amnesia, Scoville and Milner, 1957). This finding is mirrored in primates (Zola-Morgan and Squire, 1990), and rodents (Kim and Fanselow, 1992).

Presumably, memories that persisted the hippocampal damage formed in the damage-spared regions, while the forgotten events relied on the hippocampal representation. Alvarez and Squire (1994) proposed that memories are distributed across the cortex, and MTL links those geographically separated representations. The distributed cortical network stores each memory fragment in a cortical region specialised for particular information, while MTL maintains their coherence. Its damage results in a failed recall of memories it binds. According to the proposal, the cortical representations are gradually being bound together during the consolidation process when MTL co-activates these representations and their synapses change through Hebbian learning. Once the connections are strong enough, the memory becomes independent of MTL.

Memories decay over time. The lack of hippocampal dependence for remote memories, alternatively, could be due to hippocampus-specific forgetting. The hippocampus is modelled as fast learning but as having a limited capacity that causes forgetting (Marr and Brindley, 1971). Initially, the memory expression could be stronger due to additive effects of hippocampal and cortical traces. However, McClelland et al. (1995) argue against this interpretation. Memory performance was higher in animals lesioned several days after learning than in subjects lesioned the day after (Kim and Fanselow, 1992; Winocur, 1990). This difference can be explained by memory transfer from the hippocampus during the pre-lesion period, but can not be explained by additive cortical and hippocampal contributions.

Nadel and Moscovitch (1997) propose a model of the systems consolidation, in which the hippocampal involvement in memory does not change without a change in the remembered content. The model addresses the fact that the proposed consolidation processes take tens of years to transfer memory from the hippocampus as observed in patients with retrograde amnesia (Alvarez and Squire, 1994). Biological processes taking that long duration appear unlikely. Nadel and Moscovitch (1997) suggest that a new memory trace forms at the time of recall, resulting in multiple representations of memory, that each time was re-encoded with the context of memory recall. Remote memories have been reactivated more times than recent memories, and therefore left a higher number of memory traces, which explains why fewer were lost due to retrograde amnesia. When reactivated, memories are re-encoded along with the context of the memory recall in the information-specific structures. As a consequence, the observed retrograde amnesia is absolute for tasks that critically depend on the hippocampus, such as spatial memory. In this theory, consolidation reorganises memory representations but does not entail memory transfer from the hippocampus. Instead, memory consolidation means the neural representations are integrated into abstractions and schemas of related events (Sekeres et al., 2018).

What connects the two different models of memory consolidation is that they both postulate that the initial hippocampal representations of the memories transform in a process that involves the hippocampus. Therefore, it is of interest to investigate

the neural processes that could support that transformation and to track the memory representations over time.

1.4 Hippocampal states for memory encoding

Coordinated activity of neurons gives rise to oscillatory patterns in electric fields recorded in the hippocampus. The electrodes placed extracellularly record the LFP, which is the summation of synaptic activity, neuronal spiking as well as non-spike-related membrane voltage fluctuations (Buzsáki et al., 2012). The LFP of the hippocampus switches between different oscillatory patterns marking distinct states that associate with different animal behaviours (Vanderwolf, 1969). The two most prominent states are theta-gamma oscillations (theta state; Figure 1.2A) and epochs with irregular sharp-waves (sharp-wave state; Figure 1.2B). These states are interleaved with the third state of mostly irregular LFP, which dominates during immobility (Kay and Frank, 2019). Buzsáki (1989) proposed that the theta and sharp-wave states constitute two stages necessary for memory encoding: first, a labile memory trace is encoded during the theta phase; next, the synapses of that same memory trace are strengthened during sharp-waves. The sections below introduce these states and describe their significance for memory.

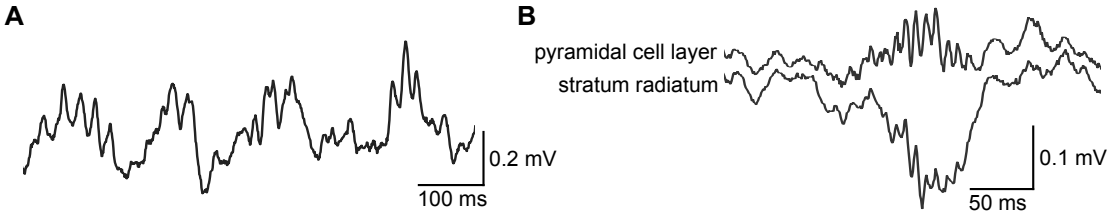

Figure 1.2: Hippocampal LFP states. (A) Theta with nested gamma oscillations recorded in the CA1. **(B)** Sharp-wave in *stratum radiatum* and the associated ripple in pyramidal cell layer.

1.4.1 Theta-gamma oscillations

Theta

Slow oscillatory activity dominates LFP of the rodent hippocampus during locomotion, exploratory behaviours such as sniffing and rearing, and during rapid-eye movement (REM) sleep (Vanderwolf, 1969; Kramis et al., 1975). Depending on the behavioural state, the exact frequency of these slow oscillations called theta varies between 4 and 12 Hz in rodents (Vanderwolf, 1969; Kramis et al., 1975).

Extracellular theta rhythm is present across the entire dorso-ventral axis but its phase is offset between regions, and the rhythm resembles a wave travelling from the septal to the temporal pole of the hippocampus (Lubenov and Siapas, 2009). The timing of cell firing is strongly modulated by the phase of theta oscillations. CA1 pyramidal neurons fire action potentials around the theta trough, when their inhibitory input is lower (Mizuseki et al., 2009). They fire sporadically, issuing spikes that repeat across several adjoining theta cycles. Few pyramidal neurons are active at the same time in this state, and different cells fire sequentially (Pastalkova et al., 2008). This sequential activation persists even when animals run in-place on a wheel in the absence of changing environmental cues, suggesting they can be internally generated (Pastalkova et al., 2008).

Because theta state dominates in the hippocampus during exploration, Buzsáki (1989) proposed that the spiking activity during theta state primes the hippocampal network to lay a new memory of the experience. The role of theta activity might extend to computational mechanisms for information processing. Each theta cycle chunks the sensory input and was proposed as a processing unit in the hippocampus (Jezek et al., 2011; Gupta et al., 2012). Multiple sensory systems converge onto the hippocampus, therefore, theta rhythm could also serve to limit the time window when external inputs affect hippocampal spiking, which could support multi-sensory integration (Mizuseki et al., 2009; Colgin, 2013).

Theta rhythm could coordinate the hippocampal activity with other brain regions by aligning their spike timing and oscillations. In the ventral striatum, neurons lock their spike timing to the CA1 theta phase during spatial memory tasks (van der

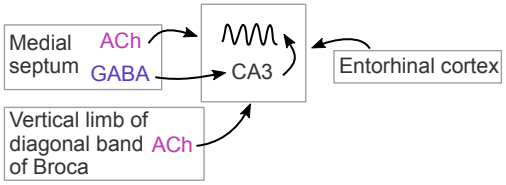

Figure 1.3: Sources of hippocampal theta oscillations. Cholinergic sources include medial septum (MS) and vertical limb of diagonal band of Broca (Kramis et al., 1975); non-cholinergic sources include EC (Kramis et al., 1975), GABAergic input to CA3 (Joshi et al., 2017) and resonant properties of CA3 recurrent circuit (Buzsáki, 2002).

Meer and Redish, 2011). In the medial prefrontal cortex, spike timing and theta lock their phase with the CA1 theta at decision points during spatial working memory tasks (Jones and Wilson, 2005; Benchenane et al., 2010). Such coordination of rhythms may be a mechanism to synchronise the activity between regions at the times when they interact while allowing them separate processing at other times (Jones and Wilson, 2005; Fries, 2015).

Theta generation

Theta oscillations are present across several brain structures. Multitude of sources has been implicated in theta generation (Figure 1.3) The MS diagonal band of Broca has been initially identified as a potential source by lesion or inactivation studies that abolished theta oscillations in the hippocampus (Green and Arduini, 1954; Petsche et al., 1962). Moreover, an early study on the rabbit demonstrated that MS neurons fire in bursts of theta frequency which could provide the theta-generating activity (Gogolák et al., 1968).

Subsequent studies made a distinction that highlighted the presence of multiple sources for the the hippocampal theta: sources that can be abolished by atropine, an antagonist of acetylcholine receptors, and other sources that were resistant to atropine (Kramis et al., 1975). Acetylcholine is a neuromodulator released in the hippocampus from the cholinergic neurons in the MS. These compose 5–10% of the MS neurons. Thus, it was proposed that the atropine-sensitive theta oscillations could be associated with MS activity while the atropine-resistant theta oscillations with EC activity (Kramis et al., 1975). The atropine-resistant origin could be maintained by the me-

dial EC GABAergic neurons that target local hippocampal interneurons and can drive theta-modulated activity (Melzer et al., 2012).

Cholinergic projections from the MS to the hippocampus can not directly be responsible for the theta currents (Buzsáki, 2002). Cholinergic activation of muscarinic receptors on the hippocampal pyramidal cells is much too slow for the generation of theta rhythm (Hasselmo and Fehlau, 2001). Instead, it might affect theta rhythm by depolarising pyramidal cells and interneurons (Madison et al., 1987), and by modulating the synaptic inhibition and conductance (Hasselmo, 2006). In addition to the cholinergic projections, MS sends GABAergic projections to the hippocampus. Inactivation of both neuronal types in the MS is needed to abolish hippocampal theta oscillations during locomotion (Yoder and Pang, 2005). MS inhibitory neurons are believed to be the main theta source as some of them fire rhythmically with theta frequency (Tóth et al., 1997; Yoder and Pang, 2005). Their subclass specifically targets the CA3 interneurons (Joshi et al., 2017), and their activity leads to a synchronous disinhibition of the CA3 pyramidal neurons, thus coordinating the CA3 excitability (Joshi et al., 2017).

Likely, there are also other factors that contribute to the hippocampal theta rhythm. These include resonant properties of neurons and of the recurrent CA3 circuit (Buzsáki, 2002). The multitude of sources makes it a robust, high-amplitude rhythm.

Gamma

Hippocampal theta oscillations co-occur with higher frequency, gamma oscillations (30–100 Hz), which were originally termed hippocampal fast activity (Buzsáki et al., 1983; Bragin et al., 1995; Csicsvari et al., 2003). A single theta cycle nests multiple cycles of gamma oscillations, and its phase modulates the gamma amplitude (Bragin et al., 1995). Gamma oscillations also appear independently of theta oscillations (Buzsáki et al., 1983) but their power is the highest during theta state (Csicsvari et al., 2003). In CA1, different rhythms within the gamma band are driven by several inputs that arrive at different times during the theta cycle (Schomburg et al., 2014). CA3 input drives the power of slow gamma, entorhinal input drives medium gamma and local CA1 network drives fast gamma oscillations (Schomburg et al., 2014). Experiments suggest a link

between memory and gamma oscillations: slow and fast gamma oscillations increase their amplitude during memory recall in spatial memory task (Schomburg et al., 2014; Fernández-Ruiz et al., 2017); and medial prefrontal cortex neurons synchronize their firing with gamma oscillations during the memory encoding stage of a spatial working memory task (Spellman et al., 2015).

1.4.2 Sleep

Consolidation of the memory is supported by sleep (Dudai, 2012). Sleep can be divided into two alternating phases: REM and non-rapid-eye movement (NREM). REM is characterized by dominating theta oscillations in the cortical and hippocampal activity, atonia of postural muscles and bursts of rapid eye movements. NREM is characterized by dominating slow, high voltage cortical oscillations. This phase is also called slow-wave sleep.

Both REM and NREM might contribute to memory consolidation. Selective deprivation of REM sleep post learning leads to impaired spatial memory in rodents (reviewed in Graves et al., 2001) and to impaired learning of perceptual tasks in humans (Avi et al., 1994). The deprivation selectively impairs new learning without affecting performance in previously learned tasks (Avi et al., 1994). Because of experimental limitations, evidence after selective deprivation of NREM sleep is lacking (Graves et al., 2001). However, this phase of sleep also might have a role. Next, I describe evidence for the role of hippocampal sharp wave ripples (SWRs) occurring during NREM sleep.

1.4.3 Sharp-wave ripples and replay

Hippocampal SWRs are the largest scale events of synchronous excitation that can be identified in the mammalian brain. They occur most frequently during slow-wave sleep, and at an intermediate rate during awake immobility (Buzsáki, 2015). They are defined by two co-occurring events in the LFP: a sharp-wave in *stratum radiatum*, and ripples which are high-frequency (100–250 Hz) oscillations in the CA1 pyramidal cell layer.

The sharp-wave is a brief, usually shorter than 120 ms, large deflection in the LFP. It is caused by a synchronous depolarisation of a large fraction of CA1 neurons by a strong bursting input from CA3 arriving via Schaffer collaterals (Buzsáki et al., 1983; Buzsáki, 1986). The depolarisation of the CA3 pyramidal cells is preceded by ramping up CA2 pyramidal neuron activity, which is thought to initiate SWRs, especially in awake animals (Oliva et al., 2016). CA2 depolarises CA1 directly and indirectly through CA3 (Oliva et al., 2016). The resulting firing of CA3 neurons drives concurrent excitatory and inhibitory currents in CA1, leading to the firing of a sparse CA1 pyramidal cell population (English et al., 2014). The interneurons and pyramidal cells fire at different phases of the ripple, suggesting the inhibitory signal modulates the time window for pyramidal cell spiking (Csicsvari et al., 1999; English et al., 2014).

Arguably, SWRs could support all three stages of hippocampal memory encoding: its initial formation, later consolidation, and recall. First, the awake SWRs could support learning through reinforcement and reevaluation processes just after the behavioural episodes (Foster and Wilson, 2006). Later, SWRs during sleep and during awake immobility could promote consolidation by reinforcing the neuronal activation representing the experienced perceptions and responses (Buzsáki, 2015). Finally, SWRs occurring during behavioural tasks could support the recall of memory (Joo and Frank, 2018).

Both LTP and LTD could take place as the result of SWRs during memory encoding and its later consolidation. The magnitude of the excitation during SWRs satisfies requirements for induction of LTP such as high-frequency stimulation (Bliss and Collingridge, 1993; King et al., 1999). The fast timescale and synchronous activity could further support spike-timing-dependent plasticity in CA1 cells (Markram et al., 1997; Buzsáki, 2015). Synapses whose postsynaptic neurons fired later than their presynaptic neurons would undergo LTP according to the STDP rules (Buzsáki, 2015). Additionally, SWRs could be a homeostatic mechanism of memory consolidation, during which all but the recently potentiated synapses undergo LTD (Norimoto et al., 2018).

During SWRs, CA1 pyramidal cells activate in sequence. The sequence repeats the order of the cell firing from a previous behavioural episode in theta state

(replay, Lee and Wilson, 2002; Foster and Wilson, 2006; Csicsvari et al., 2007; Diba and Buzsáki, 2007). The replay sequence progresses faster than the sequential firing during the initial experience. During sleep, the sequences are usually reactivated in the same order (forward replay, Lee and Wilson, 2002; Diba and Buzsáki, 2007). During immobility periods, sequences are reactivated both in forward and reverse order (reverse replay, Foster and Wilson, 2006; Diba and Buzsáki, 2007; Csicsvari et al., 2007). Most of the replay events co-occur with SWRs and can extend their duration to co-occur with several SWRs events (Davidson et al., 2009). The connections between subsequently reactivated cells could be potentiated during the SWRs (Buzsáki, 2015).

SWRs and replay occurring after experience could be mechanisms of system consolidation. They could reinforce memory traces that involve or are bound by the hippocampus (Alvarez and Squire, 1994; Nadel and Moscovitch, 1997). In turn, the SWRs and replay occurring during experience could be mechanisms of memory recall. Memory recall is thought to reactivate the neural activity that occurred during the recalled experience (Tonegawa et al., 2015; Josselyn and Tonegawa, 2020). The experience's past neuronal representations could be reinstated by the hippocampal replay. In support of this proposed function of replay, the hippocampus was observed to replay activation of cells from the previous reward-directed runs before a rat starts running (Pfeiffer and Foster, 2013), and to replay the previous activity patterns before a human subject recalls an image (Norman et al., 2019).

Learning enhances the incidence of SWRs, promoting memory encoding and consolidation. Experiments that disrupt or prolong SWRs demonstrate their causal role in both stages. Disruption of SWRs during spatial learning (Jadhav et al., 2012) and during post-learning sleep (Girardeau et al., 2009; Ego-Stengel and Wilson, 2010) impairs the learning progress, which, in contrast, improves if the SWRs are artificially prolonged (Fernández-Ruiz et al., 2019). The naturally occurring SWRs correlate with learning. The incidence of SWRs increases during a novel experience (Cheng and Frank, 2008) and during post-learning sleep (Eschenko et al., 2008). Lastly, the incidence of long-duration SWRs during a spatial memory task correlates with improved recall (Fernández-Ruiz et al., 2019). Spatial memory tasks usually involve animals navigating towards the reward. The reward promotes the incidence of SWRs, which frequently

occur during immobility after reward consumption (Csicsvari et al., 2007; Foster and Wilson, 2006; O'Neill et al., 2006). Unexpected reward (Singer and Frank, 2009) or an increase of the reward size increases SWRs incidence (Ambrose et al., 2016), while omission or a decreases of the reward size decrease SWRs incidence (Ambrose et al., 2016). The enhanced SWRs and replay in response to reward could be a mechanism binding the rewarding outcome to the experience that preceded it (Foster and Wilson, 2006).

SWRs coordinate activity outside of the hippocampus. This might be critical for system consolidation, which needs to temporally coordinate the activity in the distributed memory network (Alvarez and Squire, 1994). During sleep, SWRs co-occur with spindle events. These are large amplitude cortical oscillations in a 10–16 Hz frequency band, which can be up to 3 s-long (Siapas and Wilson, 1998; Sirota et al., 2003; Staresina et al., 2015; Latchoumane et al., 2017). Spindles are also implicated in memory consolidation (Staresina et al., 2015; Latchoumane et al., 2017). Additionally, the SWRs modulate spike-timing outside of the hippocampus. They modulate the spiking activity of the EC in sleeping and awake animals (Chrobak and Buzsáki, 1996; Ólafsdóttir et al., 2016). Similarly, SWRs strongly modulate the firing in the medial prefrontal cortex of awake animals (Jadhav et al., 2016).

1.4.4 Role of neuromodulation by acetylcholine in controlling the hippocampal states

The MS is one of several brain regions where cholinergic neurons are located. The majority of the cholinergic input to the hippocampus arrives in stratum oriens from two adjacent areas: the MS and the nucleus of the vertical limb of the diagonal band (Mesulam et al., 1983). In the hippocampus, the released ACh activates nicotinic and muscarinic receptors (Thiele, 2013). The muscarinic receptors are a class of slow-activating G-coupled receptors (Thiele, 2013). Based on their subunit composition, they can be classified into M1–5 subtypes (Thiele, 2013). Among them, M1 is most prevalent in CA1, while M2 in the other CA subfields (Levey et al., 1991).

ACh levels vary between sleep and wake as demonstrated by microdialysis measurements (Marrosu et al., 1995; Fadda et al., 2000; Giovannini et al., 2001; Fadel, 2011). In the hippocampus, ACh levels are high during exploration, low during slow-wave sleep and intermediate during REM sleep. Different hippocampal ACh levels map onto different hippocampal states: high levels during exploration and REM sleep overlap with theta state, and lower levels during immobility and slow-wave sleep overlap with the hippocampal sharp-wave state. These different levels of cholinergic neuromodulation correspond to different stages in memory encoding.

Online memory encoding

Studies that manipulated the cholinergic transmission during experience demonstrate that a high ACh level might be necessary at that stage. Blocking cholinergic receptors with scopolamine, a muscarinic receptor antagonist, affects learning but not memory retrieval in human subjects learning word pairs (Atri et al., 2004) and in primates during visual recognition tasks (Aigner et al., 1991). Local infusions of scopolamine in the perirhinal and entorhinal cortices of primates further identify that the effects of cholinergic modulation on learning can be localised in areas that include the hippocampal formation (Tang et al., 1997).

Several mechanisms could contribute to the cholinergic effects on learning. First, ACh regulates synaptic plasticity. Depending on the concentration levels in hippocampal slices, ACh induces LTP or LTD (Auerbach and Segal, 1994, 1996). It can also modify the direction of synaptic time-dependent plasticity (Brzosko et al., 2017). Second, ACh modulates neuronal transmission from the hippocampus. During theta state, the high ACh level suppresses feedback from the hippocampus to layers 5/6 of the EC (Chrobak and Buzsaki, 1994). As a result, layer 5/6 neurons of the EC have a low firing rate in this state (Chrobak and Buzsaki, 1994). Hippocampal projections to other cortical areas could also be inhibited by the cholinergic release (Hasselmo, 1999). During SWRs, the activity of layer 5/6 EC neurons is higher than during theta rhythm (Chrobak and Buzsaki, 1994). In this state, the synaptic transmission from the hippocampus is improved (Hasselmo, 1999). Therefore, the cholinergic levels can bidirectionally regulate information flow from the hippocampus.

Offline memory encoding

Memory encoding following the experience might require low-to-medium ACh levels that contrast with high ACh levels during online memory encoding. Cholinergic tone and MS cholinergic neuron discharge are at their lowest during slow-wave sleep and awake immobility. These states are associated with the highest SWRs incidence (Fadda et al., 2000; Zhou et al., 2019; Ma et al., 2020).

SWRs are a mechanism proposed to support the offline formation (Buzsáki, 1989) and later consolidation of the memory (Joo and Frank, 2018). SWRs incidence decreases when the ACh level is optogenetically elevated in urethane anaesthetised and sleeping mice (Vandecasteele et al., 2014; Zhou et al., 2019; Ma et al., 2020). In addition, theta-gamma oscillations increase upon cholinergic activation during sleep (Vandecasteele et al., 2014). The increase in theta-gamma oscillations is consistent with *in vitro* results in hippocampal slices that cholinergic release can induce and maintain theta and slow gamma oscillations in CA1 and CA3 (Fisahn et al., 1998; Fellous and Sejnowski, 2000; Dine et al., 2016).

Any changes in hippocampal theta oscillations due to ACh release might be accompanied by changes to the sleep architecture. In human subjects, drug-increased ACh level results in a relatively prolonged REM sleep (Schredl et al., 2001). The prolonged REM sleep improved memory consolidation in elderly patients whose ACh level is low (Schredl et al., 2001).

The different levels of ACh during NREM sleep and awake immobility could explain a change in the direction of cell reactivation during SWRs (Atherton et al., 2015), which also could be relevant for memory consolidation. The reverse replay during immobility after an animal has explored the environment can be triggered by the lingering excitability of cells (Atherton et al., 2015). In this case, the replay often starts with the most recently excited neurons and travels through the hippocampal circuit loop reactivating the previous neurons in the sequence from the reactivated experience (Csicsvari et al., 2007; Davidson et al., 2009). Medium level ACh during the awake SWRs would facilitate the otherwise spike-subthreshold synaptic drive and LTP (Hasselmo, 1999). During sleep, when ACh is low, forward replay would follow

the direction of synaptic changes, which replicate activation order from the experience (Atherton et al., 2015).

To summarize, ACh levels modulate the hippocampal state and both the high ACh levels during the experience and low-to-medium ACh during immediately after the experience might be necessary for memory encoding.

1.5 Hippocampal cognitive map for remembered locations

1.5.1 Place cells and other spatially modulated cells

An animal's ability to navigate its environment is thought to rely on the spatially modulated activity in hippocampal neurons (O'Keefe and Nadel, 1978). O'Keefe and Dostrovsky (1971) discovered hippocampal cells which preferentially fire at specific locations in the environment. These cells are known as place cells and the locations of their activity as place fields. The activity of place cells is modulated by the animal orientation in the environment (O'Keefe and Dostrovsky, 1971; Muller and Kubie, 1987). Nevertheless, their activity provides an allocentric, map-like marker of the position in space (O'Keefe and Nadel, 1978). They emerge immediately with no prior experience of the environment (Hill, 1978). However, their activity is specific to each environment (O'Keefe and Conway, 1978). Place cells are distributed in a random-like pattern across the entire space (Rich et al., 2014), so the potential reader of the activity in a population of place cells can decode the animal's location at any time during the animal's navigation (Wilson and McNaughton, 1993).

Hippocampal states dictate the timing of the place cell activity and their relation to the animal's spatial location. During theta state, which dominates during running and exploratory behaviour, place cells fire at their specific locations in bursts timed preferentially around theta trough (O'Keefe and Recce, 1993). Within a single theta cycle, sequences of place cells fire in an order. As an animal moves through the place field of a cell, the cell fires in a progressively earlier phase of the theta cycle (theta

precession, O'Keefe and Recce, 1993). During awake SWRs, sequences of the activated place cells are longer (Davidson et al., 2009). The sequences usually start or end with place cells with their field at the animal's current location and progress in the same or reversed order as during behaviour but on a faster timescale (Foster and Wilson, 2006; Diba and Buzsáki, 2007; Csicsvari et al., 2007).

Diversity of place cells across the hippocampal formation

Place cells were initially discovered in CA1 (O'Keefe and Dostrovsky, 1971) and were since found in other areas of the hippocampal formation: CA3 (McNaughton et al., 1983), DG (Jung and McNaughton, 1993), subiculum (Sharp and Green, 1994) and EC (Quirk et al., 1992). The place cells in these regions differ in their spatial tuning and stability of their spatial coding. CA1 and CA3 place cells have the most spatially tuned activity but they change the location of the place field (remap) over time more than the DG cells which remain stable (Hainmueller and Bartos, 2018).

The place cells also differ along the dorso-ventral axis. Consistent with the differential effects of dorsal and ventral hippocampus lesions (Moser et al., 1993, 1995; Bannerman et al., 1999; Ruediger et al., 2012; Bast et al., 2009), place field sizes increase from the dorsal to the ventral pole of CA3 (Kjelstrup et al., 2008; Royer et al., 2010) and CA1 (Jung et al., 1994; Maurer et al., 2005; Keinath et al., 2014). However, decoding of the spatial position of the animal from the population of ventral and dorsal CA1 place cells gives non-different precision (Keinath et al., 2014). Therefore, while its representation changes, spatial location encoding is present across the entire dorso-ventral axis.

Origin of place cell activity

The localised firing of place cells most likely integrates the sensory perception and self-motion signals (McNaughton et al., 2006). The visual perception can not solely lead to place cell activity. This is because place cells persist and can form in darkness (Quirk et al., 1990). Additionally, the visual cues differ with the animal's orientations, and the orientation was observed to modulate place cell activity only in some studies (Muller and Kubie, 1987).

Self-motion signals could update the internal representation of the current position in a process of path-integration (McNaughton et al., 1996). The position updating could be based on two parameters of movement: the direction of travel and the distance travelled. The first could be assisted by cells tuned to a particular head direction, which were discovered in the subicular complex (Taube et al., 1990) and later found in other brain areas (Taube, 2007). The head-direction tuning could emerge from tracking the head's self-motion and its angular velocity (McNaughton et al., 1991). The travelled distance could be measured using velocity signals or grid cells in the medial EC. Grid cells have firing fields that are equally spaced across the environment in a hexagonal arrangement (Hafting et al., 2005). Their firing is localised regardless of changes in locomotion direction and velocity (Hafting et al., 2005). Their periodic pattern could allow them to encode a metric of distance. Grid cells are organised into modules, each module sharing the same scale, which defines the distance between the cell's fields. Within a module, cells differ in the angular orientation of their fields. This arrangement allows the grid code to encode a high precision spatial location, even in large environments (Fiete et al., 2008). Additionally, their activity relayed through the direct projections to the hippocampus could drive the emergence of place cells (McNaughton et al., 2006). The firing of grid cells is not always stable in space. This instability introduces a difficulty for the utility as the metric of distance. After the physical space was stretched, the pattern of grid cells changed (Barry et al., 2007). Additionally, the grid shape of their fields can be distorted by changing the shape of the environment (Krupic et al., 2018). These two observations suggest that the grid cells are anchored to visual cues.

Over time, path-integration errors accumulate. The accumulating errors could account for the less location-specific activity of place cells when animals navigate in darkness (Quirk et al., 1990). To improve the precision of the estimated location, the environmental cues need to be integrated into the estimate (McNaughton et al., 1996). For the place cells to signal allocentric location, perception of visual cues in a self-centred, egocentric frame needs to be transformed to an orientation-independent, allocentric frame. Several classes of cells that have spatial receptive fields in an egocentric frame were found in the brain (reviewed by Bicanski and Burgess, 2020). The

responses of these cells to stimuli in an egocentric frame could be combined with the head-direction signal to arrive at allocentric representations that could generate place cell activity (Bicanski and Burgess, 2020). To increase their spatial tuning, place cells could combine the signals originating from the visual and olfactory system with self-motion signals.

1.5.2 Changes in spatial cell activity after learning

CA1 place cells appear early during exposure in a novel environment (Hill, 1978). McNaughton et al. (2006) proposed that path-integration signals are responsible for this early place cell activity, while the learning of visual landmarks leads to correction of the tracking by the self-motion. The latter develops over time and improves the precision of the place cells: with extended exposure to the environment, the place cells increase their spatial specificity and fire more reliably in the same locations (Cacucci et al., 2007; Roux et al., 2017). SWRs were proposed to stabilise the place fields (Csicsvari et al., 2007; Dupret et al., 2010). Interrupting the naturally occurring awake SWRs prevents this stabilisation in CA1 (Roux et al., 2017). In tasks where mice learn a fixed reward location, the frequency of awake SWRs correlated with memory performance (Csicsvari et al., 2007; Dupret et al., 2010). Therefore, the increased tuning and stabilisation of place cells due to their reactivation during SWRs (Roux et al., 2017) could support navigation to the reward.

The hippocampus was proposed to build a cognitive map to store information about learned spatial relations between locations, including objects in the environment (O'Keefe and Nadel, 1978). The encoding of object locations would be linked to the spatial representations, influencing place cell responses. In line with the reasoning that hippocampal activity encodes the learned object locations, the activity of dCA1 place cells increases at salient locations and objects (Deshmukh and Knierim, 2013; Sato et al., 2020), and their activity persists even when those objects are removed (Deshmukh and Knierim, 2013). dCA1 place cells accumulate at learned reward locations (Dupret et al., 2010; Boccara et al., 2019; Zaremba et al., 2017; Kaufman et al., 2020; Sato et al., 2020) and their activity increases when animals approach the reward (Zaremba et al., 2017; Kaufman et al., 2020). The place cell accumulation correlates with the

strength of memory for the reward location and persists when the animals navigate towards the learned location after the reward is removed from the environment. This effect seems to be restricted to CA1, as CA3 representations do not change the same way after learning (Dupret et al., 2010). The accumulation is due to both existing place fields shifting towards the reward and previously non-spatially modulated cells becoming consistently active at the reward location (Mizuta et al., 2021).

Grid cells are also modulated by the memory of reward. They increase their activity selectively inside reward-proximal fields (Butler et al., 2019). When reward is delivered at multiple locations, their grid pattern shifts towards the reward location (Boccara et al., 2019). This evidence from the place and grid cells suggests that the brain's spatial representations form and subsequently update to incorporate memory of reward location.

1.5.3 Models of navigation to remembered reward location

Place cells and other spatially modulated cells provide the basis for theoretical models of how animals navigate towards a learned reward location. Two classes of solutions were proposed: one that changes connection strengths between cells in a network that control the animal's locomotion and the other that explicitly encodes the goal location so it can be compared with the current location.

Navigation based on network-weight changes

The model by Redish and Touretzky (1998) proposes that Hebbian learning leads to changes in the hippocampal CA3/CA1 fields that produce activation of place cells in a reward-directed sequence. In the model, repeated reactivation of the reward-directed paths leads to co-activation of recurrently connected CA3 place cells. As a result of Hebbian learning, their connections strengthen in an asymmetric direction, and they fire in a sequence that leads towards the reward.

Redish and Touretzky (1998) omits how the firing of place cells leads to the animal selecting particular actions. This is solved by a class of models learning the best actions in a given location by reinforcing choices that previously led to reward

(reinforcement learning). These models train a network of weights that connect locations to appropriate locomotor actions at that location, such as turning west. Training updates their synaptic weights (Arleo and Gerstner, 2000; Foster et al., 2000). Reward needs to affect the learning of distant actions. The solution by Foster et al. (2000) applies temporal difference (TD) learning, which associates location signalled by a place cell with a prediction of how close the reward is. The reward prediction at a given location is calculated as a time-discounted reward value: at the reward location, the reward is maximal, and so is the reward prediction; with distance from the reward, its value decays exponentially. Adjacent locations have similar reward predictions, so moving between them causes a gradual change in reward prediction. Learning gradually updates the reward prediction values based on the error between all successive reward values experienced after visiting a particular location and the reward prediction (reward prediction error). Such error could be relayed by the dopaminergic neurons of the ventral tegmental area (Arleo and Gerstner, 2000) whose activity tracks the reward prediction error (Schultz et al., 1997). The associations between the locations and reward prediction are used to learn the best action for a location, which can be learned simultaneously as learning reward predictions. Foster et al. (2000) propose the synaptic changes can happen as a form of learning where synapses between place cells and action cells that fire together strengthen if the reward prediction was too low, and weaken if the prediction was too high.

The models described above allow fast learning of a new reward location. However, their major drawback is that they are slower to update after the reward location is changed. That is because the spatial relationship between locations is encoded in the network in a way that depends on the reward location.

Another drawback of the models proposed by Arleo and Gerstner (2000); Foster et al. (2000) is that they assume a static representation of space. However, place cell activity changes after learning (e.g. Dupret et al., 2010). In a successor representation framework, a form of TD learning was proposed to modify the place cell activity (Stachenfeld et al., 2017). In the model, the place cells encode successor states and can be combined with reward prediction values during navigation. The successive states could link individual states represented in the wider brain network, and this

way affect decision-making or locomotion (Sosa and Giocomo, 2021). The successor representation model explains some experimental results such as asymmetric shapes of place fields that follow the travelling direction (Mehta et al., 2000) and higher firing rate at the reward, but fails to explain other results such as accumulation of place cells at reward (Dupret et al., 2010; Zaremba et al., 2017; Kaufman et al., 2020; Sato et al., 2020).

Navigation based on the encoding of reward location

An alternative solution for the brain is to explicitly encode reward location. The brain could encode a snapshot of the activity of the spatial cells at the reward. This encoding would be used during navigation to calculate displacement from the current to the reward location (Burgess and O'Keefe, 1996; Foster et al., 2000; Bush et al., 2015; Erdem and Hasselmo, 2012).

A dedicated set of goal cells could take a snapshot of place cell activity at the reward (Burgess and O'Keefe, 1996). During later navigation, the goal cell activity would be proportional to that of place cells active at the time of the snapshot, therefore the activity of the goal cells would scale with reward proximity. The animal could probe the activity in different directions and follow the one that increases activity in the goal cells, or additionally decode the reward direction (Burgess and O'Keefe, 1996). Alternatively, a mapping from place cell activity could be used to learn the coordinates of their place fields, so that the reward location coordinates could be compared with the coordinates of the currently active place cells (Foster et al., 2000).

An issue with the navigation based on place cells is that their activity remaps after changes in the environment (Muller and Kubie, 1987) and over time (Ziv et al., 2013). The snapshot of reward would need to be re-learned as the place cell representations change. This issue is addressed by models based on grid cells, which preserve their pattern of firing across environments (Hafting et al., 2005). Grid cell signal could be combined to form place selective activity, reminiscent of place cells, but which is invariant over time (path integration, McNaughton et al., 2006). The snapshot of grid cell activity at reward could be encoded in a dedicated set of goal cells. Later during navigation, the animal could simulate movement away from the current location

that follows different directions and choose the one that activates the goal cells (McNaughton et al., 2006). Alternatively, the animal moving towards the learned reward location could follow a displacement vector. The vector can be calculated as a difference between the current and reward positions encoded by grid modules (Bush et al., 2015). Such calculation is possible because decoding jointly from activity of several grid modules encodes a set of possible positions of the animal (Fiete et al., 2008). Interestingly, an artificial neural network trained through reinforcement learning to control a computer agent navigating an environment develops grid-like responses in some of the network units (Banino et al., 2018). The agent can navigate to a selected reward location, taking shortcuts on the way.

The experimental results show the grid cell fields are replicated across different environments (Hafting et al., 2005); however the fields can still be affected by reward location learning (Boccara et al., 2019; Butler et al., 2019). Because both place cells and grid cells change after learning of reward location, their dynamic representations could encode reward information. Therefore, the network-level in place cells and grid cells changes, most likely, would accompany any encoding in the dedicated goal-cell populations.

1.6 Aims of the thesis

I aim to address the following three questions about the hippocampal encoding and recall of reward memory:

1. Does acetylcholine differently affect learning and the hippocampal activity depending on the behavioural phase of a spatial memory task?

2. Do memories for different reward locations share hippocampal representations that persist in time?

3. Do dorsal and intermediate hippocampus differently encode learned reward location?

Much is known about encoding spatial memory for reward location but how the cholinergic system affects this process is unclear. Neuromodulation by ACh affects

the hippocampal states observed in the oscillatory rhythms. These states are different during the navigation and immobility at reward and I tested the hypothesis that they have different roles in memory encoding. Using optogenetic stimulation of MS cholinergic neurons, Chapter 3 investigates how cholinergic stimulation affects learning and hippocampal activity during navigation and immobility at the reward.

When an animal navigates, hippocampal place cells fire in specific locations in the environment. The neural activity when the animal passes through the same locations changes after learning. Chapter 4 investigates how the memory of reward location is encoded in the hippocampal activity as the mice approach the learned reward location. Previous studies demonstrate the memory of reward modulates the activity of dCA1 place cells. I hypothesise that the reward location is encoded differently in the iCA1 whose anatomical connections differ. I test whether CA1 cells respond in a way reminiscent of goal coding cells proposed by some navigational models or whether the activity changes at the network-level support reward-directed navigation.

Chapter 2

Methods

2.1 Animals

All animal experiments were performed under the Animals (Scientific Procedures) Act 1986 Amendment Regulations 2012 following ethical review by the University of Cambridge Animal Welfare and Ethical Review Body (AWERB) under personal license held by the author and under project licence held by the supervisor.

A total of 16 adult male wild-type (WT, C57Bl/6), 51 ChAT-Ai32 mice, 5 ChAT-Cre mice (Jackson Labs strain #006410) and 13 Thy1-GCaMP6f mice (Jackson Labs strain: #024276; Dana et al., 2014) were used for the experiments. ChAT-Ai32 mice were bred from ChAT-Cre mice that express Cre-recombinase under the control of the choline acetyl-transferase promoter and mice of the Cre-reporter Ai32 line (Jackson Labs strain #012569), which carries a Cre-dependent, enhanced YFP (eYFP)-tagged *channelrhodopsin-2* (ChR2)-containing expression cassette (Madisen et al., 2012).

Mice were housed with 2-4 cage-mates on a 12:12 h light cycle. Thy1-GCaMP6f mice were housed in cages with running wheels, in a room with reversed light cycle. Other mice were housed inside standard cages in a room with daylight-aligned light cycle.

2.2 Surgery

Surgeries were carried out following minimal standard for aseptic surgery. Meloxicam (2 mg/kg intraperitoneal) was administered as analgesic 30 min prior to surgery initiation. Mice were anaesthetised with isoflurane (5% induction, 1-2% maintenance, Abbott Ltd, Maidenhead, UK) mixed with oxygen as carrier gas (flow rate 1.0–2.0 l/ min) and placed in a stereotaxic frame (David Kopf Instruments, Tujunga, CA, USA). The skull was exposed after skin incision and Bregma and Lambda were aligned horizontally.

2.2.1 Optogenetic implants

To modulate the cholinergic activity, an optic fibre was implanted above the MS. A hole was drilled at coordinates 1.0 AP, 0.0 ML in mm from Bregma, and an optic fibre (200 µm, 0.22 NA; Doric Lenses) was lowered to -3.6 DV at low speed (1 mm/ min). Once positioned just above the MS, the optic fibre was secured to the skull using dental cement (Super-Bond C & B; Prestige Dental, Bradford, UK). Six ChAT-Cre mice underwent viral transduction of MS cholinergic neurons upon injection of viral particles. Two mice were injected with 0.5 µl of AAV5/9-EF1a-dio-EGFP-WPRE and three with 0.5 µl of AAV5/9-EF1a-dio-ChR2(H134R)-EYFP-WPRE (titers ranging 1.2 to 13×10^{12} vg/ml; UNC vector Core; USA), which were delivered through a metal cannula fixed to a 5 µl Hamilton syringe.

2.2.2 Electrophysiology implants

To perform recordings in freely moving animals, 10 mice were implanted with paired wire LFP electrodes, each consisting of two twisted 75 µm teflon-coated silver wires (AGT0510, World Precision Instruments, Hitchin, UK). The tips were spaced 150–300 µm apart in vertical direction. Mice were implanted bilaterally in CA1 at coordinates -1.7 AP, ±1.2 ML, 1 & 1.35 DV in mm from Bregma, DV being taken from the surface of the brain to the lower of the electrodes. Ground and reference silver wires were connected to a stainless microscrew implanted over the cerebellum at -5.3 AP, ±1.5 ML.

To record the electromyogram activity, a 75 µm teflon-coated silver wire was implanted in the neck muscle. All wires were connected to a 32 pins Omnetics connector (Genalog, Cranbrook, UK).

The exposed brain was covered with a protective dura gel (Cambridge NeuroTech, UK) to prevent damage upon cementing of the electrodes. LFP electrodes were individually glued to the skull using UV-cured dental cement (Tetric EvoFlow) and the implant was secured to the skull using dental cement (Super-Bond C & B; Prestige Dental, Bradford, UK).

2.2.3 Calcium imaging

For experiments using calcium imaging, mice underwent two surgeries: the first one to implant a GRIN lens directly above the cells of interest, and the other to fix an aluminum baseplate above the GRIN lens for later attachment of the miniature microscope. The procedures followed the protocol as described in Resendez et al. (2016). A craniotomy was drilled above the implantation site. For the dCA1 implanted mice, the craniotomy was 1.5–2 mm in diameter. The cortical tissue and 2 layers of corpus callosum fibres above the hippocampal implantation site were aspirated. Saline was applied throughout the aspiration to prevent desiccation of the tissue. A GRIN lens (1 mm diameter, 4.3 mm length, 0.4 pitch, 0.50 numerical aperture, Grintech) was stereotaxically lowered at coordinates -1.75 AP, 1.75 ML, 1.35–1.40 DV (in mm from Bregma) and fixed to the skull surface with ultraviolet-light curable glue (Loctite 4305) and further fixed with dental adhesive (Metabond, Prestige Dental) and dental acrylic cement (Simplex Rapid, Kemdent). A metal head bar was attached to the cranium using dental acrylic cement for head-fixing the mouse during the microscope mounting. For the iCA1 implanted mice, a 0.9 mm diameter hole was drilled, and no tissue was aspirated. The GRIN lens (0.6 mm diameter, 4.95 mm length, 1.0 pitch, 0.5 numerical aperture, Grintech) was lowered inside a 21 gauge needle using a custom-made stereotaxic guide that allowed precise placement of the lens. The lens was placed at coordinates -3.16 AP, 3.6–3.8 ML, 3.40–3.70 DV and the needle guide was retracted allowing for fixation of the lens to the skull surface.

If the GCaMP6f expression was visible in the implanted mice, 4 weeks later the mice were anaesthetised for the purpose of attaching a baseplate for the microscope above the top of the GRIN lens. The baseplate was fixed into place with dental cement (Tetric EvoFlow) and the miniscope was unlocked and detached from the baseplate.

At the end of the implantations, 0.3–0.5 ml saline was injected subcutaneously for hydration and mice were placed in a post-surgery chamber +34.0 °C until full recovery from anaesthesia. The mice were allowed to recover for 5 days before habituation started and during these 5 days were monitored daily and given oral Meloxicam as an analgesic.

2.3 Behavioural testing

Mice were kept on a restricted feeding schedule for the duration of behavioural testing to maintain at least 85% of their free food body weight. The mice were habituated to the food reward of condensed milk before the behavioural testing.

Behavioural tests were recorded with an overhead webcam video camera. The video was recorded at 24 Hz frame rate. The mouse body location was tracked with DeepLabCut software (Mathis et al., 2018), and custom software was written to map the mouse coordinates to the relative location on the maze. The extracted tracks were smoothed by applying locally weighted scatterplot smoothing (LOWESS) which used a moving average of coordinates in 15 video frames. Periods of running were identified when the running speed smoothed with a moving average 0.5 s window exceeded 4 cm/s.

2.3.1 Y-maze task

Effects of cholinergic modulation on long-term spatial memory were assessed using the appetitive Y-maze task. In the task, mice have to learn to find a food reward on a three-arm maze. Acquisition of this spatial memory depends on the hippocampus function (Bannerman et al., 2012). We used food reward of approximately 100 µl of condensed milk mixed 1:1 with water. The food reward remained at a fixed location

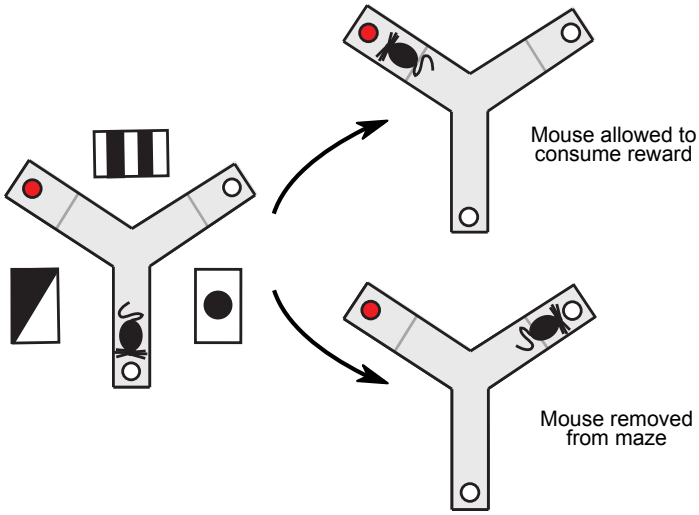

Figure 2.1: Schematic of Y-maze task for spatial learning of reward location. Mice were trained on an elevated maze to find food reward (red dot) placed at the end of one of the three arms. If they chose the correct arm they were allowed to consume the reward but were removed from the maze if they chose the incorrect arm. The reward location remained fixed relative to the room's visual cues across all learning trials.

in relation to visual cues in the room. The three-arm maze, elevated 82 cm from the floor, consisted of grey-painted 50×13 cm arms bordered by 1 cm high white plastic walls, which extended from a central triangular platform. Plastic food wells (1.5 cm high) were positioned 5 cm from the distal end of the arms.

Before the start of the learning task, mice were habituated to the maze in a different room to where behavioural testing would occur. During testing, mice were only allowed to make a single choice of the arm in each trial and were only allowed to consume the reward if they chose the correct arm, otherwise, they were removed from the maze and the trial was ended (Figure 2.1A). Target arm assignments were counterbalanced such that at least one mouse of each experimental group was designated to each arm. Each mouse received ten trials per day for 6–10 consecutive days, five starts from the left of the target arm and five starts from the right in a pseudo-random order with no more than three consecutive starts from the left or right. The interval between the within-day trials averaged 10 minutes during which the mice were placed to a holding cage. The maze was rotated either clockwise or anticlockwise after each trial to discourage the use of intra-maze cues to help solve the task.

2.3.2 Cheeseboard maze task

Changes in the CA1 activity after learning of reward locations were investigated in a spatial navigation task on a 120 cm diameter cheeseboard maze with 177 evenly spaced wells, similar to the one used previously by Dupret et al. (2010).

For the first three days, the mice foraged for rewards baited in randomly selected wells. The rewarded wells were baited with approximately 100 µl of condensed milk mixed 1:1 with water. The mice explored the cheeseboard in three or four trials for a total of 30 minutes per day. A different, random set of wells was baited in each trial. Next, the mice performed a spatial learning task. The mice had to learn two locations with baited wells (Figure 2.2). The baited wells had fixed locations that were at least 40 cm apart chosen pseudorandomly for each mouse. Mice started the trial in one of the three locations on the maze: south, east or west. The maze was rotated and wiped with a disinfectant (Dettol) in-between the trials to discourage the use of intra-maze cues. Landmarks of black and white cues were installed on the walls surrounding the maze. The trials were terminated once the mice had consumed both rewards or after 300 s, whichever was sooner. Each learning day consisted of 8 trials with 2 to 4-minute-long breaks between the trials.

After the first 5-day-long learning period, memory retention was tested on the next day in a 4–5-minute-long unbaited trial. The trial was started from a previously unused starting position (north). The performance was measured by the number of reward zone crossings counted when the mouse crossed a circular zone within 20 cm from either of the reward locations. The number of crossings was normalised by the total travelled distance.

Following the learning sessions and memory retention test for the first set of locations, one of the two reward locations was translocated. The new location was pseudorandomly chosen to be at least 40 cm away from the current and previous reward locations. The learning of the new sets of locations was performed over two days and tested in an unbaited trial the following day as described above.

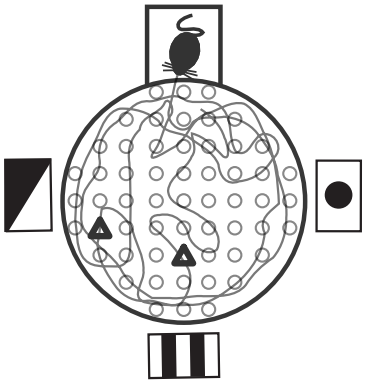

Figure 2.2: Schematic of cheeseboard task for spatial learning of reward location. Mice learned sets of two locations with baited wells (triangles) on a cheeseboard maze – a 120-cm-diameter maze with 177 evenly spaced wells (circles). The reward location remained fixed relative to the room's visual cues across all learning trials. Mouse movement during a sample trial is overlaid on top of the maze.

2.4 Histological processing

Following the behavioural experiments, mice were terminally anaesthetised by intraperitoneal injection of pentobarbital (533 mg/kg) and then transcardially perfused with phosphate-buffered saline (PBS) followed by 4% paraformaldehyde. Brains were removed and post-fixed for 24–48 hours, then rinsed and subsequently cryoprotected overnight in 30% (w/v) sucrose dissolved in phosphate-buffered saline (PBS). Coronal sections of the hippocampus were cut using a microtome (Leica) with 80–100 µm thickness for identification of GRIN lens location and 40–50 µm for other purposes. After rinsing in PBS, the sections were mounted in Fluoroshield with DAPI (Sigma). Sections were examined with a Leica Microsystems SP8 confocal microscope using the 10× and 20× magnification objectives. The placement of the electrodes was aided by the application of Dil on electrodes prior to their insertion in the brain.

To verify the expression of ChR2 fused with the eYFP tag and visualise the location of cholinergic neurons, sections were immunostained for eYFP and ChAT. After rinsing in PBS, sections were incubated for one hour in a blocking solution comprising PBS with 0.3% (weight/volume) Triton X-100 and 5% (weight/volume) donkey serum (Abcam) containing 1% (weight/volume) bovine serum (Sigma). Sections were then incubated for ≥15 hours at 4 ℃ with chicken anti-GFP (1:1000, Abcam AB13970) and goat anti-ChAT (1:500, Milipore AB144) antibodies. The sections were then washed,

followed by 2 hours of incubation in a blocking solution containing anti-chicken Alexafluor488 (1:400; Life Technologies A11039) and anti-goat Alexafluor594 (1:1000, Abcam AB150132) at room temperature. Finally, the sections were rinsed and mounted in Fluoroshield with DAPI (Sigma). The eYFP+ and ChAT+ cells were quantified manually using the ImageJ software.

2.5 Optogenetic stimulation

Task-phase specific effects of optogenetic stimulation were tested on the Y-maze by four different stimulation protocols (Figure 2.3A). The stimulation started either from the beginning of the trial (navigation and throughout cohorts), or when the mouse reached the goal zone (goal cohort). Light stimulation ceased when the mouse reached the goal zone for the navigation cohort. Estimated location of the optical fibre implants in the compared groups are shown in Figure 2.3B–D.

Optogenetic activation was achieved by light-sensitive cation channel ChR2, which opens upon activation with blue light. The activation was performed using a blue laser at 473 nm (Ciel, Laser Quantum, Cheshire, UK), powered at 25 ± 1 mW with 50-ms-long pulses at 10 Hz. Stimulation was controlled using custom made procedures in Igor Pro (WaveMetrics, Oregon, USA).

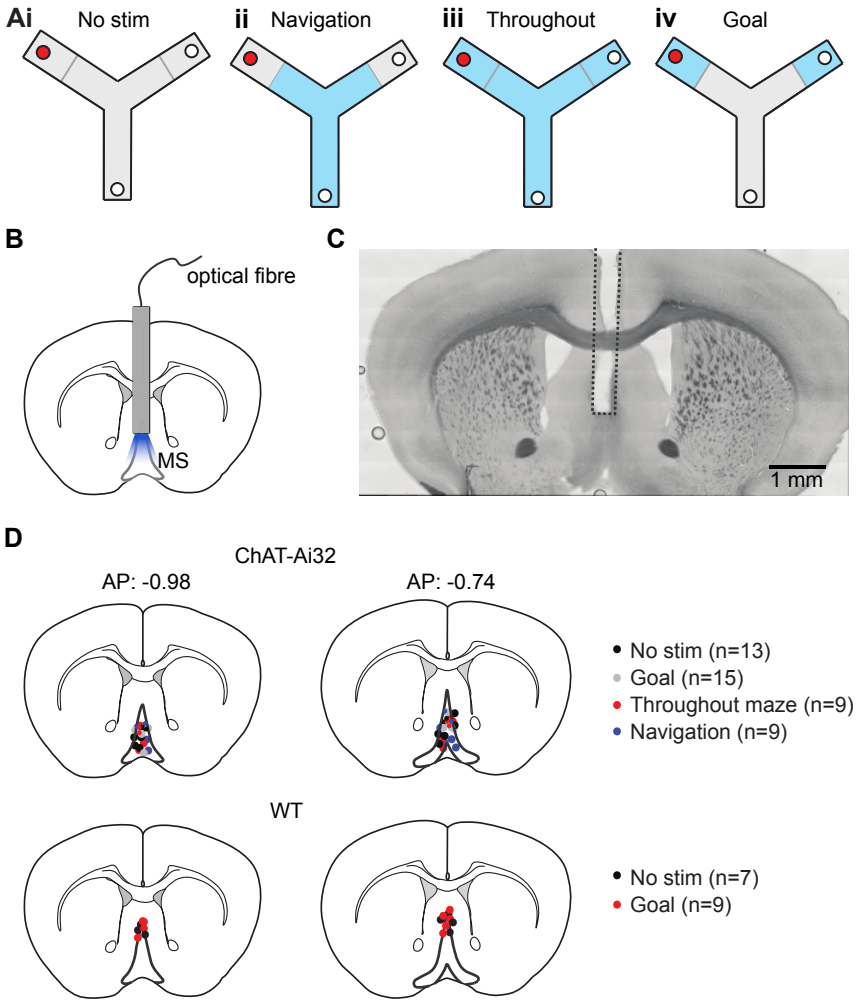

Figure 2.3: Optogenetic stimulation during Y-maze task and optical fibre implant location. **(A)** Mice were pseudo-randomly split into four groups to test four optogenetic stimulation conditions: (i) no stimulation, (ii) stimulation only until the goal zone was reached (grey line), (iii) stimulation throughout the maze, and (iv) stimulation only inside the goal zone. Blue indicates a stimulation area in the four conditions. **(B)** Placement of the optical fibre above MS. **(C)** Bright-field image of a coronal section of the brain with the dashed lines showing implantation site. Scale bar: 1 mm. **(D)** Estimated locations of the implant tip. AP, Anterior-Posterior in mm from Bregma.

2.6 Electrophysiological recordings

2.6.1 Recordings in anaesthetised mice

To test the effectiveness of the protocol for optogenetic stimulation, multi-unit activity was recorded from the MS during the stimulation in two anaesthetised ChAT-Ai32

male mice. The experiment was conducted by Dr Sze-Man Clara Tang, and the method description below is adapted from her Ph.D. thesis.

Mice were anaesthetised with intraperitoneal injections of 1.2 g/kg urethane (Sigma-Aldrich, Missouri, USA) and their head was fixed in a stereotaxic frame (Kopf Instruments, Tujunga, USA). A heating pad was used to help maintain body temperature at 35 ± 1 ℃. The head was shaved, levelled and a craniotomy was made above the MS. Optical activation in the MS (1.0 AP, 0.0 ML, –3.6 DV in mm from Bregma) was performed with a stripped optical fibre (200 µm, 0.22 NA; Doric Lenses). Multi-unit activity in the MS was recorded using an extracellular tungsten microelectrode (127 µm diameter, 1 MΩ; A-M Systems). During the experiment, the surface of the exposed skull was covered with saline (0.9% NaCl). Surgery was terminal and at the end of the experiment, a 3 mA current was passed through the recording electrode for 2 s, causing a lesion at the recording site. Coronal slices of the MS using a vibratome (VT1200S, Leica Biosystems, Milton Keynes, UK) and visualised under a bright-field microscope to verify the recording site.

2.6.2 Recordings in freely moving mice

Electrophysiological data was acquired from five ChAT-Ai32 male mice, three ChAT-Cre mice expressing ChR2 (both referred to as ChAT-ChR2) and two ChAT-Cre mice expressing GFP in the MS (ChAT-GFP). The mice were implanted with LFP electrodes for electrophysiological recordings in the CA1 (Figure 2.4A) and optic fibre for optogenetic stimulation in the MS as described in the section above. The LFP was recorded in sleeping mice and in mice performing the appetitive Y-maze task.

Staggered wire electrodes were used to record the field potentials. The electrodes targeted the CA1 pyramidal cell layer. The signal recorded from one electrode was subtracted from that in the other (Figure 2.4B). The differential signal enhances signal differences between the hippocampal layers like the locally generated phase-reversed signals, such as theta, gamma, and ripple events (Buzsáki et al., 1983; Buzsaki et al., 1992). This subtraction procedure also cancels out synchronous changes on both electrodes, like those caused by movement artefacts. In addition, EMG signal was recorded to detect any muscle movements that could correlate with mobility of the

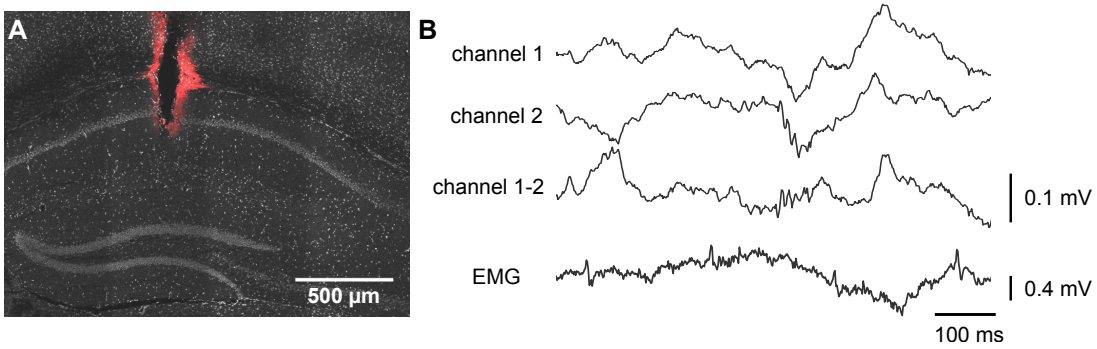

Figure 2.4: Recording LFP from CA1 implanted electrodes. (A) Location of the recording electrodes marked in red by DiI in a DAPI-stained image of CA1. **(B)** LFP signal recorded during sleep. The differential between channel 1 and channel 2 signals (top two traces) was taken as the LFP signal (middle trace). The electromyography (EMG) signal (bottom trace) was used to exclude from the SWR detection periods with detected muscle movement.

mice. Changes in the consecutive samples of the EMG signal were detected. If the change exceeded a threshold set to 2 standard deviations, a 500 ms-long window of the signal centred on the noise timestamp was removed.

For recordings during sleep, after connecting the electrodes to the Whisper recording acquisition system (Neural Circuits, LLC, VA, USA) and connecting the optic fibre to the laser, the mouse was placed in a cage (different to their home cage), to which the mouse was habituated over a period of two days. The floor of the cage was covered with standard bedding. The recordings started after the mice visibly stopped moving for an extended period of time and consisted of 30-s-long laser stimulation at 473 nm, power 25 $\pm$ 1 mW using 50-ms-long pulses at 10 Hz alternating with 60–120 s intervals without the stimulation. An overhead webcam camera tracked the movement and position of the mouse. The videos were manually reviewed together with the recorded EMG signal to exclude trials that were interrupted by the mice moving.

For Y-maze task, the mice underwent the same habituation and learning protocol as described above in the appetitive Y-maze task section. During learning, mice were connected to the laser and to the Whisper acquisition system and placed at the starting arm of the maze. The laser was activated in the goal zone on alternating trials to allow within-subject comparison. Data from these five mice was not used in the behavioural analysis as the stimulation protocol (stimulation performed in 50% of

the trials) was different from that used in behaviour only (stimulation performed in all trials).

All recordings were performed using the Whisper acquisition system sampling at 25 kHz, laser stimulation was triggered using custom made procedures in Igor Pro and synchronised with the electrophysiological and webcam recordings.

2.7 Electrophysiology data analysis

The analysis used one of the bilaterally implanted CA1 LFP electrodes that was selected based on the quality of signals for both theta oscillations and ripples. For ripple detection, the method from Vandecasteele et al. (2014) was adapted. The signal was downsampled to 1.25 kHz and 100–250 Hz bandpass filtered with Type II Chebyshev phase-preserving filter (filter order = 4, stopband attenuation = 20 dB). Next, the filtered signal was squared, mean-subtracted, and smoothed by applying a moving average with 10-ms-long window. Ripples were detected when the squared signal crossed 2 standard deviations for 20–300 ms duration and its peak crossed 7 standard deviations. Only ripples with spectral peak frequency $\geq$140 Hz were identified as SWRs (Figure 2.5; Sullivan et al., 2011). Spectral peak frequency of a ripple was estimated as the frequency with maximum power spectral density (PSD) estimated with multitaper method on the signal from the ripple start to end. Ripple incidence was calculated as the number of detected ripples divided by the recording duration.

PSD was estimated using Welch's method (MATLAB built-in pwelch function with 0.5 s window and 0.25 s overlap) for frequencies spanning the range from 1 to 200 Hz. To visualise instantaneous changes in PSD during Y-maze trials, spectrograms were created with continuous wavelet transform using Morlet wavelets (MATLAB built-in cwt function with default parameters). Theta band was defined as 5–12 Hz and slow gamma as 25–45 Hz. The slow gamma frequency upper bound was chosen to exclude any line noise contamination at 50 Hz. To estimate relative theta and slow gamma power, the FOOOF tool was used (Donoghue et al., 2020). It models the estimated PSD as the sum of an aperiodic component and Gaussian peaks in narrowband frequencies. The aperiodic component was fitted on the PSD log-log plot with straight lines, which

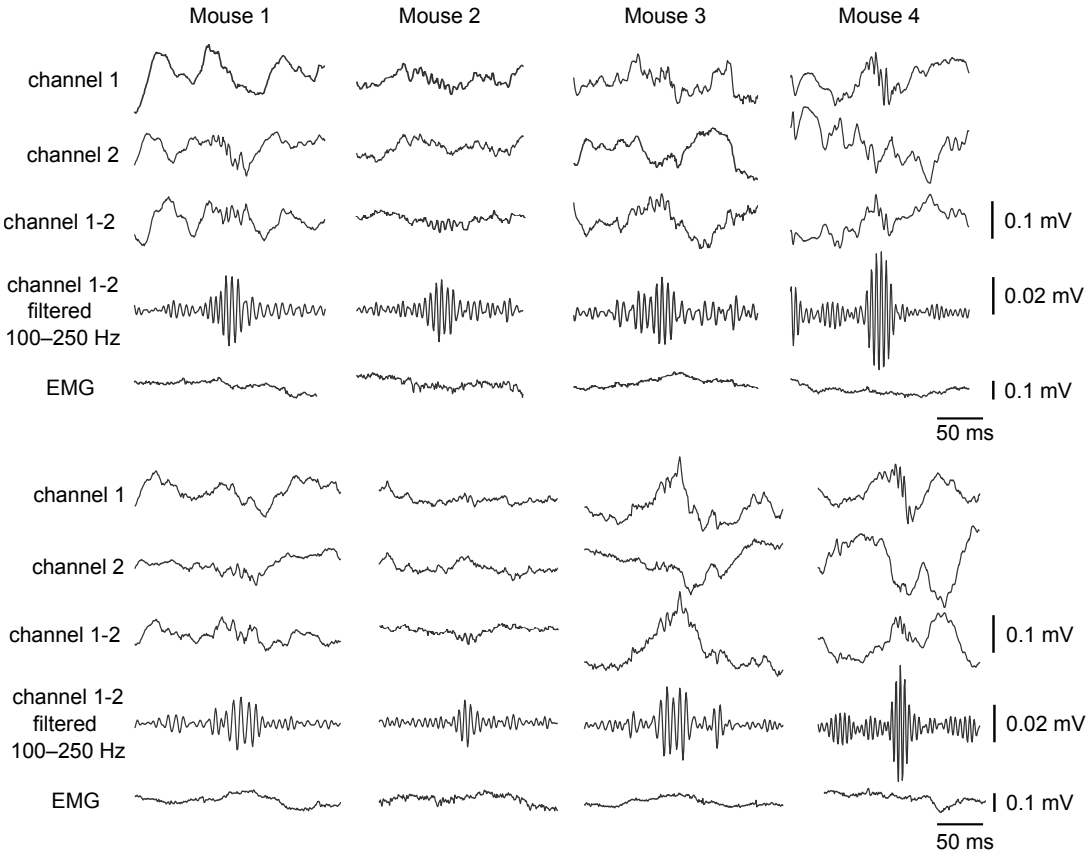

Figure 2.5: Detected SWRs. Example traces with LFP signal centred around the time of SWR peak amplitude recorded in different mice.

corresponds to a pink noise-like (1/f) background. To minimize the model error — the difference between the actual and the modelled PSD — the aperiodic component was estimated in two frequency ranges separately (3–15 Hz and 15–150 Hz). Relative theta and slow gamma peaks and their spectral peak frequencies were taken from the Gaussian peaks fitted above the aperiodic component.

2.8 Calcium imaging

The mice used for the experiment expressed GCaMP6f (Chen et al., 2013) fluorescent protein under the Thy1 promoter. The use of transgenic mice ensured constant-over-time fluorescent expression. Calcium imaging was acquired using Miniscope — a head-mounted microscope (v3 and v4 Miniscope; Ghosh et al., 2011; Ziv et al., 2013). Microscope emitted blue excitation light ($\tilde{4}70$ nm spectral peak) whose power was adjusted to approximately match the mean brightness of the image across mice. Fluo-

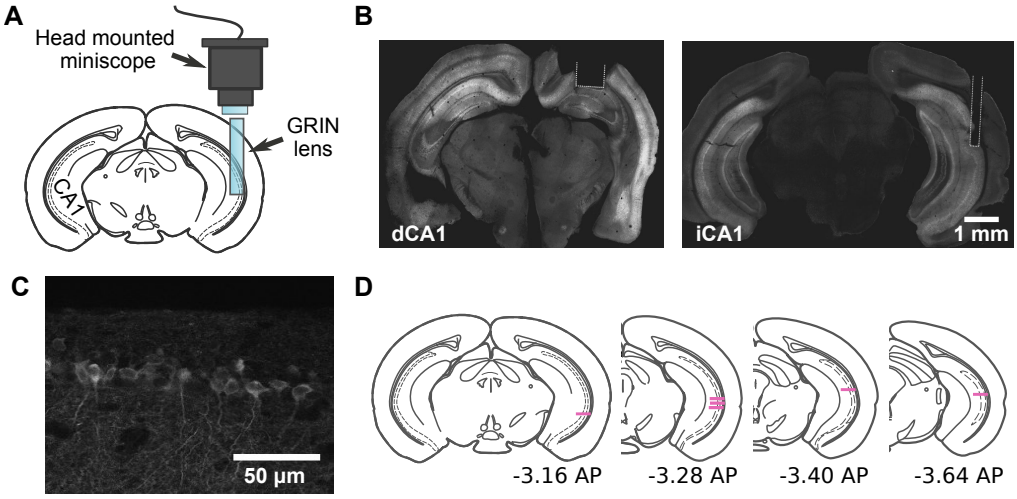

Figure 2.6: Location of the dCA1 and iCA1 implanted GRIN lenses for calcium imaging. (A) Schematic showing configuration of the implanted GRIN lens and the head-mounted miniscope during calcium imaging. **(B)** Coronal section of the brain with the dashed lines showing implantation site of the GRIN lens implanted above dCA1 (left) and iCA1 (right) pyramidal cells expressing GCaMP6f. **(C)** dCA1 pyramidal cells expressing GCaMP6f located below the edge of the implanted GRIN lens. **(D)** Reconstructed location of the recorded cells under the GRIN relay lens implanted in the iCA1 of six imaged mice. Horizontal bars mark the bottom of the relay lens.

rescence emissions were passed through an emission filter (bandpass filter, 525/50 nm) and collected by a CMOS imaging sensor. Before the start of the recording, the mouse was head-fixed on a running wheel to attach the microscope and adjust its focal plane so it matched the field of view from the previous recordings. Afterwards, the mouse with the Miniscope attached was placed in a start box for 3–5 minutes before recording sessions started. The calcium imaging was acquired at 20 Hz, and synchronously started with webcam camera recording.

2.9 Calcium signal processing

CaImAn software was used to motion-correct any movements between the calcium imaging frames, identify the cells and extract their fluorescence signal from the video recordings (Giovannucci et al., 2019). The method for cell and signal detection was based on constrained non-negative matrix factorization (Pnevmatikakis et al., 2016), which separates sources of the fluorescence changes. Because the 3-dimensional imaged volume is projected onto 2-dimensional image, some cells in the 2-dimensional projec-

tion can have overlapping region of interests (ROIs). Constrained non-negative matrix factorization isolates sources of the changes in the overlapping ROIs. The isolation is possible because each source results in correlated fluorescence values in neighbouring pixels, and different sources change fluorescence at different times. The identified sources will include neurons and their processes, and the neuronal activity can be attributed to specific cells.

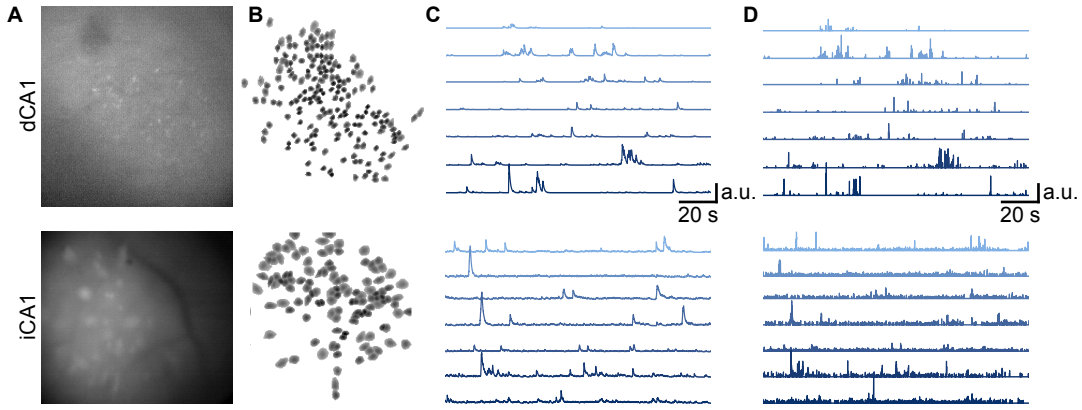

Figure 2.7: Calcium imaging from the hippocampus. (A) Example field of view of the microscope cropped to the area with detected cells. The image shows a maximum projection calculated on a 50-s-long imaging video. **(B)** ROIs of cells detected across all sessions in a day from an example mouse. **(C)** Background-subtracted fluorescence traces of example cells shown in (B). **(D)** Deconvolved fluorescence traces shown in (C). The top panels show examples from dCA1 and the bottom panels from iCA1 recordings.

CaImAn extracted background-subtracted calcium fluorescence values and deconvolved the signal. The deconvolved signal can be interpreted as a scaled probability of a neuron being active. The calcium imaging videos recorded in the same-day trials were motion-corrected to a common template frame and were concatenated. Signal extraction and further processing were performed on the resulting long video, allowing the detection of cells and signals present across the trials. To improve the computational performance, the videos were cropped to a rectangle containing the imaged cells and the video width and height was downsampled by a factor of 2.

The identified putative cells were automatically filtered using CaImAn. The results were visually inspected and the filtering parameters adjusted to exclude non-cell like shapes and traces. The criteria used for the filtering included a threshold for signal to noise ratio of the trace, the minimum and maximum size of the component's

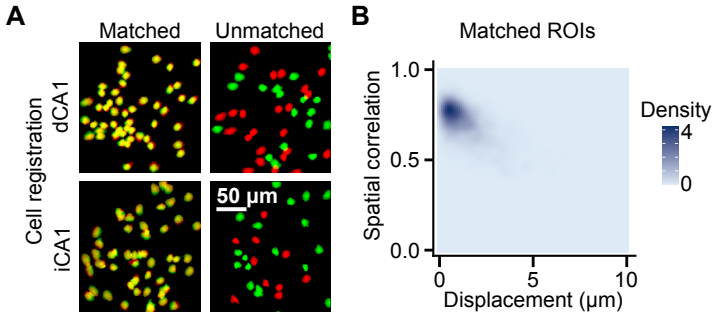

Figure 2.8: Matching cell identities between days. (A) Matching of cell identity (cell registration) based on the ROIs in calcium recordings from two different days. An example with iCA1 cells found on one day is shown in green and on the other day in red. The figure shows a fragment of magnified recording's field of view. **(B)** Spatial correlation of the matched ROIs as a function of the distance between their centroids.

ROI, the threshold for consistency of the ROI at different times of the component's activation, and a threshold for the component's resemblance to a neuronal soma as evaluated by a convolutional neural network provided with CaImAn software.

The deconvolved traces were smoothed in time with a Gaussian kernel (σ = 75 ms). To reduce the data size for the analysis, the trace was then time binned by averaging the values in 200 ms non-overlapping bins. Using the trace smoothed in time reduced the importance of the exact location for boundary between the time bins.

For the comparison of dCA1 and iCA1 activity, calcium event rates are reported. A calcium event was detected whenever the cell's deconvolved signal crossed 20% of its maximum value.

The identity of cells between the recordings on different days was matched using a registration algorithm implemented in CaImAn (Giovannucci et al., 2019). The algorithm aligned the image with ROIs of cells from all days to the image from the reference day and matched the cells when their centres of mass were closer than 10 µm. The matched cells had low displacement (mean distance 1.9 µm, IQR: 1.1–3.1 µm) and highly correlated regions of interest (median 0.72, IQR: 0.66–0.77, Figure 2.8B).

2.10 Calcium data analysis

2.10.1 Place cell detection and analysis

To assess how spatial locations modulated the cell activity, its place map was calculated. Place map shows mean neural activity per spatial bin calculated during running periods. The total activity inside 6 x 6 cm bins was summed from the smoothed deconvolved signal. The mean neural activity in the spatial bin was then calculated as a ratio of the total activity to the total occupancy in the bin after both maps were smoothed across the space using a 2D Gaussian kernel with $\sigma = 12$ cm. The place map was filtered to include spatial bins with total occupancy that exceeded 1 s (5 time bins, thresholded on unsmoothed total occupancy). The size of place fields scales with the environment (Harland et al., 2021). To facilitate comparison with other studies, the field size is reported as percentage of the maze area.

Spatial information of a cell's activity was calculated using the place map values. Spatial information (W. E. Skaggs, B. L. McNaughton, K. M. Gothard, 1993) was defined as:

$$spatial\_information = \sum_{i=1}^{N} p_i \frac{\lambda_i}{\lambda} log_2 \frac{\lambda_i}{\lambda} \tag{2.1}$$

where λ represents the mean value of the neural signal, p_i represents the probability of the occupancy of the i-th bin, and λ_i represents the bin's mean neural activity. Dividing by λ ensures the metric is independent of the cell's average activity. The units of spatial information calculated on calcium fluorescence can be reported as bits per action potential (Climer and Dombeck, 2021). However, because the actual action potentials were not measured, spatial information is reported as arbitrary units.

Spatial information was compared to the value expected by chance. The chance level was calculated by circularly shifting the activity with regard to the actual location. For each cell, the activity was circularly shifted within the trial by a time offset chosen randomly (minimum offset 10 s for baited and 20 s for unbaited trials). If the cell's spatial information exceeded 95% values calculated on 1000 random shifts of its activity, it was defined as a place cell.

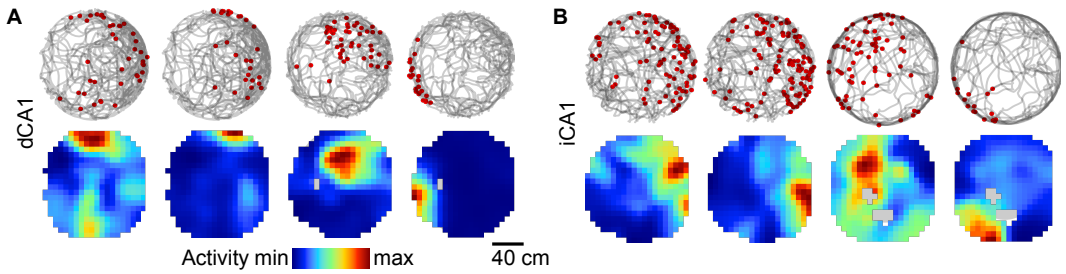

Figure 2.9: Computing place maps. (A) Examples of dCA1 place cells. Locations of calcium events marked with a red dot are overlaid over mouse movement paths (top); place maps are shown below. Grey pixels represent unsampled locations. **(B)** As in (A) but for iCA1 place cells.

A limited number of neuronal responses sampled per spatial bin can lead to an upward bias in the estimated spatial information (Treves and Panzeri, 1995). To correct for this bias, the spatial information values are reported relative to the spatial information expected by chance. The value expected by chance was estimated as the mean spatial information from the time-shifting procedure used for place cell detection. This procedure did not require binning the neuronal responses from the calcium imaging as required by analytical estimation (Panzeri et al., 2007), and has been used previously to estimate mutual information bias (Akrami et al., 2018).

The field size was defined as the fraction of a place map with values exceeding half the maximum value. Centres of place fields were identified in the place map by finding local maxima exceeding half the global maximum. The local maxima were restricted to be at least 25 cm apart and have at least one adjacent spatial bin exceeding half the global maximum.

2.10.2 Calculation of place fields at reward location

The centre of mass for the field was calculated and used to report the field's distance from the reward locations. For place cells with multiple place fields, the shortest distance from the reward was used. Fields $\leq$20 cm from the reward location were referred to as reward fields. For the count of reward locations where a place cell had a reward field, only cells that were classified as a place cell in at least half of the test trials were considered. The distribution of the expected counts was generated by a process that shuffled cell identities assigned to test trial place maps. The count of reward fields

was summed for each resulting cell. A significantly higher fraction of cells with zero or many fields at reward location means their count exceeded that in 95% of the shuffles.

2.10.3 Bayesian decoders

Two Bayesian decoders were constructed from the neural activity: the first decoding spatial location of the running mouse, the second decoding if the mouse was running inside a reward zone.

The decoders used smoothed deconvolved activity after it was binarised. The binarised trace had value 1 when the value exceeded the 90th percentile of the cell's values for that day (active cell); otherwise, the binarised trace had value 0 (inactive cell).

The Bayesian decoder assumed activity of the cells was independent given the output, and it chose the output to maximize posterior probability given the neural data:

$$\hat{s} = argmax_s P(s) \prod_{i=1}^{ncells} P(r_i|s) \tag{2.2}$$

For decoding the mouse location during running, s represents the spatial bin, P(s) represents the prior occupation probability in the spatial bin s, and $P(r_i|s)$ represents the probability of the i-th cell being active in the spatial bin s.

For decoding whether the mouse was running in the proximity of learned reward location, s represents whether the mouse is inside a reward zone (within 20 cm from the reward), P(s) represents prior occupation probability inside or outside of a reward zone, and $P(r_i|s)$ represents the probability of the i-th cell being active inside or outside of a reward zone.

The probabilities $P(r_i|s)$ and $P(s)$ in equation 2.2 were calculated on a training dataset and were used to decode $\hat{s}$ in dataset used for evaluation.

Two decoders were trained and evaluated:

(1) The decoder for the spatial location was trained and evaluated using a cross-validation method as follows: The day's session was split into five equal parts. A

single part was reserved for evaluation and the others for training the decoder. The decoder was trained and evaluated, and the process was repeated five times, each time with a different part of the data reserved for evaluation. The decoder was compared to a baseline random decoder which predicted spatial location based on prior occupancy probabilities. The decoder errors were reported as a distance between the actual and the predicated spatial bin. Because fewer cells were recorded in the iCA1 than in the dCA1, I also compared decoders trained on equally sized populations by randomly sampling 30 cells from each recorded session (72% of the iCA1 recordings had more than 30 cells). The spatial decoding from equally sized neuronal populations was repeated 50 times with different cell samples.

(2) The decoder of whether the mouse was inside a reward zone was trained on data from two unbaited test trials, which were performed on different days and shared a single learned reward location. The training dataset was filtered to times when the mouse was in proximity of the learned reward location (distance $\leq$15 cm), or the mouse was well away from the reward location (distance $\geq$40 cm). The decoder was evaluated on data from another unbaited test trial. In this trial, one of the learned reward locations was different from the ones in the training dataset, and one of the learnt reward locations was missing from the current ones. Only data from the proximity of either of these two locations was used for evaluation (the reward zone vs the previous reward zone). The evaluation was restricted to trials that shared at least 10 cells with the training trials. The decoder assumed equal prior P(s) of the zones. The resulting decoder's performance was compared with a baseline random decoder. The decoder errors were reported as the percentage of correct predictions.

2.10.4 Downsampled data comparison

To verify that differences in maze occupancy between foraging and test trials were not the reason for the changes in place cell properties, the data was randomly downsampled. For each spatial bin in the two sessions, an equally sized subset of timestamps was selected to match the lower of the two occupancies. The selected timestamps were

used to construct place maps and to identify place cells. The random downsampling procedure was repeated 100 times, and the statistics about the place field locations and their distance to reward locations were aggregated from 100 downsampling repetitions.

2.10.5 Population activity on reward approach

To analyse the population activity during an approach to reward locations, periods of running that exceeded a minimum duration of 3 s were used. In the baited trials, the running bouts were aligned by the time of the tracked mouse body stopping within 7 cm from the reward. For the bouts stopping at non-rewarded locations, only the stops at distance >24 cm from the reward were included. In the unbaited trials, the running bouts were included if they crossed a location <18 cm from a learned reward location and covered a distance >12 cm. The deconvolved z-scored activity was aligned to the timestamp when the mouse was the closest to the learned reward location. The mean population z-scored activity was calculated for 1 s-long bins and the activity at 4–5 s before the bout finish was compared to the activity at 0–1 s.

2.11 Quantification and statistical analysis

Results are reported using two statistical methods. First, I estimated p-values using null hypothesis significance testing. The p-values are low for small effects assessed on large sample sizes; they depend on unseen data, and on the plan for how many animals to test experimentally (Wagenmakers, 2007). Therefore, I also report Bayes Factors (Keysers et al., 2020) — a measure of relative evidence for two competing hypotheses. It is calculated as a ratio of posterior probabilities: the probability of the alternative hypothesis given the observed data over the probability of the null hypothesis given the observed data. I assumed equal prior probability of the alternative and null hypothesis. In addition to providing further statistical support to significant p-values, Bayes Factor analysis gives evidence for the absence of differences where the effects are non-significant (Keysers et al., 2020).

Mixed-effects models were used for the statistical analysis to allow for unbalanced sampling and correlated samples. Both apply to these data, for example, due to

correlations between the samples of cell activity recorded at the same timestamp, or recordings from the same mouse on different trials. The effects were assessed with linear and log-linear mixed-effects models. The fixed effects were the statistically tested effects such as implant location (dCA1 vs iCA1) or cell type (place cell vs non-place cell); the random effects were modelled as mouse-specific and session-specific random variables. The random effects were also included in the estimation of the linear regression model.

For the frequentist approach, the model coefficients were estimated using the restricted maximum-likelihood method. The residual errors were checked for linear model assumptions: zero mean, no correlation with the predicted values and homoscedasticity. To satisfy these assumptions, some models used a log-linear transformation of the response variable. The significant effects and their interactions were reported and the post-hoc tests were performed on differences in least-square means of the paired groups. The tests used Satterthwaite estimation of degrees of freedom and adjusted p-values using Holm-Bonferroni correction.

For the Bayes factor analyses, the mixed-effects models mirrored the frequentist models and had the same fixed and random effects. The priors were specified as Cauchy distribution with $\sqrt{2}/2$ scale for fixed effects and 0.5 scale for random effects. These priors follow the expectation that the differences between mice are smaller than the effects of interest. Bayes factor for the effect of interest was calculated as the probability of the full model over the probability of the model excluding the tested effect and was reported as BF_{10}. Following Jeffreys' thresholds (Jeffreys, 1961), the magnitude of evidence from the data was graded as

- strong evidence for difference ($BF_{10} > 10$),
- moderate evidence for difference ($10 > BF_{10} > 3$),
- inconclusive ($3 > BF_{10} > 0.33$),
- moderate evidence for no difference ($0.33 > BF_{10} > 0.1$),
- strong evidence for no difference ($0.1 > BF_{10}$).

The effect sizes were reported with 95% credibility intervals (CI; equal-tailed interval). The interval can be interpreted as a range within which the effect falls with 95% probability given the evidence from the observed data. Credibility intervals were estimated from the samples of the model's posterior distribution.

Statistical analysis was performed in R version 3.6.3. The linear mixed-effects models were built in R with package 'lme4' and p-values for the fixed effects were obtained using Satterthwaite estimation of degrees of freedom implemented in the 'lmerTest' R package. Least-square means were calculated and tested with 'lsmeansLT' function from the same package. Bayesian linear mixed-effects models were created using 'BayesFactor' R package and 'lmBF' function.

Data was reported as mean ± SEM unless otherwise stated.

Chapter 3

Cholinergic control of hippocampal states for encoding memory

3.1 Introduction

The LFP in the hippocampus switches between distinct states: theta-gamma oscillations and epochs with irregular sharp-waves (O'Keefe and Nadel, 1978; Buzsáki, 1989). These two patterns correspond to distinct behavioural states: in sleeping animals, theta state dominates REM sleep and sharp-waves occur during non-REM sleep; in awake animals, theta state is pronounced during mobility while sharp-waves occur during immobility periods (O'Keefe and Nadel, 1978; Buzsáki et al., 1983; Buzsáki, 1986). Buzsáki (1989) proposed these two states of the hippocampal LFP constitute two stages necessary for memory encoding: first, a labile memory trace is laid during the theta state; next, the synapses are strengthened during sharp-waves. I asked whether ACh facilitates differentially the two stages of memory encoding in the hippocampus.

The local release of ACh controls hippocampal network states. ACh levels in the hippocampus are high during exploration, promoting theta activity, and lower during subsequent rest when theta rhythm terminates and sharp-waves occur (Fadda et al., 2000; Giovannini et al., 2001; Fadel, 2011). Optogenetic activation of cholinergic neurons in sleeping animals promotes theta-gamma oscillations in CA1 of the hippocampus and suppresses SWRs through the activation of M2/M4 muscarinic receptors (Vandecasteele et al., 2014; Zhou et al., 2019; Ma et al., 2020). This suggests

that the changing cholinergic tone allows the switching between theta/gamma oscillations SWRs. Disruption of cholinergic activity at different stages of learning and memory impairs performance in memory tasks (for review, see Hasselmo and Sarter, 2011; Solari and Hangya, 2018). However, the differential effects of ACh in distinct phases of memory encoding are not well understood.

To clarify the function of the MS cholinergic system in hippocampus-dependent memory, I investigated the behavioural phase-specific effects of optogenetic cholinergic stimulation in the appetitive Y-maze long-term memory task. This reward-based spatial memory task has two distinct behavioural phases: one of navigation toward a reward and another after arriving in the goal area (Bannerman et al., 2012). In this Chapter, I show the effect of cholinergic stimulation on theta-gamma oscillations and SWRs during sleep when the effects of cholinergic stimulation of the LFP were the largest. Next, I describe how the cholinergic stimulation affected the learning of reward location depending on the task phase. The simultaneous recordings of the LFP in the dorsal CA1 indicated that impaired memory was related to the disruption of awake SWRs immediately following the experience.

The results and their discussion presented in this chapter were published in Jarzebowski et al. (2021b). The work was completed in collaboration with Dr Sze-Man Clara Tang and Dr Audrey Hay, who both helped design the study. Dr Sze-Man Clara Tang conducted behavioural experiments and tested the optogenetic stimulation efficacy, which she also presented in her Ph.D. thesis; Dr Audrey Hay surgically implanted recording implants for electrophysiology.

3.2 Effects of cholinergic stimulation on hippocampal state during sleep

3.2.1 Functional expression of ChR2 in cholinergic neurons

I investigated the effects of cholinergic modulation on hippocampal state and memory in a spatial navigation task. To this end, I optogenetically controlled the activity of cholinergic neurons using ChAT-Ai32 crossbred mice that expressed enhanced

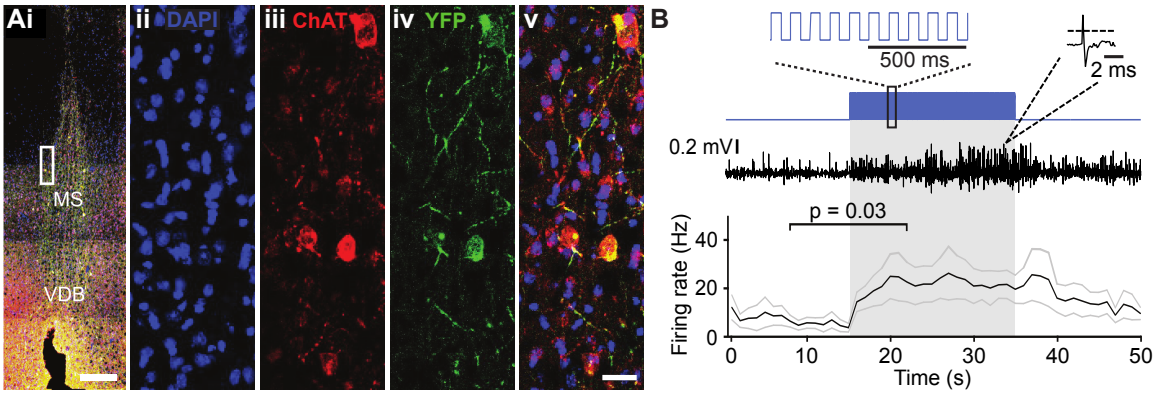

Figure 3.1: Medial septum neurons increase activity upon optogenetic stimulation of ChR2 tagged neurons. (Ai) Overlay of DAPI, ChAT, and eYFP-positive immunostaining in a coronal section of the MS in a ChAT-Ai32 mouse. Scale bar 500 µm. VDB, ventral diagonal band. **(Aii-v)** Higher magnification of the MS (rectangle in Ai), triple immunostaining of DAPI (blue, ii), ChAT (red, iii), and eYFP (green, iv), showing their colocalisation (overlay, v). Scale bar 50 µm. **(B)** Sample trace of multi-unit recording from the MS in a ChAT-Ai32 mouse. Top: the stimulation protocol (blue) beginning at 15 s. Inset shows a section of the 50-ms-long square stimulation pulses at 10 Hz. Middle: an example recording trace; inset shows an example unit recorded. Bottom: mean spike frequency (n = 6). *p = 0.03, two-tailed paired Wilcoxon signed-rank test. Grey lines represent mean ± SEM. Data collected by Dr Sze-Man Clara Tang.

YFP-tagged channelrhodopsin-2 (ChR2-eYFP) under the control of the choline-acetyl transferase (ChAT) promoter. Double immunostaining for ChAT and YFP confirmed the MS cholinergic neurons expressed ChR2 (Figure 3.1A). In sections sampled from two mice, 98 out of 150 ChAT+ cells counted were YFP+ (YFP+/ChAT+ = 65%). In independently sampled sections, 111 out of 111 YFP+ cells counted were ChAT+ (ChAT+/YFP+ = 100%).

The optogenetic stimulation of the ChR2 expressing neurons increased multi-unit activity in the MS of urethane-anaesthetised mice, confirming the effectiveness of the optogenetic protocol. Light delivery (473 nm light, 50 ms pulses at 10 Hz) through an optic fibre increased multi-unit activity recorded 200 µm ventrally from the optic fibre tip (baseline spike frequency: 7.9 ± 2.8 Hz vs. spike frequency during light delivery: 22.7 ± 7.3 Hz, two-tailed Wilcoxon matched pair signed-rank test: p = 0.03; n = 6 recordings from two mice; Figure 3.1B).

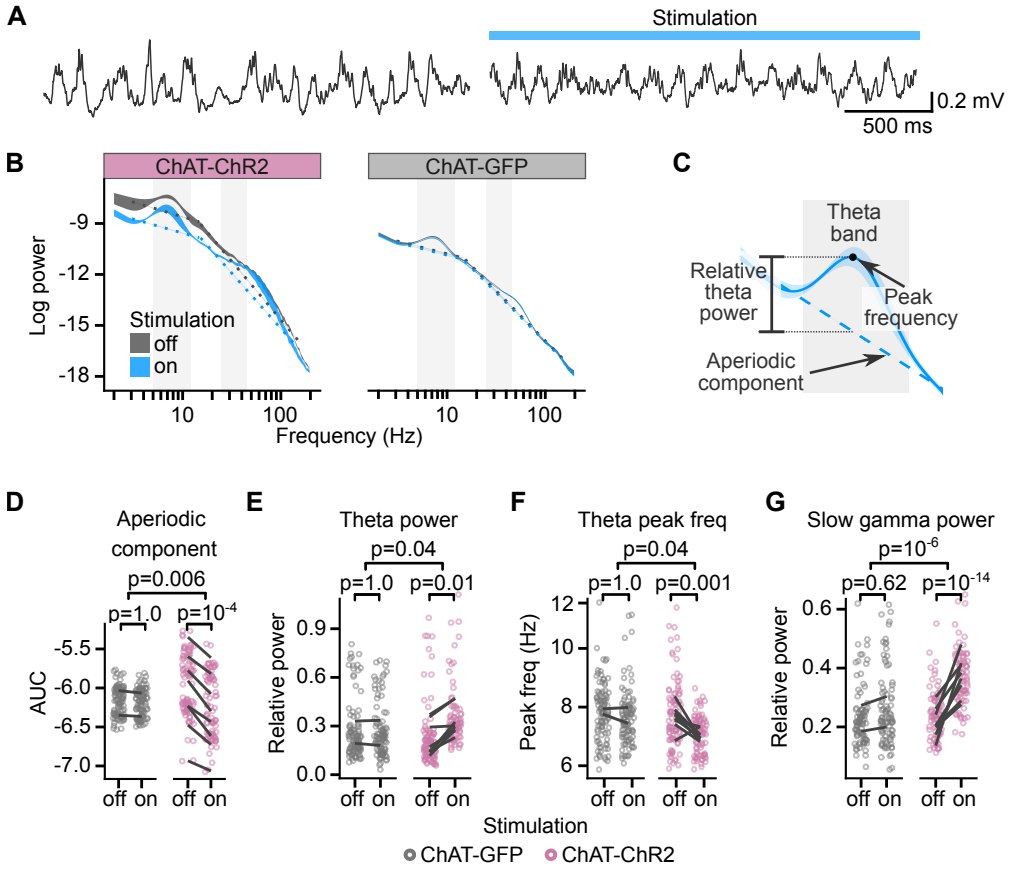

Figure 3.2: Cholinergic stimulation during sleep reduced aperiodic and increased relative theta-gamma activity in CA1. **(A)** LFP signal recorded from CA1 during sleep before (left) and during (right) optogenetic stimulation of the MS. **(B)** Mean PSD of the LFP signal from a single mouse during the subsequent epochs with the stimulation off and on. Ribbons extend ±1 SEM. Grey background marks the frequency range of theta and slow gamma bands. The dashed lines show the fitted aperiodic component. **(C)** PSD parameters assessed for the stimulation effect: the aperiodic component **(D)**, relative theta power **(E)**, spectral peak frequency in the theta band **(F)**, and slow gamma power **(G)**. The aperiodic component was fitted for two frequency ranges, 3–15 and 15–150 Hz, and compared using the total area under the curve (AUC). Values are plotted for individual trials. Lines connect means for individual animals. p-values were calculated with linear mixed-effects models for mouse group–laser interaction.

3.2.2 Increased theta-gamma power

First, I investigated how the hippocampal state changes as the result of optogenetic stimulation of the MS cholinergic neurons. Previous studies reported that cholinergic stimulation increases theta-gamma oscillations in sleeping animals (Vandecasteele et al., 2014), while other studies reported such effect was not found in sleeping or immobile awake animals (Zhou et al., 2019; Ma et al., 2020).

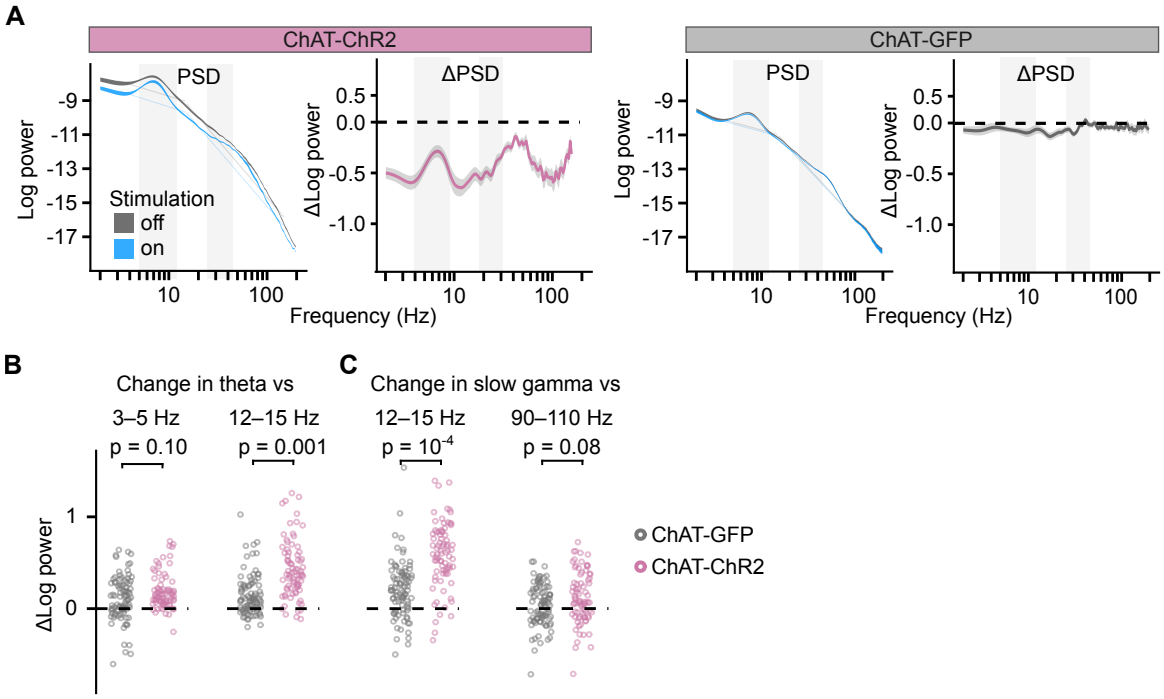

Figure 3.3: Cholinergic stimulation during sleep reduced absolute theta and gamma power less than it reduced their neighbouring frequency bands. (A) Left: PSD ± 1 SEM during sleep epochs with the stimulation on and off. Right: difference between log power calculated on subsequent epochs with stimulation off and on as a function of frequency. PSD and its difference are shown for one ChAT-ChR2 and one ChAT-GFP mouse. Grey background marks the frequency range of theta and slow gamma bands. **(B)** Change in theta power as the result of optogenetic stimulation compared to change in surrounding frequency bands. **(C)** As in (B) but for slow gamma power. Values are shown for log power differences in subsequent epochs with stimulation off and on. p-values were calculated with linear mixed-effects models for the mouse group effect (ChAT-ChR2 vs. ChAT-GFP).

I recorded LFP signal while the mice slept in a cage, to which they had been familiarised over the two previous days and I alternated periods without optogenetic stimulation (60–120 s) and periods with optogenetic stimulation (30 s). I compared the signal in the 30-s-long epochs preceding the stimulation with the 30-s-long epochs during the stimulation without a distinction between SWS and REM sleep. Only epochs during which the mouse was asleep for their full duration were used for the analysis (n = 369 epochs from 10 animals, IQR of 5–16 epochs in succession without interrupted sleep).

Upon the stimulation, I observed a reduction of the PSD across the full 1–200 Hz frequency range (Figure 3.2B,D), as reported previously in freely behaving mice (Vandecasteele et al., 2014).

PSD from electrophysiological recordings measures the summation of periodic activity and aperiodic activity. The intensity of the aperiodic component of the PSD has a pink noise distribution (1/f) (Donoghue et al., 2020). Broadband power of the aperiodic component decreased with light stimulation in the ChAT-ChR2 but not in the ChAT-GFP mice (linear mixed-effects model on area under curve [AUC] of estimated aperiodic component on PSD log-log plot, significant mouse group × laser interaction: $F_{(1,4.6)} = 22$, $p = 0.006$, $BF_{10} = 10^{14}$, $n = 369$ epochs from 10 mice; post-hoc test for laser effect in ChAT-ChR2: $t_{(7.1)} = 10.1$, $p = 10^{-4}, BF_{10} = 55$, $CI = [-0.08, -0.27]$; Figure 3.2D).

To quantify the power of theta and gamma oscillations, I measured relative peaks above the estimated aperiodic component (Figure 3.2B–C; Donoghue et al., 2020). Even though theta power was low during sleep outside of REM sleep, 99 ± 0.1% of the control and 100 ± 0% of the stimulated epochs had a relative theta peak. Optogenetic stimulation had a significantly different effect in the ChAT-GFP and the ChAT-ChR2 animals on the relative theta power (log-linear mixed-effects model, mouse group × laser interaction: $F_{(1,4.8)} = 7.3$, $p = 0.04$, $BF_{10} = 14$, $n = 368$ epochs with theta peak from 10 animals; Figure 3.2E). In the ChAT-ChR2 mice, the power increased by 51 ± 9% (post-hoc test: $t_{(9)} = 4.8$, $p = 0.01$, $BF_{10} = 35$, $CI = [24\%, 112\%]$) and the spectral peak frequency in the theta band decreased from 7.7 ± 0.2 to 7.2 ± 0.1 Hz (log-linear mixed-effects model, mouse group × laser interaction: $F_{(1,4.8)} = 7.3$, $p = 0.04$, $BF_{10} = 1.6$; Figure 3.2F, post-hoc test: $t_{(30)} = 4.5$, $p = 0.001$, $BF_{10} = 6.0$, $CI = [-0.2, -1.0]$ Hz).

To independently confirm that the stimulation increased relative theta power, I looked at the difference in the PSD between subsequent epochs with the stimulation off and on (Figure 3.3A). Differences for a given frequency can be caused by a change in oscillatory power, change in the aperiodic component, or by a shift of the spectral peak frequency or change of the peak's width (bandwidth). To minimise the impact of the peak frequency shift and change in bandwidth, I compared maximum changes within frequency bands that were wider than the bandwidth of the theta peak and shift in theta peak frequency. In the ChAT-ChR2 mice, the negative change in the theta band was significantly smaller than in the 12–15 Hz band (linear mixed-effects

model: $F_{(1,10)} = 21$, $p = 0.001$, $BF_{10} = 5355$; Figure 3.3B). I concluded that the stimulation reduced the power in the theta frequency band significantly less than in higher frequency bands.

The stimulation also increased by 30 ± 4% the slow gamma oscillations (25—45 Hz, log-linear mixed-effects model: mouse group × laser interaction: $F_{(1,232)} = 26$, $p = 10^{-6}$, $BF_{10} = 671$, $n = 338$ epochs with slow gamma peak from 10 animals, post-hoc test for laser effect in ChAT-ChR2: $t_{(295)} = -8.2$, $p = 10^{-14}$, $BF_{10} = 772$, $CI = [18\%, 89\%]$; Figure 3.2G). The spectral peak frequency in the slow gamma of 38 ± 1 Hz did not significantly change (linear mixed-effects model, mouse group × laser interaction: $F_{(1,10)} = 0.4$, $p = 0.57$, $BF_{10} = 0.17$). I independently confirmed the increase in relative slow gamma power by looking at the PSD change between subsequent epochs with the stimulation off and on. In the ChAT-ChR2 mice, the negative change of power in the slow gamma band was significantly smaller than in the 12–15 Hz band (mouse group effect in the linear mixed-effects model: compared to the 12–15 Hz band: $F_{(1,8)} = 35$, $p = 10^{-4}$, $BF_{10} = 7300$; compared to the 90–110 Hz band: $F_{(1,10)} = 3.7$, $p = 0.08$, $BF_{10} = 10$; Figure 3.3C).

3.2.3 Reduced SWRs

Optogenetic stimulation reduced the SWR incidence throughout the stimulation in ChAT-ChR2 mice but not in ChAT-GFP mice (Figure 3.4A–C). SWR incidence in ChAT-ChR2 mice was reduced from 0.21 ± 0.01 to 0.03 ± 0.01 Hz (85 ± 3% reduction, linear mixed-effects model, mouse group × laser interaction: $F_{(1,22)} = 47$, $p = 10^{-6}$, $BF_{10} = 10^5$, $n = 369$ epochs from 10 animals; post-hoc test for laser effect in ChAT-ChR2: $t_{(86)} = 9.7$, $p = 10^{-14}$, $BF_{10} = 27$, $CI = [-0.05, -0.18]$ Hz; Figure 3.4C). The stimulation did not change the spectral peak frequency of the remaining SWRs of 168 ± 1 Hz (mouse group × laser interaction: $F_{(1,262)}) = 0.51$, $p = 0.48$, $BF_{10} = 0.11$, $n = 2554$ ripples; Figure 3.4D), nor ripple duration of 38 ± 0.3 ms (log-linear mixed-effects model, mouse group × laser interaction: $F_{(1,28)} = 0.9$, $p = 0.35$, $BF_{10} = 0.12$; Figure 3.4E). Hence, the results above confirm that optogenetic activation of MS cholinergic neurons during sleep almost completely suppresses SWRs in CA1 (Zhou et al., 2019; Ma et al., 2020).

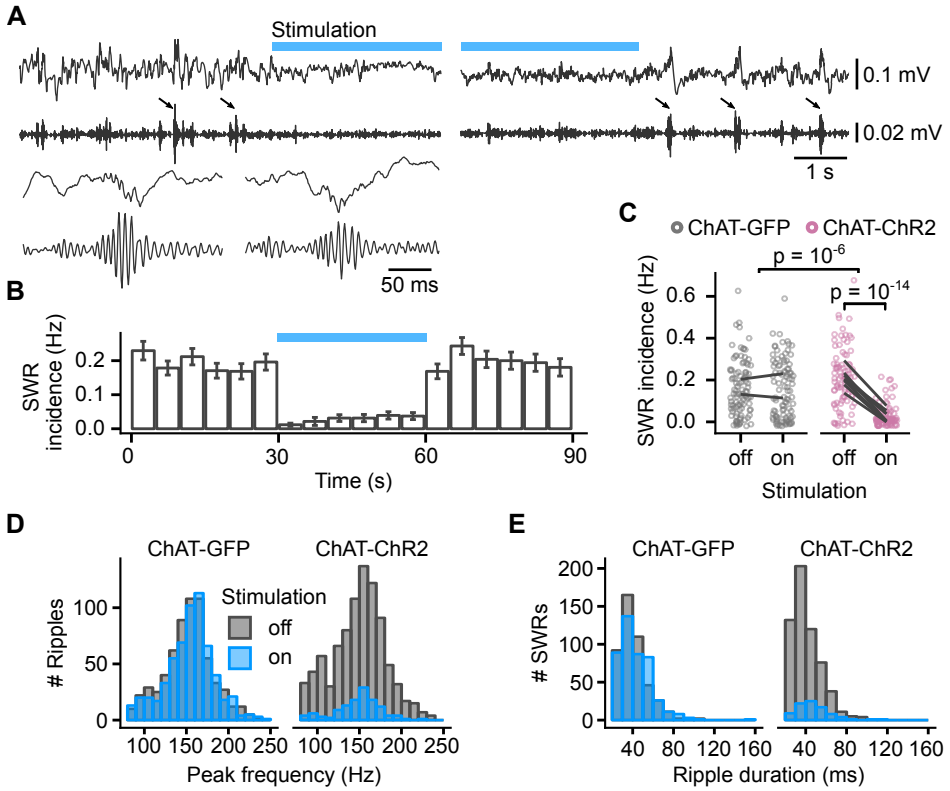

Figure 3.4: Cholinergic stimulation reduced SWRs incidence during sleep. **(A)** LFP from CA1 of a sleeping mouse recorded before, during, and after optogenetic stimulation (top trace). For ripple detection, the signal was 100–250 Hz bandpass filtered (second trace). The detected SWRs are marked with arrows. The insets (lower left) show the signal for two example SWRs at greater time resolution than above. **(B)** Histogram of SWR incidence before, during, and after 30 s of stimulation with 50-ms-long pulses at 10 Hz (n = 103 epochs from eight ChAT-ChR2 mice). **(C)** Comparison of SWR incidence during the stimulated and non-stimulated epochs for ChAT-GFP and ChAT-ChR2 mice. Lines connect mean incidence in individual mice. p-values were calculated with linear mixed-effects model for the mouse group × laser interaction; groups were compared with post-hoc test on least-square means. **(D)** Histogram showing spectral peak frequency for sleep ripples during 30-s-long epochs with the stimulation on and off. **(E)** Histogram showing duration of SWRs (detected ripples with spectral peak frequency ≥140 Hz) during 30-s-long epochs with the stimulation on and off.

3.3 Task-phase specific effects of cholinergic stimulation on learning

Having shown that cholinergic stimulation affects the hippocampal oscillatory state and SWRs during sleep, I investigated the effect of cholinergic stimulation during different phases of the appetitively motivated Y-maze task, a hippocampus-dependent

task commonly used to study long-term spatial memory (Bannerman et al., 2012; Shipton et al., 2014). Following the two stage model for memory encoding (Buzsáki, 1989), the cholinergic-modulation during the hippocampal theta state could affect the early memory encoding, while the changes to the SWRs could affect the long-term potentiation of the encoding.

In the spatial memory task, mice had to learn to find a food reward on an elevated three-arm maze that remained at a fixed location in relation to visual cues in the room, while the mice pseudo-randomly started from one of the other two arms. Because short-term memory errors caused by re-entry during a single trial have previously been shown to interfere with the acquisition of this spatial long-term memory task (Schmitt et al., 2003), mice were only allowed to make a single choice of the arm in each trial. The trials were divided into two phases: navigation and reward consumption where SWRs generally occur in navigation tasks (Csicsvari et al., 2007; Dupret et al., 2010). The navigation phase encompassed the maze arms except for the distal ends (20 cm from the edge), which were considered goal zones. Cholinergic activation was achieved by light stimulation delivered via an optic fibre as before. ChAT-Ai32 mice were split into four groups to test four experimental conditions: (i) no stimulation (n = 13), (ii) optogenetic stimulation during navigation – from the start of the trial until they reached the goal zone (n = 9), (iii) optogenetic stimulation throughout the maze (n = 9), and (iv) optogenetic stimulation in the goal zone only – from the entry of the goal zone until the mice were removed from the maze either after they had eaten the food or they had reached the empty food well (n = 15).

Each mouse received 10 trials per day for 6–10 consecutive days, and I set a learning criterion of ≥80% rewarded trials in a day. Mice from all four groups of ChAT-Ai32 mice learned the task (Figure 3.5A left) but comparison between the groups revealed differences in the number of days taken to reach this criterion (one-way ANOVA on ranks $\chi^2_{(3)} = 14$, $p = 0.003$, $BF_{10} = 20$; Figure 3.5B left). Post-hoc tests indicated that the ChAT-Ai32 'goal' group was delayed at learning the task compared to the ChAT-Ai32 'no stimulation' group (4.5 ± 0.3 vs. 2.9 ± 0.3 days, Dunn test with Holm-Bonferroni correction for multiple comparisons: $p = 0.002$; $BF_{10} = 45$). Similarly, the ChAT-Ai32 'goal' group was delayed compared to the ChAT-Ai32

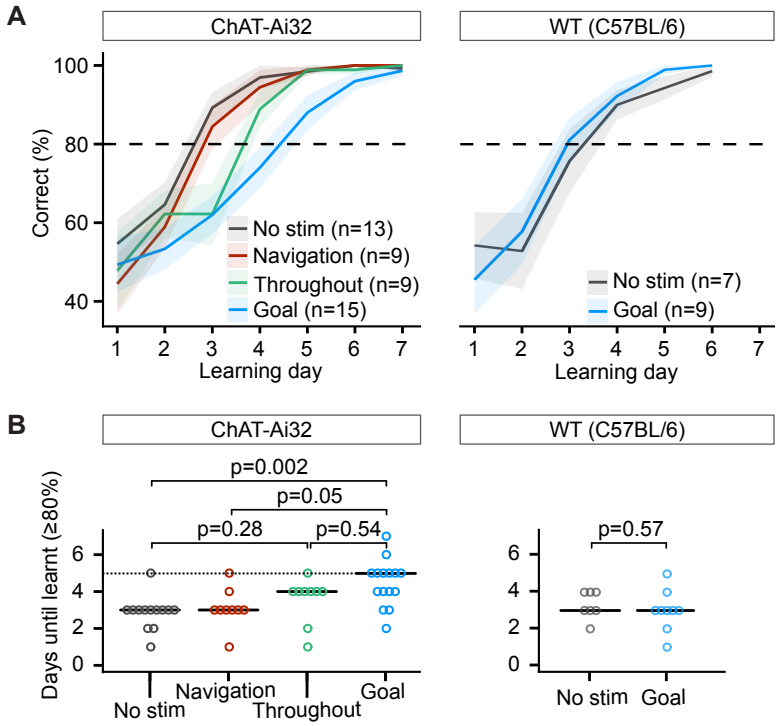

Figure 3.5: Cholinergic stimulation impaired learning of reward location. **(A)** Daily performance in the Y-maze task was measured by the percent of the trials when a mouse chose the rewarded arm. The mouse performance improved over time at rates that differed between the groups of ChAT-Ai32 mice (left) but not between the groups of WT mice (right). Ribbons extend ± 1 SEM. Horizontal dashed line marks the learning criterion of 80% correct choices. **(B)** The number of days required for each group of the ChAT-Ai32 mice to reach the learning criterion of ≥80%. Horizontal bars indicate the median within each group of the ChAT-Ai32 mice (left) and WT mice (right). The p-values for differences between groups were calculated using post-hoc Dunn tests. Data collected by Dr Sze-Man Clara Tang.

'navigation' group (4.5 ± 0.3 vs. 3.1 ± 0.4 days, $p = 0.05$, $BF_{10} = 4.4$). Whilst the stimulation for the 'goal' group lasted longer (34 ± 1 vs. 8 ± 1 s), the duration alone cannot explain the different effects of the optogenetic stimulation. The 'throughout' group received the longest stimulation (42 ± 1 s) but presented an intermediate learning curve. I found inconclusive evidence for the 'throughout' group to learn more slowly than the 'no stimulation' group (post-hoc test for difference in means: $p = 0.28$, test for higher mean days-to-criterion in the 'throughout' group: $BF_{10} = 1.6$) and learn faster than the 'goal' group (post-hoc test for difference in means: $p = 0.54$, test for lower mean days-to-criterion in the 'throughout' group: $BF_{10} = 2.0$). Therefore, the spatial location in the maze where the optogenetic stimulation took place was most likely the factor that decided the behavioural outcome. The MS neurons sustained an increased

level of firing after the optogenetic stimulation ceased (Figure 3.1B). Therefore, I cannot exclude the possibility that this sustained activity contributes to the learning deficit in the 'goal' group.

To control for possible aversive or other non-specific effects of the illumination, in an additional experiment with MS-implanted wild-type (WT) mice were split into two groups: no stimulation (n = 7) and light delivery in the goal zone (n = 9; Figure 3.5A right). I did not observe any learning difference between the 'goal' and 'no stimulation' groups of this control WT mice cohort (goal: 3.0 ± 0.37 days; no stimulation: 3.4 ± 0.37 days; one-way ANOVA: $F_{(1,14)} = 0.34$, $p = 0.57$, $BF_{10} = 0.48$; Figure 3.5B right).

The memory of the rewarded arm was retained when the mice were retested on the Y-maze task one week after the end of the acquisition period for each group of the ChAT-Ai32 mice (no stimulation: 100 ± 0%; navigation: 99 ± 1%; throughout: 100 ± 0%; goal: 94 ± 3%). After behavioural testing, implant placement and the level of eYFP expression were verified by immunohistochemistry, confirming that there were no significant differences in implant placement between the behavioural groups (Figure 2.3).

The results above show that cholinergic activation in the goal zone for as short as 50 s (95% percentile of stimulation duration) slows learning of the appetitive Y-maze task. In contrast, optogenetic stimulation during navigation or throughout the maze had no significant effect on task acquisition.

3.4 Effects of cholinergic stimulation on hippocampal state during learning

3.4.1 No detectable change in theta-gamma oscillations

Stimulating MS cholinergic neurons in the goal zone could impair task acquisition by disrupting memory encoding. To find neural mechanisms that support this hypothesis, I performed hippocampal LFP recordings during the Y-maze task. I recorded from

CA1 of five ChAT-ChR2 and two control ChAT-GFP mice implanted with recording electrodes and an optic fibre. Optogenetic stimulation was applied on alternating trials when the mouse reached the goal zone, comparing the CA1 activity between the stimulated and non-stimulated trials (111 non-stimulated and 109 stimulated at the goal rewarded trials and 56 non-stimulated and 36 stimulated at the goal unrewarded trials). To evaluate the effects of laser (on vs. off), mouse group (ChAT-ChR2 vs. ChAT-GFP), and their interaction, while accounting for correlations between the trials for the same mouse, I used a linear mixed-effects model. The cholinergic activation did not overtly affect the behaviour once the mice were at the goal location: I did not detect any effect of the laser on the time the mice spent at the goal location (linear mixed-effects model, moderate evidence for no effect of mouse group $\times$ laser interaction: $F_{(1,78)} = 0.01$, $p = 0.94$, $BF_{10} = 0.20$; moderate evidence for no effect of laser: $F_{(1,78)} = 0.1$, $p = 0.73$, $BF_{10} = 0.15$).

The theta power (5–12 Hz) peaked in the central section of the maze, where the mice typically ran the fastest (Figure 3.6A) and was reduced at the goal location in rewarded trials (Figure 3.6B, right panel).

To achieve a reliable estimate of PSD at the goal location, I analysed trials in which the LFP recording was EMG-movement free at the goal location for at least 10 seconds (201 out of 229 trials). Both theta and slow gamma (25–80 Hz) oscillations were present at the goal location in the rewarded non-stimulated trials (theta peak present in 98 $\pm$ 2% of trials; slow gamma peak present in 86 $\pm$ 7% trials; Figure 3.6C). Light did not affect the relative theta power differently in the ChAT-GFP and ChAT-ChR2 mice (linear mixed-effects model, mouse group $\times$ laser interaction: $F_{(1,5)} = 0.01$, $p = 0.94$, moderate evidence for no difference $BF_{10} = 0.19$, n = 199 trials with a theta peak; Figure 3.6D). However, theta power increased in both mouse groups indiscriminately (strong effect of laser: $F_{(1,5)} = 6.9$, $p = 0.05$, $BF_{10} = 10^5$, $CI = [7\%, 18\%]$), suggesting another, non-specific effect of the laser on theta power. I found inconclusive evidence for a change in spectral peak frequency in the theta band (linear mixed-effects model, mouse group $\times$ laser interaction: $F_{(1,5)} = 1.3$, $p = 0.31$, $BF_{10} = 2.1$; effect of laser $F_{(1,5)} = 3.5$, $p = 0.12$, $BF_{10} = 0.87$; Figure 3.6E).

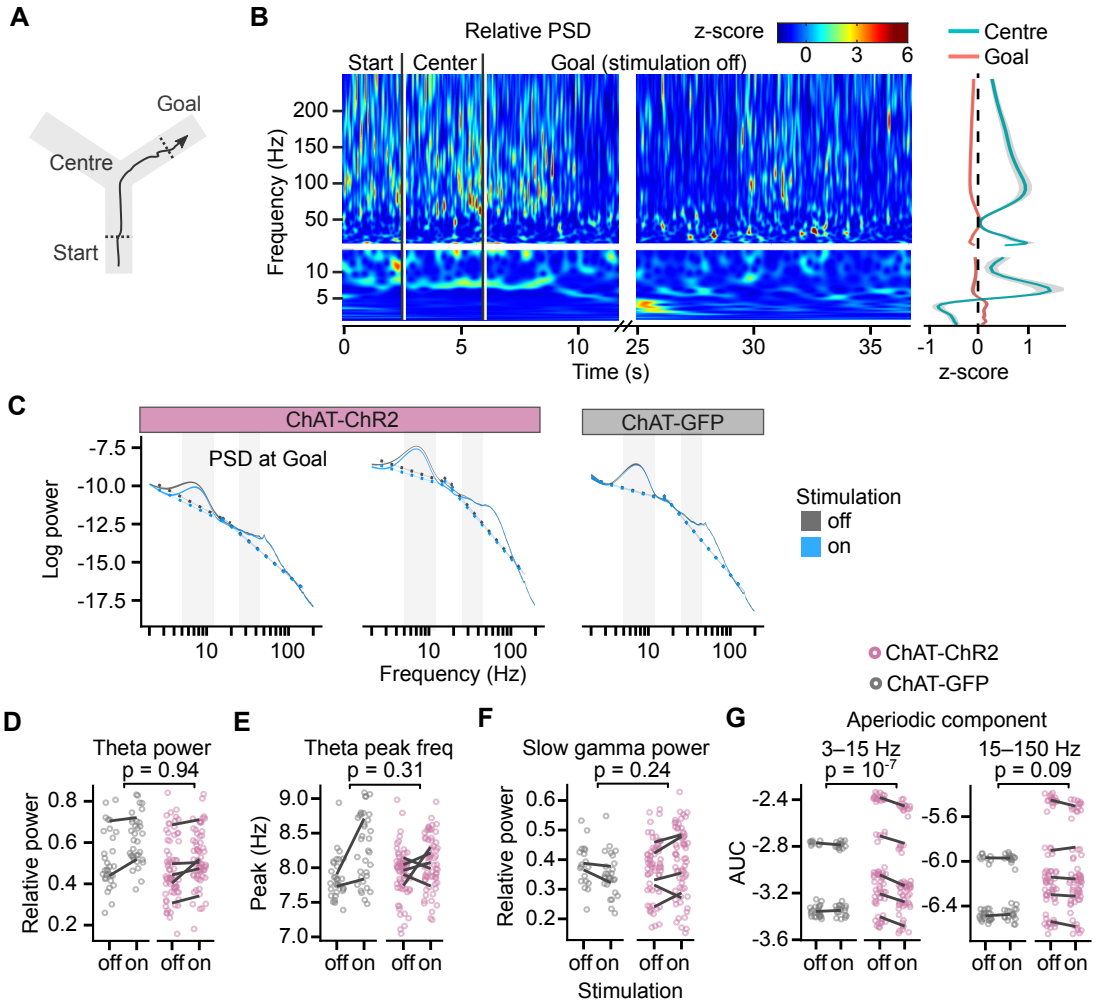

Figure 3.6: Cholinergic stimulation did not affect relative theta-gamma at reward location. **(A)** Schematic showing the maze zones. **(B)** Spectrogram of the LFP recorded in a single non-stimulated trial. The values for each frequency were z-scored to show its relative changes over time. Note transient increases in high-frequency power throughout the recording and high theta power at Centre. Right: mean z-score value at Centre and Goal as a function of frequency. **(C)** PSD of the LFP recorded from two representative ChAT-Ai32 (left) and one ChAT-GFP (right) animals on non-stimulated and stimulated-at-Goal rewarded trials. The dashed lines show the fitted aperiodic component. Ribbons extend ±1 SEM of log power. Grey background marks the frequency range of theta and slow gamma bands. PSD parameters that were assessed for the stimulation effect: **(D)** relative theta power, **(E)** spectral peak frequency in the theta band, **(F)** slow gamma power, and **(G)** the aperiodic component fitted for two frequency ranges, 3–15 and 15–150 Hz, and compared using the area under the curve (AUC). (D–G) Values are plotted for individual trials. Lines connect means for individual animals. p-values were calculated with linear mixed-effects models for the mouse group × laser interaction.

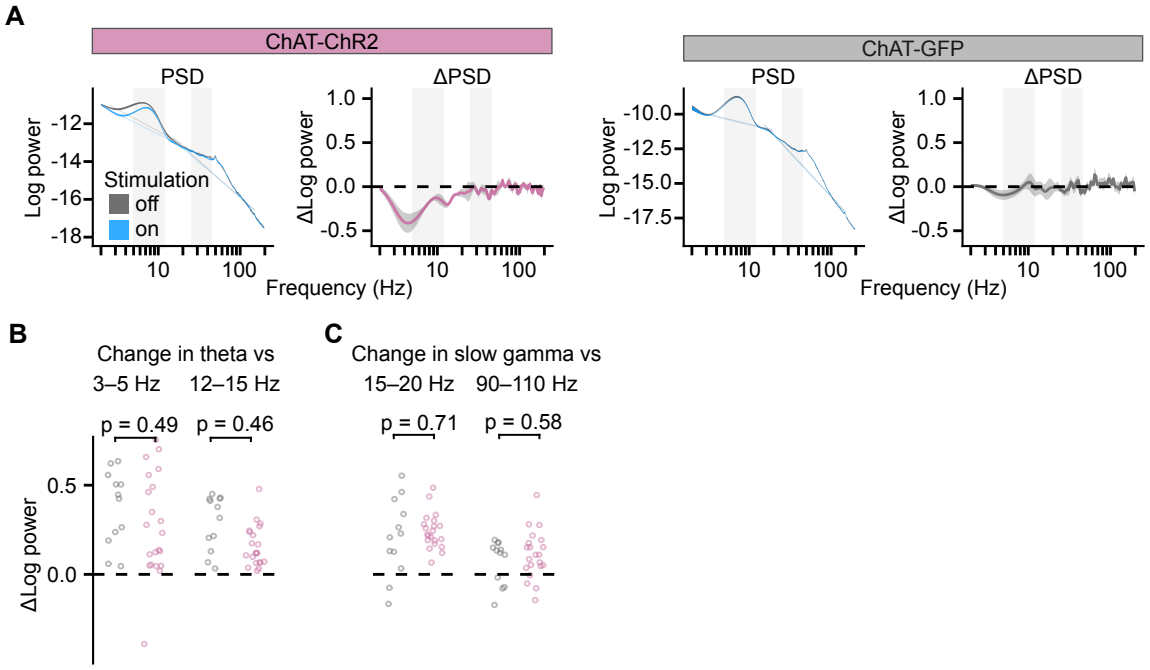

Figure 3.7: Cholinergic stimulation did not affect theta-gamma power at reward location differently than it affected the power of their neighbouring frequency bands. **(A)** Left: PSD ± 1 SEM during rewarded trials with the stimulation on and off at goal. Right: difference between day-averaged log power calculated for trials with the stimulation on and off. PSD and its difference are shown for one ChAT-ChR2 and one ChAT-GFP mouse. Grey background marks the frequency range of theta and slow gamma bands. **(B)** Change in theta power as a result of optogenetic stimulation compared to change in neighbouring frequency bands. **(C)** As in (B) but for slow gamma power. Values are shown for day-averaged log power differences in trials with the stimulation on and off. p-values were calculated with linear mixed-effects models for the effect of mouse group (ChAT-ChR2 vs. ChAT-GFP).

To independently confirm that the stimulation did not differentially affect relative theta power in ChAT-GFP and ChAT-ChR2 mice, I looked at the difference in the PSD between day-averaged trials with the stimulation on and off (Figure 3.7A). In the ChAT-ChR2 mice, the difference between the negative power change in the theta band and in the surrounding bands was not significantly different than in the ChAT-GFP mice (Figure 3.7B). Hence, the results indicate that the stimulation did not affect the theta power significantly differently between the mouse groups.

Quantification of the relative slow gamma power indicated inconclusive evidence for the effect of the stimulation (linear mixed-effects model, mouse group × laser interaction: $F_{(1,6)} = 1.7$, $p = 0.24$, $BF_{10} = 0.82$, $n = 175$ trials with a relative slow gamma peak; Figure 3.6F). This result was independently confirmed by looking

at the difference in the PSD between day-averaged trials with the stimulation on and off (Figure 3.7C).

The only effect of the laser that affected PSD of the ChAT-GFP and ChAT-ChR2 mice differently was a reduced aperiodic component of the PSD in the 3–15 Hz range (linear mixed-effects model, mouse group × laser interaction: $F_{(1,135)} = 29$, $p = 10^{-7}$, $BF_{10} = 10^5$, $n = 201$ trials; Figure 3.6G).

3.4.2 Reduced SWRs

Previous studies (Vandecasteele et al., 2014; Zhou et al., 2019; Ma et al., 2020) and the results in sleeping mice (Figure 3.4) show that activation of MS cholinergic neurons suppresses CA1 SWRs. Therefore, I investigated whether impaired place learning was associated with changes in SWRs.

The SWRs occurred at the start and the goal location (Figure 3.8A–B). Mice learned over 6 days and on day 5 reached 80 ± 10% rewarded trials. I detected significantly more SWRs in rewarded than in unrewarded trials (82 ± 7% of rewarded non-stimulated trials vs. 32 ± 13% of unrewarded non-stimulated trials, paired t-test on percentages per animal: $p = 0.02$, $BF_{10} = 3.7$, $n = 7$ animals; Figure 3.8C). The difference could be explained by shorter-duration immobility when the mice visited the non-rewarded arms: on unrewarded trials, mice spent 6.5 ± 0.5 s in the goal zone before leaving compared to 34.0 ± 1.0 s on rewarded trials. Because I detected few SWRs in the unrewarded trials, I restricted the further analysis to the rewarded trials.

I first assessed whether the incidence of SWRs changed during learning by quantifying them in the non-stimulated rewarded trials during early and late learning (Figure 3.8D). I did not observe any significant difference between early (before day 5) and late learning (day 5 or later, linear mixed-effects model, effect of early vs. late learning: $F_{(1,110)} = 0.3$, $p = 0.58$, moderate evidence for no difference $BF_{10} = 0.22$, $n = 124$ trials). However, optogenetic stimulation had a significantly different effect in the ChAT-GFP and the ChAT-ChR2 mice (log-linear mixed-effects model, mouse group × laser interaction: $F_{(1,42)} = 4.5$, $p = 0.04$, moderate evidence for difference: $BF_{10} = 3.8$, $n = 229$ trials; Figure 3.8E), whose SWR incidence at the goal location

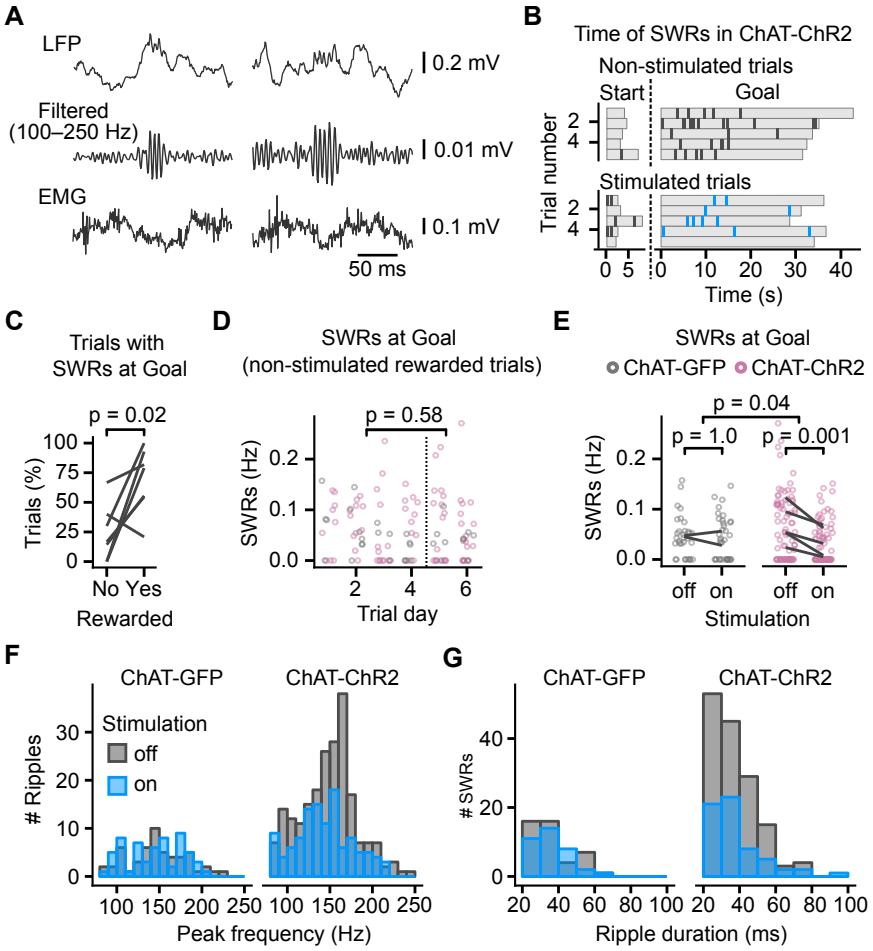

Figure 3.8: Cholinergic stimulation reduced SWRs at reward. **(A)** Example SWRs recorded at the Goal location: LFP traces (top), the same traces after 100–250 Hz bandpass filtering (middle), and simultaneously recorded EMG (bottom). **(B)** Time of SWRs recorded from a representative mouse over multiple trials the same day. Time measured relative to the trial start and arrival at Goal. Stimulated and non-stimulated trials are grouped for clarity. **(C)** Percentage of trials with SWRs at Goal compared between unrewarded and rewarded non-stimulated trials. One line per animal is shown. p-value was calculated with paired t-test. **(D)** SWR incidence as a function of trial day. Data is shown for ChAT-GFP and ChAT-ChR2 mice together, values are plotted for individual non-stimulated rewarded trials. Dashed vertical line separates early and late trials. p-value was calculated with linear mixed-effects model for the effects of early vs. late trials. **(E)** Effect of cholinergic stimulation on SWR incidence at Goal location in rewarded trials. Data is shown for ChAT-GFP and ChAT-ChR2 mice, values are plotted for individual trials. Lines connect means per animal. p-values were calculated with linear mixed-effects model for mouse group × laser interaction; groups were compared with post-hoc test on least-square means. **(F)** Histogram showing spectral peak frequency for all ripples at Goal location compared between stimulated and non-stimulated rewarded trials. **(G)** Histogram showing duration of SWRs (detected ripples with spectral peak frequency ≥140 Hz) at Goal.

was reduced by 52 ± 7% from 0.06 ± 0.01 to 0.03 ± 0.01 Hz (strong evidence for change in ChAT-ChR2 mice: $t_{(44)} = 4.2$, $p = 0.001$; $BF_{10} = 484$, $CI = [-0.04, -0.01]$ Hz, $n = 163$ trials; moderate evidence for no change in ChAT-GFP mice: $BF_{10} = 0.19$, $CI = [-0.02, 0.02]$ Hz, $n = 66$ trials). Spectral peak frequency of SWRs in the ChAT-ChR2 mice was not affected by the stimulation (frequency: 168 ± 2 Hz; linear mixed-effects model for effect of laser: $F_{(1,2.5)} = 0.09$, $p = 0.80$; $BF_{10} = 0.13$, $CI = [-7, 5]$ Hz, $n = 199$ SWRs; Figure 3.8F), nor was the SWR duration (duration: 37 ± 1 ms; log-linear mixed-effects model for effect of laser: $F_{(1,9.6)} = 0.003$, $p = 0.96$, $BF_{10} = 0.14$, $CI = [-3, 4]$ ms, $n = 199$ SWRs; Figure 3.8G).

Overall, these results show that optogenetic stimulation of MS cholinergic neurons reduced ripple incidence in CA1 in rewarded trials but did not cause a detectable change in theta-gamma power. Hence, this result suggests that the reduced SWR incidence at reward location is a mechanism relevant for the memory impairment.

3.5 Discussion

Using optogenetics, I investigated the effects of stimulating MS cholinergic neurons on learning and hippocampal LFPs when delivered at different phases of an appetitively motivated spatial memory task. I found that: (1) MS cholinergic stimulation reduces SWR incidence and promotes theta-gamma rhythm in the sleeping mice; (2) MS cholinergic stimulation at the reward location reduces SWR incidence; and (3) MS cholinergic activation at the goal location, but not during navigation, impairs spatial memory encoding. These results show that timely control of cholinergic modulation is important for spatial learning on a time scale of seconds.

The results indicate that cholinergic stimulation almost completely suppresses SWRs in sleeping animals and suppresses SWRs by about one half in awake, behaving animals. SWRs at the rewarded locations are thought to be crucial for learning (Dupret et al., 2010). Their suppression at the goal location in the experiments with the same stimulation protocol as that used in mice during learning suggests a possible explanation for the learning deficit induced by inappropriately timed cholinergic activity. Moreover, the effect of cholinergic stimulation on theta-gamma oscillations, which

was prominent during sleep, was not observed when the same stimulation was applied at the goal location during learning, suggesting that learning was impaired through a mechanism independent of theta-gamma oscillations.

The results can be interpreted as supporting the account for the two stage memory encoding in which SWRs following an experience promote encoding of its memory (Buzsáki, 1989).

3.5.1 Importance of timely regulation of cholinergic tone for memory encoding

I found that temporally controlled optogenetic stimulation of MS cholinergic neurons could affect learning of the appetitive Y-maze task. Stimulation of cholinergic neurons during navigation did not affect the performance, while, strikingly, cholinergic stimulation in the goal zone significantly impaired task acquisition (Figure 3.5). The stimulation duration differed between the groups: it was longest in the 'throughout' group, followed by 'goal' and by 'navigation' group. The only significant impairment of task acquisition was seen in the 'goal' group, indicating that it was cholinergic activation at the goal location that interfered with memory (Figure 3.5C,E). The lack of significant impairment with cholinergic stimulation throughout the task may appear surprising. However, the task performance in the 'throughout' group was not significantly different from the 'goal' group. I cannot exclude the possibility that prolonged optogenetic stimulation becomes less effective over time, either because the MS neurons become less activated or because vesicular ACh might be depleted with prolonged stimulation.

The lack of behavioural effect of the stimulation during the navigation phase, when the cholinergic tone is naturally high (Fadda et al., 2000; Giovannini et al., 2001; Fadel, 2011) may suggest that the release of ACh in the hippocampus is already optimal or maximal, or that ACh receptors are saturated. MS cholinergic neurons are slow spiking neurons with a maximal rate of 10 Hz during active exploration (Ma et al., 2020), the stimulation frequency used here. Thus, it is plausible that ACh receptor activation in the hippocampus had already reached a plateau, which was not increased

further by the stimulation. The lack of behavioural effect of the stimulation during the navigation phase suggests that the effect of optogenetic stimulation was short-lived and restricted to the stimulation period, albeit with a short period of sustained activity following the stimulation (Figure 3.1B). This observation supports the idea that cholinergic modulation is timely controlled, but further experiments, for instance using ACh sensors in the hippocampus (Jing et al., 2020), will be necessary to confirm this hypothesis.

An interesting complementary experiment would be to silence cholinergic inputs during navigation or at the goal location to further explore the role of cholinergic tone during memory encoding. There is evidence to suggest that CA1 SWRs, which occur during low cholinergic activity, play a crucial role in memory encoding: disruption of SWRs in the first 15–60 min following training impairs learning of spatial navigation tasks (Girardeau et al., 2009; Ego-Stengel and Wilson, 2010), while their disruption or prolongation during the continuous alternation task impairs or improves learning, respectively (Jadhav et al., 2012; Fernández-Ruiz et al., 2019). In exploring animals, SWRs occur during transient immobility periods, including periods at goal locations (Csicsvari et al., 2007; Dupret et al., 2010; Roux et al., 2017). These SWRs stabilise spatial representations of the CA1 place cells supporting navigation toward the newly learned goals (Roux et al., 2017) and are predictive of performance in a spatial memory task (Csicsvari et al., 2007; Dupret et al., 2010). During these SWRs, sequences of neuronal activation are replayed in both forward and reverse order (Foster and Wilson, 2006; Csicsvari et al., 2007; Diba and Buzsáki, 2007; Karlsson and Frank, 2009; Ambrose et al., 2016). I found that MS cholinergic activation for the brief time the mice spent in the reward zone, shorter than 50 s (95% percentile of stimulation duration), is sufficient to significantly impair memory encoding in the Y-maze task (Figure 3.5). Therefore, I speculate that disruption of the normally occurring replay events in the reward zone is sufficient to impair long-term memory encoding (Figure 3.8). However, selective disruption of SWRs at the reward zone did not affect rats' performance in the inbound phase of the W-maze task (Jadhav et al., 2012), which is comparable to the Y-maze task. In both of these tasks, animals could use either an allocentric place strategy or an egocentric rule-based strategy, or a combination thereof,

and the relative importance of each could lead to differences in their reliance on SWRs. Alternatively, additional effects of MS cholinergic activation on intracellular signalling cascades and synaptic plasticity (Brzosko et al., 2019), synaptic inhibition (Hasselmo, 2006; Haam and Yakel, 2017), or interference with extra-hippocampal reward-related signalling cannot be ruled out.

Because learning can be affected by the interruption of SWRs during post-learning sleep (Girardeau et al., 2009), and because the same cholinergic activation during sleep achieves a similar effect on the SWRs (Figure 3.4; Ma et al., 2020), it would be of interest to see if the cholinergic activation during post-learning sleep would also impair spatial learning. This would show whether low cholinergic states are important also for memory consolidation during sleep and provide further evidence for the role of SWRs in memory.

3.5.2 Cholinergic influence on hippocampal network activity

Hippocampal network activity varies with cholinergic tone and MS cholinergic neuron activity. MS cholinergic neurons discharge at a maximal rate when the animal is running (Ma et al., 2020), which corresponds to the highest theta power intensity in CA1 and highest cholinergic tone measured in the pyramidal cell layer of CA1 (Fadda et al., 2000; Fadel, 2011). Conversely, cholinergic tone and MS cholinergic neuron discharge are at their lowest during slow-wave sleep and awake immobility, which are associated with the highest ripple incidence (Fadda et al., 2000; Zhou et al., 2019; Ma et al., 2020). In accordance with these observations, I found that stimulation of MS cholinergic neurons reduces SWR incidence in both awake behaving animals and naturally sleeping animals, consistent with previous reports (Figure 3.4, 3.8; Vandecasteele et al., 2014; Zhou et al., 2019; Ma et al., 2020). The reduction of SWR incidence of 52 $\pm$ 7% at the goal location was smaller than the 92% median suppression reported during free behaviour (Vandecasteele et al., 2014), which could be due to a smaller effect of ACh at the reward location or an already high ACh level occluding the effect of the optogenetic stimulation.

I observed that stimulation of MS cholinergic neurons of sleeping mice causes an apparent decrease of the PSD across the entire frequency spectrum (Figure 3.2).

A similar effect was reported previously for anaesthetised and freely behaving animals (Vandecasteele et al., 2014). Signal decomposition into aperiodic and periodic components (Donoghue et al., 2020) showed that the optogenetic stimulation enhanced the periodic components with peaks in the theta and slow gamma bands and decreased the aperiodic component of the signal (1/f background). The enhanced theta-gamma activity might appear at odds with previous reports that such manipulation does not change theta-gamma power during sleep (Ma et al., 2020) and quiet wakefulness (Zhou et al., 2019). The combined effect of the cholinergic stimulation on the periodic and aperiodic signal sums to near-zero values, which could explain the different conclusions, showing the advantage of PSD decomposition (Donoghue et al., 2020) when assessing the power of periodic signals.

Because cholinergic input has been implicated in theta activity in the hippocampus (Buzsáki, 2002), I was surprised that no effect on theta-gamma oscillations by cholinergic stimulation was detected at the goal location. However, there are at least two distinct forms of theta oscillations in the hippocampus, only one of which is dependent on cholinergic receptors (Kramis et al., 1975). Pharmacological evidence *in vivo* indicates that there are two distinct mechanisms of theta oscillations in the hippocampus, an atropine-sensitive and an atropine-resistant component (Kramis et al., 1975; Buzsáki, 2002; Colgin, 2013). The atropine-sensitive component is mediated by the combination of cholinergic and GABAergic neurons in the MS (Buzsáki, 2002; Manseau et al., 2008) and is slower than the atropine-resistant theta, which is generated primarily by the EC (Buzsáki, 2002; Colgin, 2013). Moreover, atropine-sensitive theta was best detected in the anaesthetised animal, while atropine-insensitive theta was shown to predominate in the running animal (Kramis et al., 1975; Newman et al., 2013). Consistent with this division, MS cholinergic stimulation in sleeping mice, in addition to increasing theta power, shifted the spectral peak in the theta band to a lower frequency (Figure 3.2F). Both effects were limited to the ChAT-ChR2 animals.

The stimulation frequency of 10 Hz provided faster activation than the kinetics of metabotropic muscarinic receptors. Therefore, I did not expect to observe indirect effects on the network activity mirroring the stimulation frequency. Indeed, the spectral peak frequency in the theta band was lower than the stimulation fre-

quency, and PSD did not show a spectral peak at 10 Hz (Figure 3.2F). In behaving mice, the MS cholinergic stimulation at the goal location did not have a significantly different effect on theta power and spectral peak in ChAT-GFP and ChAT-ChR2 mice (Figure 3.6D–E) and theta power increased in both groups of animals. The lack of effect on theta-gamma rhythm during the memory task could be explained by the prominence of an atropine-resistant entorhinal-driven theta that would override any atropine-sensitive theta. It is also possible that the small sample of control animals (n = 2) whose theta power also increased with the laser stimulation prevented the detection of the differences between the animal groups. Alternatively, a diminishing efficacy with the prolonged optogenetic stimulation could have prevented the detection of a change in the theta-gamma oscillations. However, SWR incidence was reduced at the goal location for the entire duration of the stimulation, suggesting that any decrease in the stimulation efficacy would be biologically minor.

Chapter 4

Encoding of learned reward location in the dorsal and intermediate CA1

4.1 Introduction

Navigation towards the location of learned rewards is thought to be supported by place cells (O'Keefe and Nadel, 1978). The place cells fire in specific locations when an animal navigates through the environment (O'Keefe and Dostrovsky, 1971). Their activity encodes information about the animal's current and upcoming locations (Frank et al., 2000; Wood et al., 2000). However, it is unclear whether and how the place cell activity supports navigation towards the reward or recall of its location.

After animals learn the reward location, dCA1 place cells shift their place fields and accumulate at the rewards (Dupret et al., 2010; Zaremba et al., 2017; Boccara et al., 2019; Kaufman et al., 2020; Sato et al., 2020). The encoding of learned reward location could vary between the dorsal and the intermediate hippocampus, which differ in gene expression and cortical and subcortical connectivity (Fanselow and Dong, 2010). In the iCA1, neurons fire across larger place fields than in dCA1. (Maurer et al., 2005; Jung et al., 1994; Keinath et al., 2014) In addition to encoding spatial location, they regulate reward-seeking (Britt et al., 2012; Ito et al., 2008; Kosugi et al., 2021; LeGates et al., 2018; Riaz et al., 2017), but little is known about their activity during reward-directed navigation.

What follows are the results comparing how the dCA1 and the iCA1 activity changed after mice learned reward locations. The changed activity could represent the recalled memory of reward location, and I refer to these neural patterns of activity as the encoding of reward location. To delineate changes due to learning of reward locations, the experiment was split into two stages: first mice foraged for food rewards placed at random locations on a maze, later the mice learned fixed locations of the rewards on the same maze. I used calcium imaging with a head-mounted microscope (Ghosh et al., 2011) to track the activity of the same CA1 cells throughout the experiment. First, I describe changes in the dCA1 and iCA1 spatial representations. Next, I investigate how the place cells changed their place fields depending on the reward locations and how the population activity is modulated during the reward approach. I evaluate whether the same place cells remapped their place fields to follow the reward locations. Lastly, I report how the dCA1 and iCA1 population could encode the learned reward location.

The majority of the chapter results was published in Jarzebowski et al. (2021a). The work was completed in collaboration with Dr Audrey Hay and Dr Benjamin Grewe who both helped design the study.

4.2 Learning of reward locations on cheeseboard

To characterise the CA1 activity changes due to reward location learning, I recorded calcium imaging fluorescence during foraging on the same maze as that subsequently used for reward location learning. This section describes the behaviour and learning performance of mice during these two experiments. The data in this and the following sections comes from seven dCA1 and six iCA1 implanted mice.

First, the mice foraged for liquid rewards baited in randomly selected wells of the 120-cm-diameter maze. These sessions served to familiarise the mice with the apparatus and as a baseline for comparison with the hippocampal activity recorded after the mice learned reward locations. After foraging in daily sessions for three days, mice learned sets of two fixed reward locations in daily sessions of 8 trials. The learning period spanned five days for the first set of locations and two days each for subsequent sets, each with one reward translocated to a pseudo-random location, for a total of three

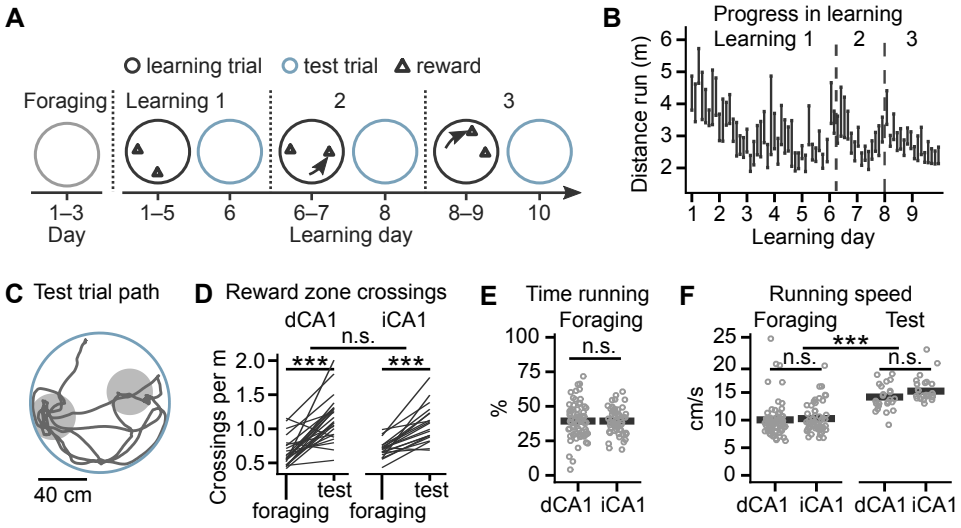

Figure 4.1: Mice learned reward locations on cheeseboard. **(A)** Timeline for the learning and test sessions shows when and how the reward locations (triangles) changed. The reward was not baited during test trials. **(B)** Progress in learning measured by distance run per trial. Vertical bars mark the mean distance ± SEM. Vertical dashed lines mark the time of reward translocations. **(C)** Example running path of a mouse during an unbaited test trial. Grey discs show the extent of the reward zone used for the analysis. **(D)** Number of reward zone crossings during the first 120 s of the test trials compared to the crossings of the zones centred on the same locations during foraging. **(E)** Percentage of foraging trials that the dCA1 and iCA1 implanted mice spent running. **(F)** Running speed of the dCA1 and iCA1 implanted mice. Data for seven dCA1 and six iCA1 implanted mice compared with post-hoc tests on least-square means of linear mixed-effects model in (D) and (E), and of log-linear mixed-effects model in (F). $^{***}p < 0.001$.

or four sets (Figure 2.2A). Mice took progressively shorter paths to find the rewards (Figure 4.1B). Their memory was tested in unbaited test trials on the day after learning each set (Figure 4.1C). Mice crossed the reward zones (20-cm-radius disks centred on the learned reward locations) 64 ± 7% more times in the first 120 s of the unbaited test trials compared to the same zones during foraging (linear mixed-effects model, effect of learning: $F_{(1,61)} = 105$, $p = 10^{-14}$; $BF_{10} = 10^{11}$, $CI = [45\%, 85\%]$, n = 44 trials; Figure 4.1D). Performance of the dCA1 and iCA1 implanted mice did not differ (linear mixed-effects model: $F_{(1,16)} = 0.03$, $p = 0.87$; moderate evidence for the lack of difference: $BF_{10} = 0.18$, $CI = [-13\%, 11\%]$, n = 44 trials; Figure 4.1D).

Because ventral hippocampal lesions can increase the mobility of mice (Bannerman et al., 1999), I confirmed that the surgical procedures did not lead to differences in mobility between the dCA1 and iCA1 implanted mice. The two groups were running

in a similar fraction of the foraging trials (linear mixed-effects model: $F_{(1,11)} = 10^{-4}$, $p = 0.99$; $BF_{10} = 0.22$, n = 39 trials; Figure 4.1E). The running speed in the test trials increased from foraging (log-linear mixed-effects model: $F_{(1,159)} = 112$, $p < 10^{-15}$; $BF_{10} = 10^{17}$; $CI = [36\%, 58\%]$) but the increase was not different between the dCA1 and iCA1 implanted mice (log-linear mixed-effects model: $F_{(1,11)} = 1.0$, $p = 0.35$; moderate evidence for the lack of difference $BF_{10} = 0.31$, n = 83 trials; Figure 4.1F).

4.3 Neurons active during foraging and learning

I imaged daily 170 ± 19 dCA1 cells from seven animals and 70 ± 11 iCA1 cells from six animals and matched the identity of active cells between days. First, I investigated how the overall number of active neurons (calcium event rate ≥ 0.005 Hz) changed over time. The highest number of cells were active during early foraging trials when the maze was novel and decreased gradually over the three days of foraging (Figure 4.2A). The number of active neurons levelled off during learning. The change is consistent with previous reports that familiarisation decreases the firing rates (Nitz and McNaughton, 2004; Karlsson and Frank, 2008) and the number of active dCA1 cells (Karlsson and Frank, 2008).

Over the 14–16 days, I recorded a total of 2,965 unique dCA1 cells from seven mice and 1,125 unique iCA1 cells from six mice (Figure 4.2B). Nearly half of the cells were not matched again after being detected once. It is likely that some of these cells reappeared on multiple days but the cell registration algorithm failed to match them. While the number of active cells dropped over the experiment duration, a subpopulation of dCA1 and iCA1 cells was active and matched on 10 or more days.

To assess how the movement of a mouse affects the calcium event rates in dCA1 and iCA1, I tested for the effects of recording site (dCA1 vs iCA1), movement (running vs immobile) and their interaction using a log-linear mixed-effects model. In immobile mice, the calcium event rates in iCA1 were 88 ± 16% higher compared to dCA1 ($t_{(11.6)} = 3.6$, $p = 0.01$, $CI = [14\%; 196\%]$). Running increased the calcium event rates in both dCA1 and iCA1 but the increase was larger in dCA1 (movement × recording site interaction: $F_{(1,2293)} = 3.1$, $p = 0.002$, $BF_{10} = 7.0$ n = 1282 cells

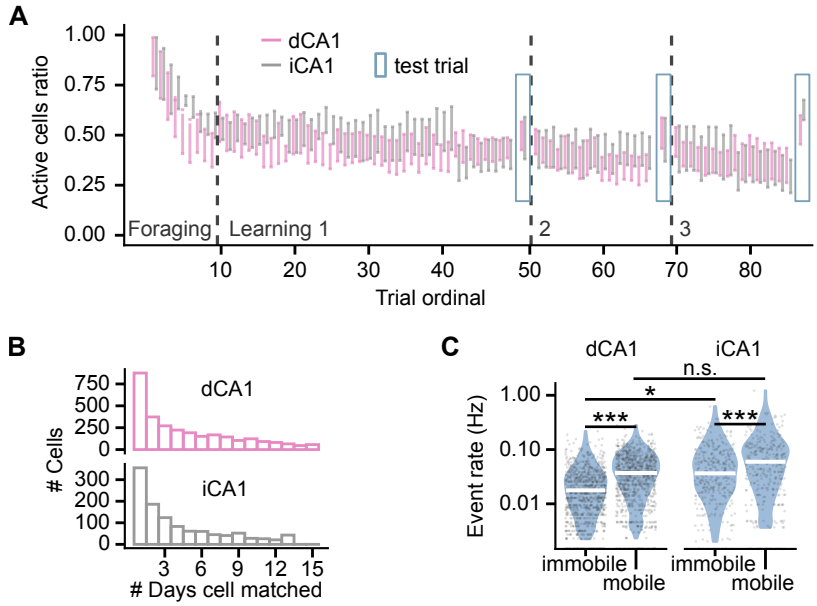

Figure 4.2: Changes in hippocampal activity over days and during running. **(A)** The number of cells active in each foraging and learning trial. The number is shown as a ratio of the animal's maximum. Data for foraging trials was calculated on the first 3 minutes to emulate the duration of the learning trials. Vertical bars mark mean ± SEM. **(B)** Histogram showing the number of recording days that a cell was active and matched. **(C)** Calcium event rates during last day foraging in mobile and immobile mice. Distribution of the values shown on violin plots of the width proportional to density; individual data points overlayed on top; horizontal bars mark the means. Data compared with post-hoc tests on least-square means of log-linear mixed-effects model. $^{*}p < 0.05$, $^{***}p < 0.001$.

from 13 mice recorded on the last-day foraging; Figure 4.2C). The dCA1 calcium event rates increased by 47 ± 5% ($t_{(2293)} = 13.3$, $p < 10^{-15}$, $CI = [42\%, 51\%]$, n = 960 cells), whereas the iCA1 event rates increased by 29 ± 11% ($t_{(2293)} = 4.5$, $p = 10^{-5}$, $CI = [16\%, 40\%]$, n = 322 cells).

The following sections of this chapter investigated hippocampal activity in running mice. This was to exclude SWR-associated activity during immobility such as that during replay when the hippocampus reactivates sequences of place cells outside of their place fields (Foster and Wilson, 2006; Csicsvari et al., 2007; Diba and Buzsáki, 2007; Karlsson and Frank, 2009).

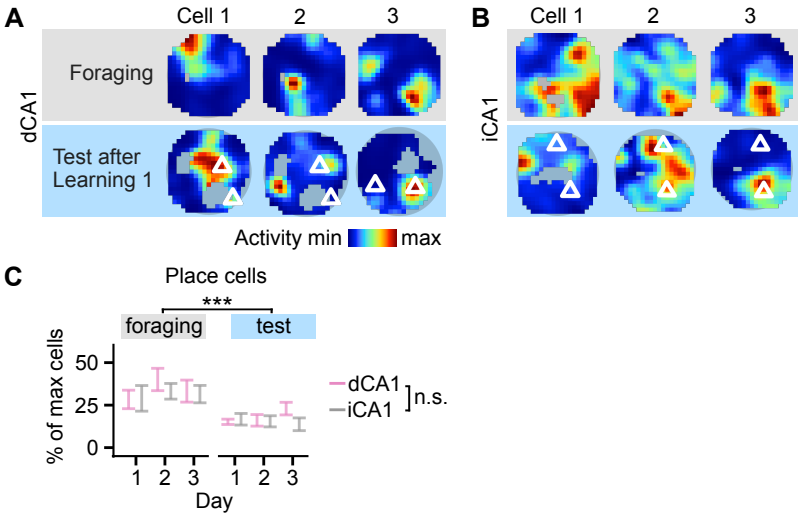

Figure 4.3: Place cells before and after learning. (A) Examples of dCA1 place maps for the same cells during foraging and the test after learning the first set of reward locations. Triangles mark reward locations. **(B)** As in (A) but for iCA1 cells. **(C)** Percentage of the dCA1 and iCA1 cells identified as place cells during foraging and test. The number is shown as a ratio of the animal's maximal number of active cells. Vertical bars mark mean ± SEM. The effects were tested with linear mixed-effects models. $^{***}p < 0.001$.

4.4 Change in spatial coding after learning

Spatial representations in dCA1 and iCA1 differ (Maurer et al., 2005; Jung et al., 1994; Keinath et al., 2014; Jin and Lee, 2021). To assess how they changed as mice learned reward locations, in this section, I compared the spatial representations during foraging trials with the spatial representations during test trials after learning.

4.4.1 Place fields, their size, and encoded spatial information

Both dCA1 and iCA1 had spatially modulated cells. Example comparison between spatial activity of the same cells from before and after learning is shown in Figure 4.3A–B. I hypothesised that familiarity with the environment may affect the number of place cells as well as the number of active cells. Therefore, I compared the absolute size of the dCA1 and iCA1 place cell populations. To make the comparison possible between animals whose number of active cells changed over time, I found the maximal number of cells active per animal. During foraging and test sessions, a similar population size of dCA1 and iCA1 cells were classified as place cells (linear mixed-effects model on the

population size relative to the animal's maximum active cells: $F_{(1,11)} = 0.34$, $p = 0.57$; inconclusive evidence for difference: $BF_{10} = 0.4$, $CI = [-11, 6]$ percentage points (pp), n = 78 trials; Figure 4.3C). The absolute number of place cells was lower in the test trials than in the foraging trials by 16 ± 2 pp (linear mixed-effects model: $F_{(1,64)} = 49$, $p = 10^{-9}$; strong evidence for difference: $BF_{10} = 5 \times 10^6$, $CI = [-20, -10]$ pp, n = 78 days), mirroring the decrease in the total number of active cells (Figure 4.2A).

To assess the effects of learning on place cells, the analysis used a data down-sampling procedure to compensate for the effects that the increased sampling of the reward locations could have on the place cell properties. The procedure randomly selected a matching count of samples per spatial bin from the foraging and test sessions. Place maps were generated for each random selection of data samples and the place cell statistics were calculated as a mean value from 100 random samples. To characterise changes in spatial coding by cells, the comparison below only includes cells that were classified as place cells in more than half of the random samples.

In agreement with reports using tetrode recordings (Maurer et al., 2005; Jung et al., 1994; Keinath et al., 2014), the iCA1 place fields during foraging were 111 ± 7% larger than dCA1 place fields (strong evidence: $BF_{10} = 12$, $CI = [24\%, 204\%]$, n = 720 cells; Figure 4.4A left). After learning, the place cells became more spatially tuned. The mean place field size of the dCA1 and the iCA1 place cells decreased similarly, by 21 ± 5% in dCA1 and 29 ± 8% in iCA1 (log-linear mixed-effects model, moderate evidence for the lack of learning × recording location interaction: $F_{(1,1034)} = 1.4$, $p = 0.23$; $BF_{10} = 0.16$, strong evidence for decrease: $F_{(1,1034)} = 33.4$, $p = 10^{-8}$; $BF_{10} = 10^4$, $CI = [-31\%, -17\%]$, n = 1043 cells; Figure 4.4A right).

Nearly half of the place cells were active in more than a single location, resulting in multiple place fields. During foraging, the mean count of place fields per place cell was similar in dCA1 and iCA1 (linear mixed-effects model: $F_{(1,11)} = 1.9$, $p = 0.19$; inconclusive evidence for difference: $BF_{10} = 0.80$, $CI = [-16\%, 4\%]$, n = 39 sessions; 4.4B left). After learning, the mean number of place fields decreased in dCA1 from 1.7 ± 0.1 to 1.5 ± 0.1 but did not significantly change in iCA1 from 1.7 ± 0.1 (linear mixed-effects model, experiment × recording location interaction: $F_{(1,73)} = 7.4$, $p = 0.008$, $BF_{10} = 6.0$; strong evidence for decrease in dCA1: $BF_{10} = 2330$; $CI = [-0.28, -0.11]$,

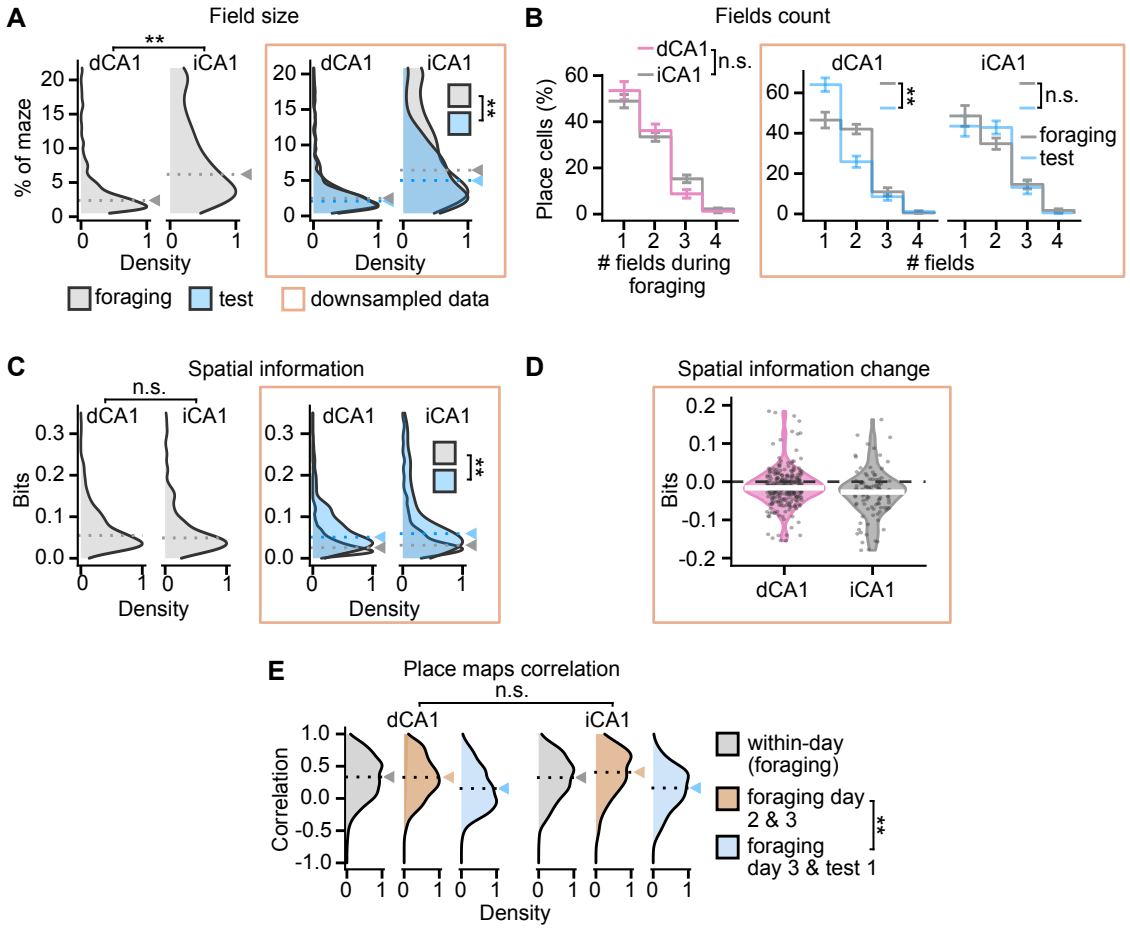

Figure 4.4: Sparser but more spatially tuned place cells after learning. (A) Distribution of field sizes of the dCA1 and the iCA1 place cells calculated on actual (left) and downsampled data (right). **(B)** Histogram of field counts per place cell calculated on actual (left) and downsampled data (right). Error bars mark mean ± SEM. **(C)** Normalised spatial information calculated on actual (left) and downsampled data (right). **(D)** Normalised spatial information change in place cells from last-day foraging to test trial after first learning, calculated on downsampled data. Horizontal bars mark median. **(E)** Stability of place cells measured as the correlation between place maps. The plot shows the distribution of correlations calculated between (1) the same-day early and late foraging trials (within-day foraging comparison); (2) foraging trials on two different days; (3) last-day foraging and test trial after learning the first set of reward locations. Dashed lines and triangles mark the means. The effect of the recording location was tested with linear mixed-effects models in (B), and with log-linear mixed-effects models in (A), (C) and (E). $^{**}p < 0.01$.

$t_{(23.5)} = -3.4$, $p = 0.03$, moderate evidence for the lack of change in iCA1: $BF_{10} = 0.32$, $CI = [-0.13, 0.30]$, $t_{(72.7)} = -1.2$, $p = 0.59$; , n = 78 sessions; Figure 4.4B right). The change in dCA1 was due to an increase in the fraction of single-field peaks from 47 ± 4% to 64 ± 3%.

Studies using tetrode recordings reported that the CA1 place cells decrease spatial information along the dorso-ventral axis (Jung et al., 1994; Keinath et al., 2014; Jin and Lee, 2021). Here, to further limit the bias that uneven sampling of the maze introduced in the measured spatial information, I report the spatial information relative to the cell's spatial information expected by chance. During foraging, the spatial information of the iCA1 place cells did not differ from that of the dCA1 place cells (log-linear mixed-effects model: moderate evidence for the lack of difference: $BF_{10} = 0.25$, $CI = [-31\%, 65\%]$; $F_{(1,10)} = 0.15$, $p = 0.71$, n = 720 cells; Figure 4.4C left). After learning, the mean spatial information increased in the dCA1 place cells by 96 ± 5% and in iCA1 place cells by 76 ± 10% (inconclusive evidence for different increase in dCA1 and iCA1, log-linear mixed-effects model, experiment × recording location interaction: $F_{(1,1037)} = 3.0$, $p = 0.084$; $BF_{10} = 0.39$; spatial information increase: $F_{(1,1037)} = 135$, $p < 10^{-15}$, $BF_{10} = 10^{26}$, $CI = [65\%, 102\%]$; n = 1043 cells; Figure 4.4C right). Data downsampling resulted in lower spatial information compared to the original data (Figure 4.4C). This is because the fewer samples led to a higher estimation of the spatial information bias that was subtracted from the spatial information values. The increase of spatial information taken together with the decrease of place field size means that the place cells increased their spatial tuning.

The majority of the place cells from foraging that were matched during the first test trial decreased their spatial information (spatial information calculated on downsampled data, median change in dCA1: -0.016 bits, n = 507 cells, in iCA1: -0.24 bits, n = 232 cells; Figure 4.4D). Consequently, only 28% of the dCA1 and 32% of the iCA1 place cells from foraging were classified as a place cell during the test trial. Because fewer cells were classified as place cells in test than in foraging but the ones that were increased their spatial tuning, the changes can be interpreted as sparsification of the spatial code.

To assess the stability of place cells between sessions and across days, I investigated correlations of their place maps. The place field correlations were different between the compared sessions (linear mixed-effects model, $F_{(1,2054)} = 63$, $p < 10^{-15}$, $BF_{10} = 1023$, n = 2065 place map correlations; Figure 4.4E) but there was no effect of the recording location ($F_{(1,10)} = 0.02$, $p = 0.88$; strong evidence: $BF_{10} = 0.17$). Corre-

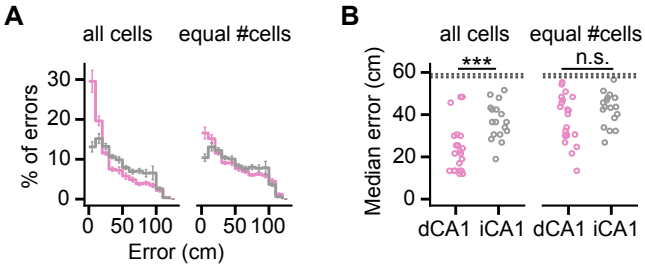

Figure 4.5: Spatial location could be decoded from dCA1 and iCA1 activity with similar accuracy. (A) Histogram of location decoding errors calculated using cross-validation on single-day activity from foraging sessions. The decoding errors show the performance of decoding location from the activity of all cells and from equally sized dCA1 and iCA1 neuronal populations. Error bars mark mean ± SEM. **(B)** Comparison of median decoding error. Horizontal dashed lines mark the performance of a random decoder. Data compared with post-hoc tests on linear mixed-effects model. $^{***}p < 0.001$.

lations between the last foraging day and the first test session were lower than between the last two foraging days by 0.12 ± 0.02% ($t_{(2052)} = 9.0$, $p < 10^{-15}$; $BF_{10} = 10^{23}$, n = 795 place map correlations); however, they were still significantly positive ($t_{(16)} = 3.2$, $p = 0.005$, n = 371 place map correlations). The decrease in the place field correlations could be due to learning or a learning-independent factor, as place cells remap over time (Ziv et al., 2013). Nevertheless, 16% of dCA1 and 12% dCA1 place cells from foraging that were matched during the test had stable place fields between the two sessions and their place map correlation exceeded 0.5.

To assess the precision of the spatial coding, I compared performance of decoding spatial location from the dCA1 or the iCA1 population activity. When decoding from the entire cell population, decoding from dCA1 had a median error of 24 ± 3 cm. This was significantly lower than decoding from the iCA1, which had a median error of 39 ± 3 cm (linear mixed-effects model, recording location × decoder size interaction: $F_{(1,63)} = 4.1$, $p = 0.05$, difference in median error: $t_{(15.5)} = -2.9$, $p = 0.04$, $BF_{10} = 4.6$, $CI = [1, 24]$ cm, n = 39 sessions; Figure 4.5A,B left). Fewer cells were recorded in the iCA1 than in dCA1, which could affect the precision of the decoded locations. Therefore, I also compared decoders trained on sized-matched populations. I trained the decoder on 30 randomly sampled cells from each session (72% of the iCA1 recordings had more than 30 cells) and repeated the procedure 50 times using different cell samples. Decoding from the sampled dCA1 had a median error of 38 ± 2 cm,

which was significantly higher than the error when decoding from all cells ($t_{(63)} = 4.8$, $p = 0.0001$). Data showed inconclusive evidence for the median error to differ between the sampled dCA1 decoder and sampled iCA1 decoder ($t_{(16)} = -1.3$, $p = 0.43$, $BF_{10} = 0.8$, $CI = [-3, 14]$ cm, n = 39 sessions; Figure 4.5A,B right). Therefore, the data does not provide sufficient evidence to conclude whether the size-matched dCA1 and iCA1 cell populations encoded the spatial location with different precision. However, if the encoded precision is different, the difference is small.

4.4.2 Accumulation of place fields at learned reward locations

I next compared how the location of dCA1 and iCA1 place fields changed as a result of learning. The dCA1 but not iCA1 place fields shifted towards the learned reward locations and gained reward fields, defined as fields within 20 cm of one of the reward locations (linear mixed-effects model on the proportion of cells with reward field, trial-type × recording site interaction: $F_{(1,13)} = 16.2$, $p = 0.001$, n = 44 trials). After learning, the proportion of dCA1 place cells with a reward field increased by 65 ± 11% ($t_{(12.1)} = 4.8$, $p = 0.002$, $BF_{10} = 42850$, $CI = [34\%, 96\%]$; Figure 4.6A); whereas it did not change significantly in the iCA1 (inconclusive evidence: $t_{(13.2)} = 1.27$, $p = 0.65$, $BF_{10} = 0.37$, $CI = [-18\%, 65\%]$; Figure 4.6B).

I verified that increased sampling of the reward locations did not account for the increase in dCA1 place cell density. The downsampling procedure as above (subsection 4.4.1) confirmed the differential effect on place fields in dCA1 and iCA1 ($F_{(1,12)} = 14$, $p = 0.003$, n = 44 trials). The proportion of place cells with a reward field increased in the dCA1 ($t_{(1,11)} = 4.9$, $p = 0.002$, $BF_{10} = 4836$, $CI = [24\%, 71\%]$; Figure 4.6C), whereas no such change was seen in the iCA1 (moderate evidence for the lack of effect: $t_{(1,13)} = 0.7$, $p = 1.0$, $BF_{10} = 0.26$, $CI = [-19\%, 37\%]$; Figure 4.6D). It is possible that while the centre of mass did not move, the iCA1 place fields could have enlarged towards the rewards. This was not the case, however, as their size decreased from foraging to test trials (Figure 4.4A).

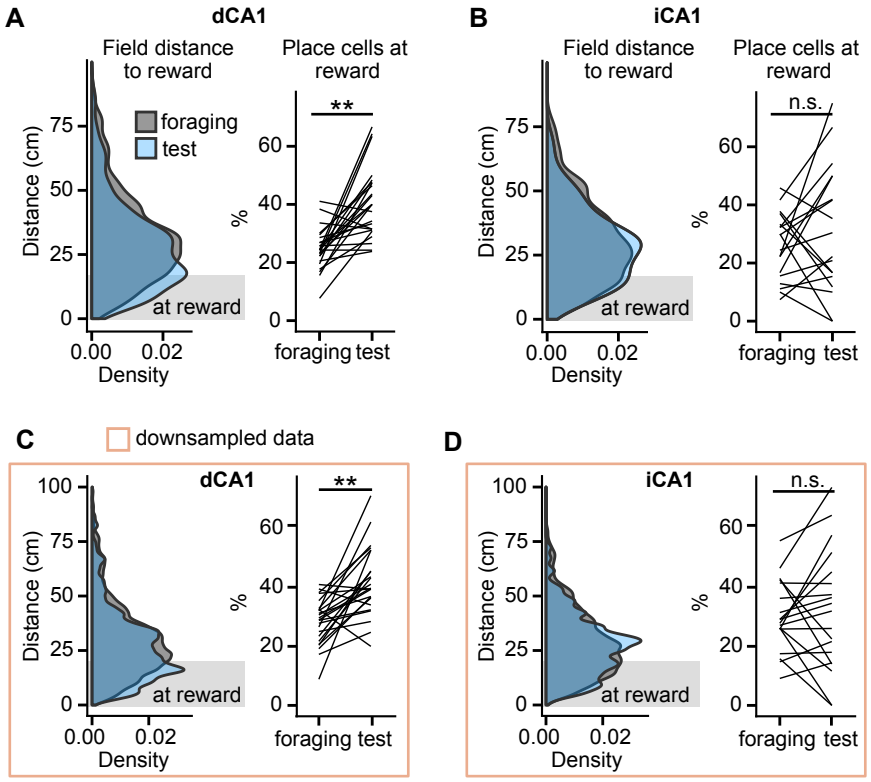

Figure 4.6: dCA1 but not the iCA1 place cells accumulated at learned reward locations. (A) Learning-induced changes of distance from dCA1 place fields to the closer of two reward locations. Left: distribution of distances shown for place fields from foraging and place fields from unbaited test after learning. Right: proportion of dCA1 place cells that had a place field inside a reward zone (reward field). Lines connect values for a single set of reward locations. **(B)** As in (C) but for iCA1 cells. **(C)** As in (A) but for place cells calculated on randomly downsampled data to match occupancies between foraging and test trials. **(D)** As in (B) but for iCA1 cells.
Data compared with post-hoc test on least-square means of linear mixed-effects model for the effects of learning, implant location and their interaction. $^{**}p < 0.01$.

4.5 Change in population activity as mice approached the reward

To gain insight into how memory of reward location affects the population activity, I analysed the dCA1 and iCA1 activity as mice approached the reward. In late learning trials (last day of learning a set of reward locations), the mean dCA1 activity increased by 0.09 ± 0.01 s.d. when mice approached the reward (log-linear mixed-effects model comparing activity at 4–5 s and 0–1 s before the reward, learning stage × reward proximity interaction: $F_{(2,1525)} = 25$, $p = 10^{-11}$; late learning increase: $t_{(1526)} = 7.8$,

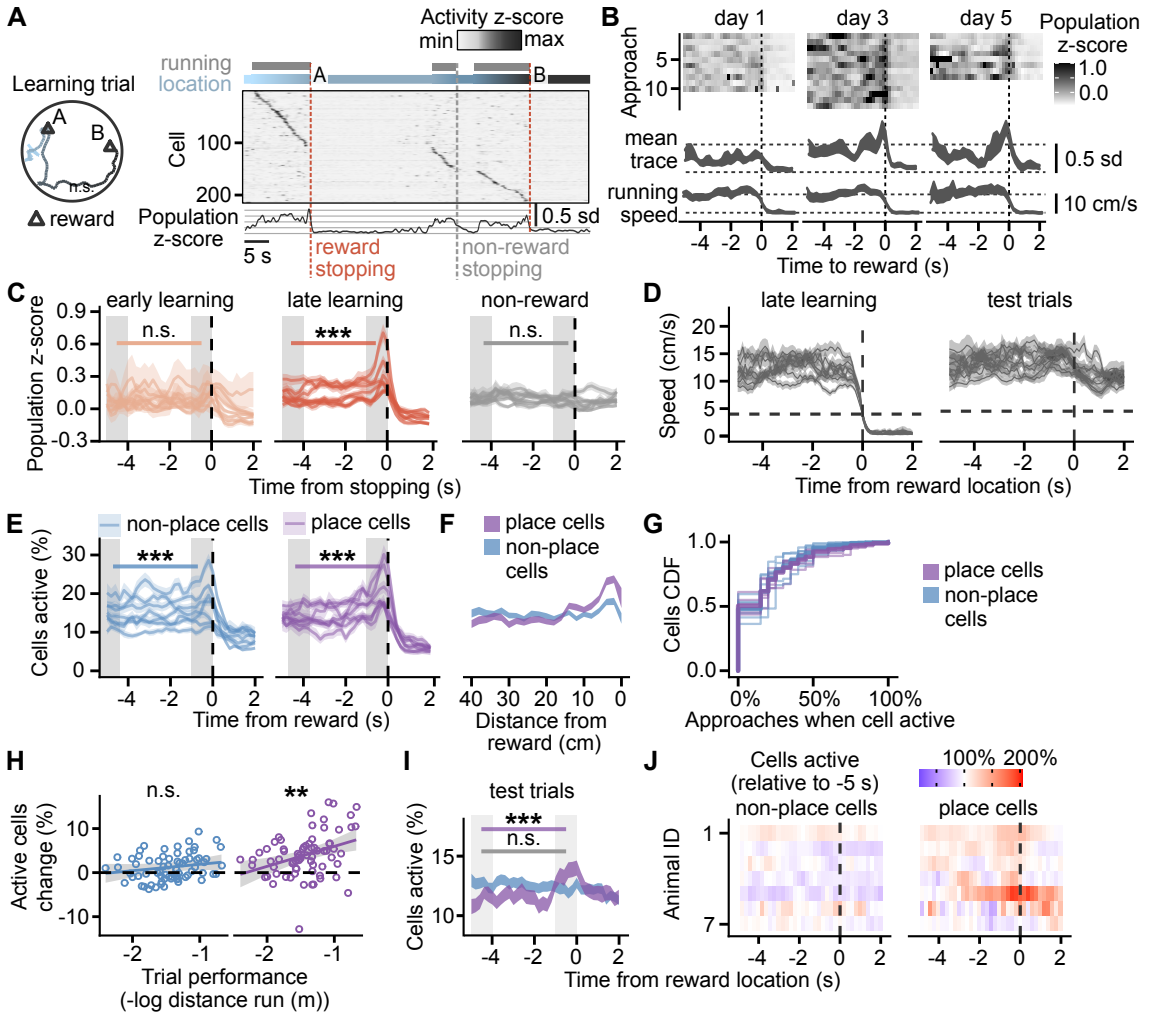

Figure 4.7: dCA1 population activity ramping-up as mice approach the reward. **(A)** Example single-trial path of a mouse (left) together with dCA1 activity (right). Each row of the raster shows z-scored activity of a single cell. The cells are sorted by the time of their maximum activity. Blue-coloured gradient above the raster indicates the colour-matched spatial location on the left; the total population activity is shown below. **(B)** Population activity during individual approaches towards the reward locations in an example mouse. Day-mean ± SEM activity and running speed are shown below. **(C)** Population activity as mice approached the reward compared between the early and late learning trials and non-reward stopping. Each ribbon shows animal mean ± SEM. **(D)** Speed profile centred on the time of dCA1-implanted mouse arriving at the reward during late learning (left) and on the time when the mouse was the closest to reward location during test trials (right). Each ribbon shows animal mean ± SEM. Horizontal line marks running speed threshold. **(E)** Percentage of active place cells and non-place cells in dCA1 as mice approached the learned reward location in late learning trials shown as a function of time from reward. Each ribbon shows animal mean ± SEM. **(F)** As in (E) but as a function of distance from reward.

Figure 4.7 *(previous page)*: dCA1 population activity ramping-up as mice approach the reward. (G) Cumulative distribution function (CDF) for the percentage of the reward approaches when the dCA1 cell was active 0–1 s before the mouse arrived at a reward. The cell's frequency was calculated separately for each reward location during late learning. The thin lines show CDF on data pooled from the same animal from multiple reward locations and learning days; the thick line shows the CDF mean. **(H)** Change in the number of active cells from the 4–5 s before the reward approach to 0–1 s shown as a function of day-mean learning trial performance. The black line shows the slope of modelled regression together with its credibility interval in grey. **(I)** Percentage of active place cells in unbaited test trials shown as time from the mouse approaching the learned reward location. Ribbons show mean ± SEM per mouse. **(J)** The percentage of active cells in test trials during the reward location approach relative to the value at -5 s from the reward location. Each row shows the animal mean as a function of time.
Population activity extracted from calcium imaging. Data compared with post-hoc tests on linear mixed-effects models in (C), (E) and (I). Linear mixed-effects model used to test for the effects of trial performance in (H). $^{***}p < 0.001$; $^{**}p < 0.01$.

$p = 10^{-13}$, $BF_{10} = 1011$, $CI = [0.08, 0.13]$ s.d., n = 70 early, 298 late, 298 non-reward approaches; Figure 4.7A–C). The effect was absent on the first day of learning (early learning, $t_{(1525)} = 0.6$, $p = 1.0$, $BF_{10} = 0.18$, $CI = [-0.03, 0.05]$ s.d.). Also, it was not a direct result of changes in running speed: the effect was absent when the mice stopped at non-rewarded locations ($t_{(1414)} = 1.6$, $p = 1.0$, $BF_{10} = 0.16$, $CI = [-0.03, 0.01]$ s.d.), and it preceded the drop in speed before the reward (Figure 4.7D). The fraction of active cells (cells whose activity exceeds z-score of 0.5) increased by 33 ± 4% among place cells, and 15 ± 3% among non-place cells (linear mixed-effects model, cell-type × reward proximity interaction: $F_{(1,1085)} = 10.5$, $p = 0.001$; increase in place cells: $t_{(1086)} = 8.0$, $p = 10^{-14}$, $BF_{10} = 1010$, $CI = [21\%, 46\%]$; increase in non-place cells: $t_{(1086)} = 3.5$, $p = 0.001$, $BF_{10} = 168$, $CI = [6\%, 22\%]$; n = 298 approaches; Figure 4.7E). The cells active at a particular reward location consisted of a repeatedly activated cell population (7 ± 1% of place cells and 4 ± 1% of non-place cells were active in more than half of the approaches) and of a changing, broader cell population: 50 ± 2% of place cells were active at reward at least once, meaning that a large fraction of these cells fired outside of their place field (Figure 4.7G). The increased activity of place cells was also visible when plotted as a function of distance to the reward (Figure 4.7F), and it correlated with day-mean performance (linear mixed-effects: $F_{(1,66)} = 10$, $p = 0.002$, $BF_{10} = 7.2$, slope: $CI = [0.8, 7.2]$, n = 68 days; Figure 4.7H right). In

contrast, there was no significant correlation between the fraction of active non-place cells and performance (inconclusive evidence: $F_{(1,36)} = 2.4$, $p = 0.13$, $BF_{10} = 0.63$, slope $CI = [-0.8, 3.1]$, n = 68 days; Figure 4.7H left).

The higher number of active place cells was not only caused by reward-associated olfactory cues, as it persisted in the unbaited test trials. When the mice were running the closest to the learned reward location, the fraction of dCA1 active place cells increased by 19 ± 11% while it did not change in non-place cells (linear mixed-effects model, cell-type × reward location proximity interaction: $F_{(1,840)} = 9$, $p = 0.003$; increase in place cells: $t_{(840)} = 3.7$, $p = 0.001$, $BF_{10} = 7.4$, $CI = [6\%, 33\%]$; strong evidence for the lack of change in non-place cells: $t_{(85)} = -0.23$, $p = 0.82$, $BF_{10} = 0.09$, $CI = [-9\%, 5\%]$; n = 230 approaches; Figure 4.7I–J). Therefore, the ramping-up of active place cells can not be explained only by reward-associated olfactory cues, which might nevertheless have contributed to the higher baseline activity during learning.

Changes in iCA1 population activity contrasted with those in dCA1. In late learning trials, the mean iCA1 activity decreased by 0.09 ± 0.01 s.d. when mice approached the reward (log-linear mixed-effects model, learning stage × reward proximity interaction: $F_{(2,1188)} = 7.3$, $p = 10^{-3}$; late learning decrease: $t_{(1189)} = -4.2$, $p = 10^{-4}$, $BF_{10} = 39$, $CI = [-0.15, -0.4]$ s.d.; n = 60 early, 253 late, 385 non-reward approaches; Figure 4.8A–C). This effect was absent during early learning trials ($t_{(1183)} = 0.82$, $p = 1.0$, $BF_{10} = 0.21$, $CI = [-0.11, 0.5]$ s.d.) and when mice stopped at non-rewarded locations ($t_{(1186)} = -1.0$, $p = 1.0$, $BF_{10} = 0.11$, $CI = [-0.02, 0.05]$ s.d.). The opposite direction of activity change between dCA1 and iCA1 was not explained by mice approaching the reward with different speeds (Figure 4.8D). The fraction of active cells did not change among place cells but it decreased among non-place cells by 32 ± 3% (linear mixed-effects model cell-type × reward proximity interaction: $F_{(1,865)} = 8.8$, $p = 0.003$; no change in place cells: $t_{(865)} = 0.3$, $p = 0.98$, $BF_{10} = 0.08$, $CI = [-15\%, 23\%]$; decrease in non-place cells: $t_{(865)} = 4.0$, $p = 10^{-4}$, $BF_{10} = 106$, $CI = [-44\%, -21\%]$; n = 253 approaches; Figure 4.8E). Large fractions of place cells and non-place cells were inactive 0–1 s before the reward in all approaches to a particular reward (46 ± 3% of the place cells, 50 ± 4% of the non-place cells; Figure 4.8G). The activity decrease was

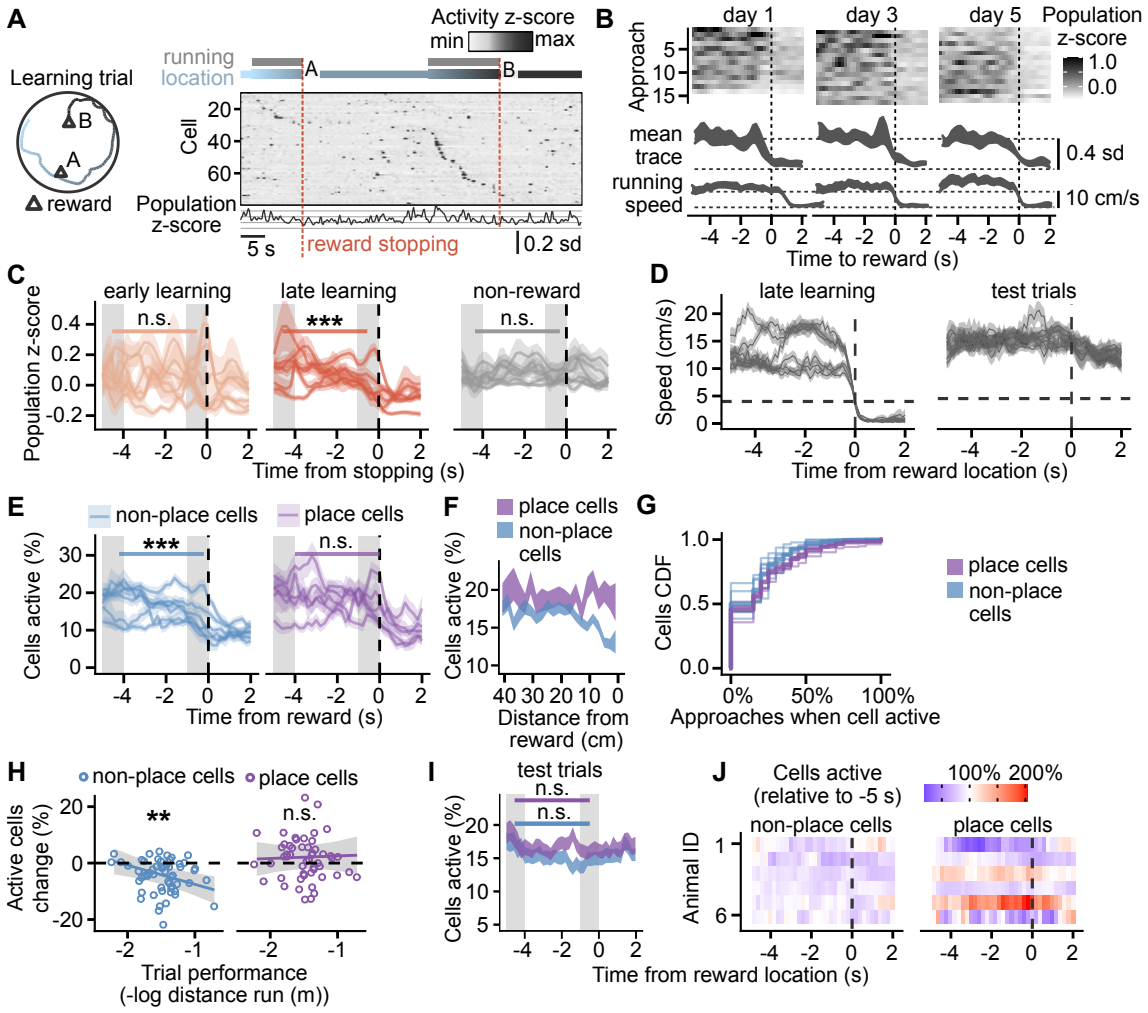

Figure 4.8: iCA1 population activity ramping-down as mice approach the reward. **(A)** Example single-trial path of a mouse (left) together with iCA1 activity (right). Each row of the raster shows z-scored activity of a single cell. The cells are sorted by the time of their maximum activity. Blue-coloured gradient above the raster indicates the colour-matched spatial location on the left; the total population activity is shown below. **(B)** Population activity during individual approaches towards the reward locations in an example mouse. Day-mean ± SEM activity and running speed shown below. **(C)** Activity as mice approached the reward compared between the early and late learning trials and non-reward stopping. Each ribbon shows animal mean ± SEM. **(D)** Speed profile centred on the time of an iCA1-implanted mouse arriving at the reward during late learning (left) and on the time when the mouse was the closest to reward location during test trials (right). Each ribbon shows animal mean ± SEM. Horizontal line marks running speed threshold. **(E)** Percentage of active place cells and non-place cells as mice approached the learned reward location in late learning trials shown as a function of time from reward. Ribbons show animal mean ± SEM. **(F)** As in (E) but as a function of distance from reward.

Figure 4.8 ***(previous page)*****: iCA1 population activity ramping-down as mice approach the reward. (G)** CDF for the percentage of the reward approaches when the cell was active 0–1 s before the mouse arrived at a reward. The cell's frequency was calculated separately for each reward location during late learning. The thin lines show CDF on data pooled from the same animal from multiple reward locations and learning days; the thick line shows the CDF mean. **(H)** Change in the number of active cells from the 4–5 s before the reward approach to 0–1 s shown as a function of day-mean learning trial performance. The black line shows the slope of modelled regression together with its credibility interval in grey. **(I)** Percentage of active place in unbaited test trials shown as time from the mouse approaching the learned reward location. Ribbons show mean ± SEM per mouse. **(J)** The percentage of active cells in test trials during the reward location approach relative to the value at -5 s from the reward location. Each row shows the animal mean as a function of time.
Population activity extracted from calcium imaging. Data compared with post-hoc tests on linear mixed-effects models in (C), (E) and (I). Linear mixed-effects model used to test for the effects of trial performance in (H). $^{***}p < 0.001$; $^{**}p < 0.01$.

also visible when plotted as a function of distance to the reward (Figure 4.8F), and it correlated with day-mean performance (linear mixed-effects: $F_{(1,55)} = 8$, $p = 0.005$, $BF_{10} = 7.0$, slope $CI = [-10.5, -1.2]$; Figure 4.8F), whereas there was no correlation between the fraction of active iCA1 place cells and performance (linear mixed-effects: $F_{(1,49)} = 0.9$, $p = 0.77$; $BF_{10} = 0.31$, slope $CI = [-5.4, 6.6]$, n = 58 days, Figure 4.8H).

In the unbaited test trials, the fraction of active iCA1 place cells and non-place cells did not change when mice approached the learned reward locations (linear mixed-effects model cell-type × reward location proximity interaction: $F_{(1,859)} = 0.7$, p = 0.41, reward location effect: $F_{(1,859)} = 1.9$, $p = 0.16$; strong evidence for the absence of change in place cells: $BF_{10} = 0.08$, $CI = [-18\%, 12\%]$; moderate evidence for the absence of change in non-place cells: $BF_{10} = 0.24$, $CI = [-26\%, 3\%]$; n = 246 approaches; Figure 4.8I–J). The decrease in the fraction of active non-place cells correlated with the performance only in baited trials, suggesting it was related to the reward-associated olfactory stimulus or different speed profile when mice approached reward location in the learning and test trials (Figure 4.8D).

4.6 Tracking of reward location by individual cells

A subpopulation of dCA1 place cells was reported to remap to track the reward locations (Gauthier and Tank, 2018). To investigate whether some dCA1 or iCA1 cells signalled location-independent anticipation of reward, I compared their activity between test trials performed after the mice learned different reward locations. Of the cells active on the first test trial, 60 ± 6% were active again on the second and 50 ± 5% on the third test trial (Figure 4.9A). I followed the remapping of place cells present in two subsequent test trials (Figure 4.9B top). Of the 89 dCA1 place cells with a reward field (place field within 20 cm of reward location) at the previous reward location, 25% retained their place field, and 31% remapped to either of the current reward locations. However, their place fields were not closer to the current reward locations than those of cells previously without a reward field (log-linear mixed-effects model comparing distances to the closer reward: $F_{(1,378)} = 0.94$, $p = 0.33$, moderate evidence for the lack of difference: $BF_{10} = 0.16$, $CI = [-6, 2]$ cm, n = 279 cells; Figure 4.9B–C left).

In contrast, iCA1 cells with a reward field at the previous reward location had place fields closer to the current reward locations than the cells previously without a reward field (log-linear mixed-effects model comparing distances from place field to the closer of the two rewards: $F_{(1,90)} = 17$, $p = 0.0001$; strong evidence: $BF_{10} = 122$, $CI = [6, 19]$ cm, n = 74 cells; Figure 4.9B–C right). The effect was not due to different place field sizes in the two groups of the iCA1 place cells (linear mixed-effects model for mean field size: $F_{(1,89)} = 1.2$, $p = 0.29$; moderate evidence for the lack of difference $BF_{10} = 0.32$, $CI = [-2.5\%, 1.0\%]$, n = 74 cells; 4.9D).

The subpopulations of iCA1 place cells with zero or multiple reward fields were larger than expected by chance – one remapped avoiding and the other remapped tracking reward locations. To test this, I looked at cells present in at least two test trials and classified as place cells in more than half of them. Of 106 iCA1 place cells, 47.1% had zero reward fields, and 4.7% had reward fields at more than half of reward locations, significantly more than the respective 40.0% and 2.9% expected by chance (Figure 4.10A–B right). The distribution of the expected counts was generated by a process that shuffled cell identities assigned to test trial place maps. A significantly

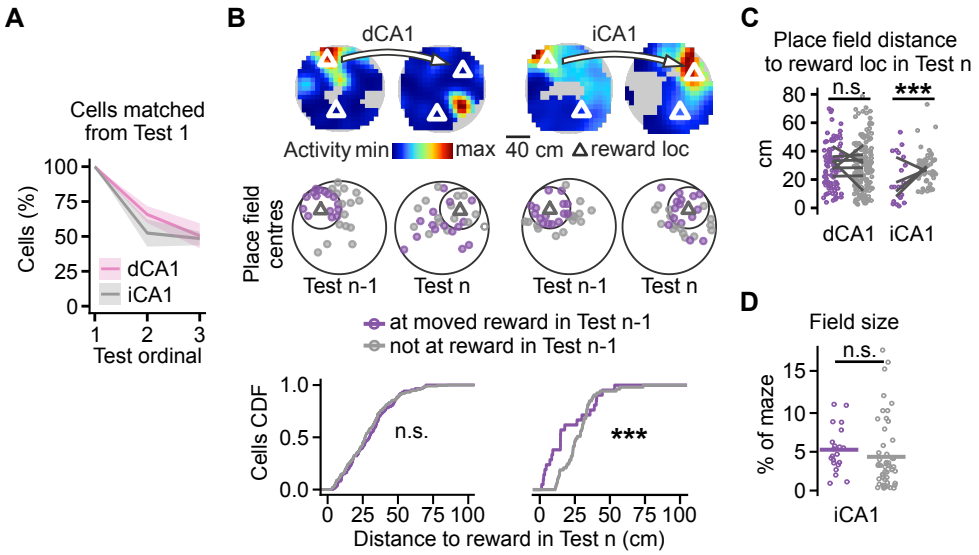

Figure 4.9: Subpopulation of the iCA1 but not dCA1 cells tracked the learned reward location. **(A)** Percentage of cells from the first test trial active again in the later test trials. **(B)** Remapping of place cells after learning a changed reward location. iCA1 place cells with a field at the previous reward location had their fields subsequently closer to the current reward locations than the cells previously without a reward field. Top: Example place maps of the same cells from the previous (Test n-1) and current test trial (Test n). Middle: place fields centres for a random cell sample. Visualization preserves distances to the reward but the exact locations differ. Bottom: CDF of distances from the place field centres to the closer of the reward locations. For cells with multiple place fields, the one closest to the reward was considered. **(C)** Data points show distances for cells used for the CDF in (B). Lines connect animal averages. Only 4 out of 6 iCA1 animals had cells with a reward field that could be matched on a subsequent trial. Statistics as in (B). **(D)** Place field sizes of iCA1 place cells previously active at the moved reward location and of the place cells previously without reward field. $^{***}p < 0.001$.

higher fraction of cells with zero or many fields at reward location means their count exceeded that in 95% of the shuffles. In comparison, of 423 dCA1 place cells, 33.8% had zero reward fields, and 2.1% had reward fields at more than half of reward locations – fractions similar to the respective 34.1% and 2.5% of cells expected by chance (Figure 4.10A–B left).

To investigate whether cells with reward fields during test trials were active in anticipation of reward, I analysed their activity as the mice approached either of the two reward locations during the previous-day learning. dCA1 and iCA1 cells with reward fields in test trials had higher activity than other place cells as the mice approached either of the two rewards (log-linear mixed effect models on activity -1–0 s from the reward, dCA1: $F_{(1,2134)} = 20$, $p = 10^{-5}$; $BF_{10} = 498$, $CI = [0.1, 0.2]$ s.d.;

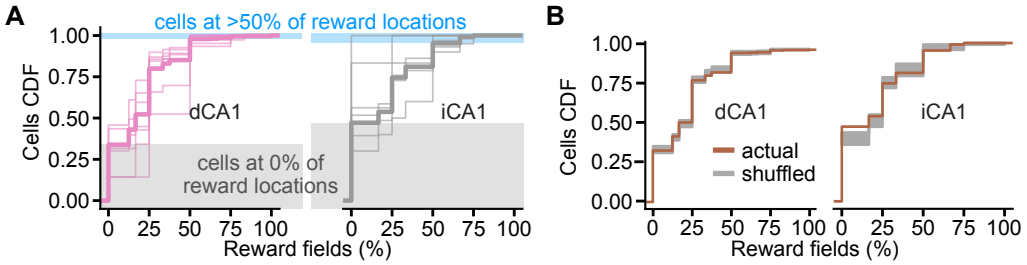

Figure 4.10: Subpopulation of iCA1 cells that remapped to track the reward location was larger than expected by chance. (A) CDF for the frequency with which cells had a reward field during the test trials. For example, a cell that had reward fields at two rewards during the three trials had a frequency of 33%. Thin lines show CDF calculated per animal; the thick lines show data pooled from dCA1 and iCA1 animals. **(B)** CDF as in (A) calculated on data pooled from dCA1 and iCA1 animals compared to the number of cell occurrences at reward expected by chance.

iCA1: $F_{(1,591)} = 19$, $p = 10^{-5}$; $BF_{10} = 224$, $CI = [0.1, 0.4]$ s.d.; n = 278 learning trials; Figure 4.11A–B). The difference between the two populations increased as mice approached the reward in iCA1 but not in dCA1, suggesting that iCA1 cells form distinct subpopulations (log-linear mixed-effects model comparing the difference at 4–5 s and 0–1 s before reward, recording site × reward proximity interaction: $F_{(1,456)} = 5.9$, $p = 0.016$; strong evidence for no change in dCA1: $t_{(455)} = -0.2$, $p = 0.90$, $BF_{10} = 0.10$, $CI = [-0.1, 0.1]$ s.d.; strong evidence for change in iCA1: $t_{(456)} = -3.3$, $p = 0.006$, $BF_{10} = 21.2$, $CI = [0.1, 0.4]$ s.d.; n = 278 learning trials; Figure 4.11C).

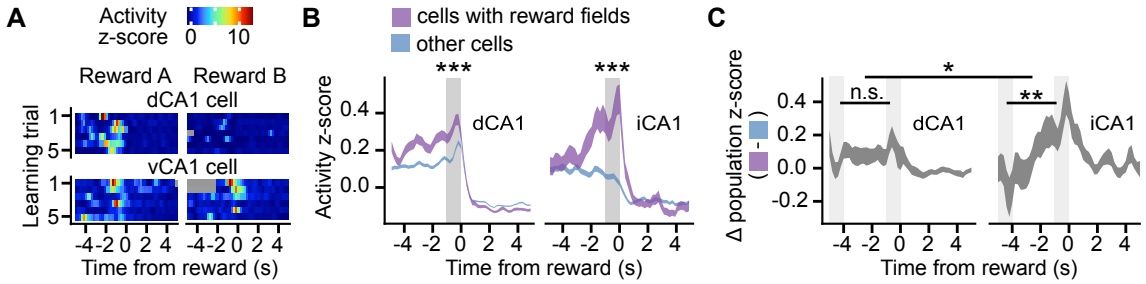

Figure 4.11: Cells with the reward fields were active in anticipation of the reward during learning. **(A)** Activity in single-day learning trials of example dCA1 cell and iCA1 cell that had a reward field in the next-day test trial. Each row shows activity in a single trial centred on the time of the mouse arriving at reward. Grey marks periods from before the recording start or after its finish. **(B)** Averaged activity during late learning trials aligned to the time of mice arriving at the reward. Shows activity of two cell groups: cells with reward fields in a next-day test trial and the cells without a reward field. The trace has a width of ± SEM; grey rectangles mark 1-s-long periods used for the statistical comparison. **(C)** Within-trial difference between the two cell groups from (B). Linear mixed-effects model for the effects of reward proximity, recording site and their interaction; effect of reward proximity in dCA1 and iCA1 tested with least-square means. Grey rectangles mark 1-s-long periods used for the statistical comparison. Data compared with post-hoc tests on least-square means of log-linear mixed-effects models. $^{***}p < 0.001$, $^{**}p < 0.01$, $^{*}p < 0.05$.

4.7 Encoding of reward location by population activity

Last, I assessed the similarity of the hippocampal encoding for memory of different reward locations. I first created a binary decoder predicting from the instantaneous activity of the dCA1 or iCA1 cell population whether the mouse was running inside a reward zone in a given instant of the test trial (Figure 4.12A). When tested on the same dataset as used for training, decoding from dCA1 and iCA1 had accuracies of respectively 31 ± 2% and 30 ± 3% above that of random predictions based on reward zone occupancy probability (Figure 4.12B left). To show that the activity generalises across reward locations, I evaluated the decoders at one new and one of the previous reward locations from another test trial. Decoding from the iCA1 had an accuracy of 10 ± 3% above that of the random predictions. This was significantly higher than decoding from the dCA1 which had an accuracy of 11 ± 4% below that of the random predictions ($F_{(1,20)} = 12$, $p = 0.002$, $BF_{10} = 7.1$, $CI = [3\%, 33\%]$, n = 20 trials; Figure

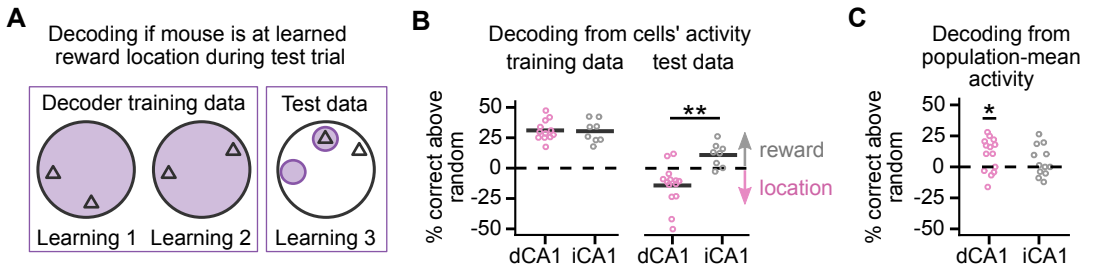

Figure 4.12: Population activity encoded learned reward locations. **(A)** Training and test data used for binary decoders predicting whether the mouse was running in the learned reward location proximity. The decoders were trained on the activity from test trials on two different days. They were tested on activity from another day when the decoder had to flip its prediction for the two tested locations: the previously rewarded location was unrewarded and vice versa. **(B)** Accuracy of decoding from the activity of cell population is shown as the difference from random predictions based on reward zone occupancy probability. Decoders evaluated on the same data as used for training (left) and on the data from test trials with different reward locations than in training (right). In the latter, the decoder had to give the opposite answer to the training data for the same location. Accuracy below the random level means the decoder predicted location rather than predicting reward zone. **(C)** Accuracy of decoding from the population-mean activity is shown as the difference from random prediction. Horizontal bars mark the means. $^{**}p < 0.01$, $^{*}p < 0.05$.

4.12B right). Decoding from the iCA1 had higher accuracy despite having to use fewer recorded cells: 38 ± 7 iCA1 vs 61 ± 9 dCA1 cells. The dCA1 decoder predicted the reward zone to be at the same location as in the training dataset even though it was moved, which means it decoded the mouse location rather than reward location.

Because the number of active dCA1 cells ramped up when mice approached the learned reward location (Figure 4.7), I tested another decoder based on the dCA1 population-mean activity. The decoder used two inputs representing the population activity: the fraction of active place cells and the fraction of active non-place cells. Decoding performed with an accuracy of 10 ± 4% above chance ($t_{(13)} = 2.7$, $p = 0.02$, $BF_{10} = 3$, $CI = [1\%, 16\%]$, n = 14 dCA1 trials; Figure 4.12C). Thus, the ramping-up activity of dCA1 place cells encoded reward location independently of their spatial coding.

4.8 Discussion

The main findings of this chapter are that both dCA1 and iCA1 activity predict reward location; however, they do so using different codes. The dCA1 anticipated the reward with increased population activity. The increase correlated with learning performance as measured by distance the mouse run to find the rewards. The activity engaged changing place cells, allowing independent reward and spatial coding. In iCA1 the same cells were active in anticipation of the reward, while the overall population decreased its activity. The iCA1 cell population provided a code for learned reward location that persisted across reward locations and time. The sections below discuss the findings of this chapter and put them in perspective.

4.8.1 Comparison of spatial coding in the dCA1 and iCA1

In agreement with previous reports, I found that iCA1 place cells have larger place fields than dCA1 place cells (Figure 4.4A; Maurer et al., 2005; Jung et al., 1994; Keinath et al., 2014). However, the dCA1 and iCA1 place cells did not differ in their within- and between-day stability (Figure 4.4G). The fraction of the dCA1 and iCA1 place cells and their spatial information per unit of activity were not different (Figure 4.4F). Previous studies using tetrode recordings reported lower spatial information per spike in the iCA1 (Jung et al., 1994; Keinath et al., 2014; Jin and Lee, 2021). Calcium imaging could be less sensitive to individual spikes (Huang et al., 2021) and underestimates spatial information and could have failed to capture the difference in the spatial information (Climer and Dombeck, 2021). Additionally, the involvement of the iCA1 in spatial navigation increases with task complexity (Contreras et al., 2018), which could affect the comparison between studies. While the iCA1 place cells had larger place fields, the dCA1 and iCA1 population activity encoded animal location with comparable accuracy (Keinath et al., 2014).

The functional contributions of the dCA1 and iCA1 place cells might be different during spatial learning and navigation. As reported before, they have different

effects on spatial learning depending on the stage of the learning task (Fanselow and Dong, 2010; Bast et al., 2009; Ruediger et al., 2012).

4.8.2 Sparser but more spatially tuned place cells after learning

The changes observed in dCA1 and iCA1 populations suggest that spatial representations become sparser after learning (Karlsson and Frank, 2008). First, together with the absolute number of active cells, the absolute number of place cells decreased after learning (Figure 4.3C). Second, the smaller population of place cells was more spatially tuned: their place fields were smaller, and their spatial information higher (Figure 4.4A,C). The decrease of place field sizes was associated with a higher fraction of single-field place cells in dCA1 but there was no change in iCA1 (Figure 4.4B). The place maps of the same cell recorded during the last-day foraging and first test had lower correlations than place maps between different-day foraging (Figure 4.4E). The lower place map correlations could have been caused by changes in the place maps due to learning a set of reward locations. However, the correlated place maps from foraging trials come from consecutive-day sessions, while the place maps from test trials come from sessions two-to-three days apart. Therefore, the longer time could contribute to the correlations difference.

The changes in spatial tuning are in agreement with previous reports that place cells increase their tuning with experience in the environment (Cacucci et al., 2007; Karlsson and Frank, 2008) and with reward location learning (Roux et al., 2017). However, place fields change over time (Ziv et al., 2013), and it is possible that the changes summarised above appeared independently of learning.

The behaviour of the animals differed between the foraging and test trials, which too confounds the effect of learning on the spatial tuning of cells. The mice ran faster in test than in foraging trials (Figure 4.1F). Running speed increases place cell firing rates (Maurer et al., 2005). Thus, if place cells increased their firing rates preferentially inside the place field, the place map contrast would increase, resulting in higher spatial information which is what I observed. A supra-linearly increased contrast of the place map due to the higher running speed could also explain smaller place field

sizes. This is because it would lead to fewer pixels of the place map exceeding a linear threshold used in the place field size calculation.

4.8.3 Reward anticipation coding in the dCA1

Consistent with previous reports, dCA1 place cells accumulated at the learned reward locations (Figure 4.6; Dupret et al., 2010; Zaremba et al., 2017; Boccara et al., 2019; Kaufman et al., 2020; Sato et al., 2020). Place field centres of mass shifted towards the reward location, which is a change that can not be explained by the higher running speed of mice during test trials than during foraging. The relative fraction of place cells at the reward increased, but the absolute count of active cells was lower after learning than during the first foraging sessions (Figure 4.2A). A previous study reported that the dCA1 place fields become asymmetric, and the cells become active earlier during the reward approach (Mehta et al., 2000). Such change is compatible with the accumulation of dCA1 place cells at the reward location because the activity peak of the asymmetric place cells could remain at the same location and because remapping and emergence of new place cells could lead to the place cell accumulation.

As mice approached the reward, the number of active place cells ramped-up (Figure 4.7). Ramping dCA1 activity was previously reported during reward anticipation in immobile animals (Hok et al., 2007; Duvelle et al., 2019). Therefore, the ramping signal can predict the reward location independently of the spatial representations during movement.

The ramping-up activity in anticipation of reward is also present in other brain regions that are involved in reward processing: striatum (Hollerman et al., 1998; Hassani et al., 2001), orbitofrontal cortex (Schoenbaum et al., 1998; Tremblay and Schultz, 1999) and amygdala (Schoenbaum et al., 1998). Activity in some of their neurons increases following a reward-predicting cue and the same neurons sustain their firing until the reward is delivered. Additionally, these neurons seem to respond to learning and reward rather than to an increased attention: the neurons in the striatum increase their activation when the reward magnitude decreases (Hassani et al., 2001). The source and function of these anticipatory signals could be related to the

ones observed in dCA1. If that was the case, magnitude of reward would also be expected to modulate dCA1 activity during reward anticipation, which requires further investigation.

I found evidence against the hypothesis that dCA1 cells with place fields close to reward remapped to track the translocated reward better than other place cells (Figure 4.9C). Thus, rather than a set of neurons specialised for encoding reward locations, a random subset of place cells accumulating at reward locations accounted for the total number of observed place fields at reward per dCA1 place cell (Figure 4.9D). This is at odds with the conclusion of Gauthier and Tank (2018). There are several differences between the two studies: (1) I compared the cell activity across multiple days and reward locations, and in the absence of reward; (2) I used a 2-dimensional maze and the mice were freely moving; (3) the null hypothesis I tested takes into account the accumulation of place cells at reward locations. The presented results suggest that the dCA1 place cells that are active at reward locations are part of a flexible spatial rather than a dedicated reward-coding population.

The results do not exclude the possibility that cells are attracted to the reward stochastically, following probabilities that differ between them. Because cells in the deep sublayer are more strongly modulated by reward (Danielson et al., 2016), and because spatial modulation of the dCA1 cells differs along the proximo-distal axis (Henriksen et al., 2010), responses across the dCA1 pyramidal cells may be more heterogeneous than I report here. Lee et al. (2020) proposed that place cells differ in the propensity to form place fields, which is scaled by salient locations. In their model, the expected number of reward fields per cell follows a Gamma-Poisson distribution, which is compatible with the low number of place cells frequently located at rewards (Figure 4.9D).

Encoding the reward-anticipatory signal with a variable ensemble of neurons could be beneficial for learning. For example, it could allow flexible global remapping of place cells between the environments (Chadwick et al., 2015), as well as allow construction of flexible sequences for mnemonic representations (Buzsáki and Tingley, 2018), and a continuous drift of memories to integrate new experience (Mau et al., 2020).

What mechanism supports the reward-anticipatory increase in the dCA1 activity? Lee et al. (2020) found that the membrane potential of some cells is depolarized at the reward locations, suggesting a selective increase in excitability. The increased excitability could be due to local disinhibitory activity (Turi et al., 2019), and due to neuromodulation by noradrenaline and dopamine (Kaufman et al., 2020). The neuromodulation could also induce LTP (Brzosko et al., 2019), resulting in increased activity during reward anticipation of neurons whose synapses were potentiated. Evidence for a role of LTP comes from Dupret et al. (2010) who reported that the accumulation of place cells at reward locations depends on NMDA receptors, which are required for some forms of LTP (Bliss and Collingridge, 1993).

4.8.4 Reward anticipation coding in the iCA1

The density of iCA1 place fields was unaffected by the memory of reward location. In a study where mice alternated between two marked reward locations, the iCA1 place cells accumulated at the reward locations and were sensitive to the reward value (Jin and Lee, 2021). Possibly, the iCA1 place cells accumulate at reward during stereotypical running; or in some form of value association. Heterogeneity among the intermediate-to-ventral CA1 cells (Ciocchi et al., 2015; Gergues et al., 2020) could have also contributed to the difference.

The iCA1 cell responses I observed were diverse: reward anticipation increased the activity of some and decreased the activity of other cells. A population of place cells increased their activity and remapped to track the changing reward locations (Figure 4.9C–D), similar to the goal-encoding cells suggested to exist in dCA1 (Gauthier and Tank, 2018). These cells were active as the mice approached the learned reward locations during the unbaited test trials and the preceding-day learning trials (Figure 4.11), supporting the interpretation that they signalled reward anticipation.

Reward anticipation modulated another cell subpopulation by decreasing its activity. The number of iCA1 place cells that did not have any reward fields was larger than expected by chance (Figure 4.9D). This cell population and the reward-tracking place cells can be related to the opposing approach and avoidance functions that are controlled by the ventral hippocampus (Riaz et al., 2017; Schumacher et al.,

2016). A population of iCA1 non-place coding cells decreased activity when the mouse approached the reward in late learning trials (Figure 4.8). The suppressed iCA1 activity during reward approach resembles a similar suppression during goal-directed lever pressing (Yoshida et al., 2019). Yoshida et al. (2019) reported that the serotonin-mediated inhibition of the iCA1 was required for mice to sustain goal-oriented activity. Possibly, the suppressed population activity helped to sustain the goal approach once the reward location was learned.

4.8.5 Function of reward-predictive encoding

Both dCA1 and iCA1 activity predicted the mouse's location relative to the learned reward location. The same patterns of activity at the reward persisted across different reward locations and across several days (Figure 4.12). The described dCA1 and iCA1 signal might direct the animal during navigation by increasing their activity in the proximity of a goal (Burgess and O'Keefe, 1996), or by signaling reward expectation (Foster et al., 2000).

The different encoding of reward-anticipation in dCA1 and iCA1 affects how the signal can be relayed downstream. iCA1 neurons have divergent outputs (Gergues et al., 2020). The reward-anticipatory subpopulation could include the nucleus accumbens-projecting neurons controlling appetitive memory (Ito et al., 2008; Britt et al., 2012; LeGates et al., 2018; Zhou et al., 2019; Davis et al., 2020; Shpokayte et al., 2020), and exclude those controlling aversion or fear (Ciocchi et al., 2015; Xu et al., 2016; Jimenez et al., 2018; Shpokayte et al., 2020). In dCA1, the ramping-up of population activity in reward-anticipation resembles that seen in the dopaminergic system (Schultz et al., 1997). Such signal could indiscriminately excite the downstream targets of the dCA1, including the nucleus accumbens-projecting neurons that enable conditioned place preference (Trouche et al., 2019). Both the dCA1 and iCA1 reward-predictive signals could contribute to the ventral striatal ramping-up activity during the learned reward location approach (van der Meer and Redish, 2011) and link locations with reward prediction.

Chapter 5

General discussion and conclusions

This thesis studies memory for reward location during two stages: its initial encoding and its later recall. For the stage of initial memory encoding, I focus on the supporting hippocampal states and how they are controlled by ACh. For the stage of memory recall, I focus on the changes in the CA1 activity which could represent the encoded memory of the reward locations. In the following sections, I summarise the main findings, discuss their validity and their significance.

5.1 Main findings

In Chapter 3, I aim to answer how cholinergic neurons affect the hippocampal activity during reward location learning depending on the behavioural phase of the learning task. The optogenetic stimulation of the cholinergic MS neurons affected spatial learning only when applied at the goal location but not when applied during navigation. These two phases of the task correspond to different hippocampal states. At the goal location, the CA1 activity favoured the occurrence of SWRs. Cholinergic activation during that state suppressed their incidence. Therefore, the study gives corroborating evidence for a role of SWRs in memory encoding (Girardeau et al., 2009; Jadhav et al., 2012; Ego-Stengel and Wilson, 2010). Optogenetic stimulation of the cholinergic neurons during navigation did not affect the learning, possibly because the cholinergic level was already naturally high. These results emphasise the need for precise timing

of the cholinergic release, which is high during navigation but needs to be low to allow memory encoding during SWRs.

In Chapter 4, I find that the memory of reward location is encoded both in the activity of dCA1 and iCA1 cells. By comparing the activity at multiple reward locations over an extended period of time, I address the question of whether the same cells encode the memory of reward independently of its location. This form of encoding was proposed as a general form of reward memory in the hippocampus that could be unambiguously relayed downstream of the hippocampus (Gauthier and Tank, 2018). I found such representations in the iCA1. Its cells target specific brain areas outside of the hippocampus (Ciocchi et al., 2015) and therefore might be well suited to relay the reward memory information. For example, specific intermediate and ventral CA1 projections to the nucleus accumbens and to the lateral septum were suggested to convey reward-related signals and were found to regulate reward-seeking (Britt et al., 2012; Ito et al., 2008; Ciocchi et al., 2015; LeGates et al., 2018; Kosugi et al., 2021). In contrast, the dCA1 activity encoded the memory location by an increase in overall population activity. The findings support a hypothesis that the memory network for reward in dCA1 involves a changing subset of place cells, and the increased activity of its entire population could serve to relay such signal.

5.2 Validity of the approach

5.2.1 A multitude of behavioural factors affecting the CA1 activity

Chapters 3 and 4 integrate observations from animal behaviour and the co-occurring CA1 activity. There are multiple factors in the animal's experience that could have contributed to the activity. For example, hippocampal activity is modulated by movement speed (Buzsáki et al., 1983) and odours (Keinath et al., 2014). To minimise the impact of factors unrelated to the animal's location on the maze and its distance from the reward, I averaged the activity recorded from multiple trials. Averaging ensures that

the neural correlates include only behavioural factors that are repeated consistently at a given location or at a defined time period during the task.

In Chapter 3, I focused on the activity during immobility at the reward when SWRs are known to occur (Csicsvari et al., 2007; O'Neill et al., 2006). I summarised these effects by calculating SWRs incidence and PSD of the LFP during the corresponding task phase. Averaging the signal over the entire time period at the reward diminishes the impact of brief changes due to the animal's behaviour.

In Chapter 4, I focused on the factors that related to the animal's mobility, its location, and its distance from the learned reward location. Factors that could have contributed to the activity during repeated approaches to the reward include olfactory cues, for which I controlled in unbaited test trials. Mice decelerating before the reward could also affect the activity; however, this factor can not explain the differential effect on dCA1 and iCA1 activity. Finally, there might be other relevant behavioural factors that I failed to observe. These, as discussed above, would need to consistently differ between the mice groups to explain the differential effects. Such differential effects are unlikely, and I reason the changes in the hippocampal activity after learning of reward location were due to its memory.

5.2.2 Limitations of the findings

In Chapter 3, the optogenetic stimulation of the MS decreased incidence of SWRs at the reward location. It is possible that this decrease did not directly lead to the memory impairment. There are several non-hippocampal mechanisms that could have contributed to the memory effects and I discuss these in the following section. Nevertheless, given that learning spatial location on the Y-maze depends on the hippocampus and given evidence from other studies on the role of SWRs in memory formation (Girardeau et al., 2009; Fernández-Ruiz et al., 2019), the decreased SWRs incidence likely contributed to the effects on learning the reward location.

Chapter 4 shows that both the dCA1 and iCA1 activity anticipated the reward location. The activity correlated with the approach to the reward location after learning, and could not be explained by olfactory cues of the reward. Also, the fact

the activity changed after the animals learned the location and that the changes to dCA1 and iCA1 activity were different suggests these changes are not directly related to running, deceleration or other type of movement at reward. Multiple brain areas increase their activity in anticipation of reward, including striatum (Hollerman et al., 1998; Hassani et al., 2001), orbitofrontal cortex (Schoenbaum et al., 1998; Tremblay and Schultz, 1999) and amygdala (Schoenbaum et al., 1998). Their activity scales with the reward, and, similarly can not be solely explained by movement. Therefore, the sources and function of the anticipatory signals in these brain areas could be related to the ones observed in dCA1 and iCA1. In addition, it is not clear whether the anticipatory activity in dCA1 or iCA1 is required for the expression of reward location memory or some other aspects of reward-approach behaviour.

5.2.3 Evidence from optogenetic modulation of the medial septum

Optogenetic stimulation selectively modulates the activity of cells expressing a light-sensitive opsin. In this work, I used optogenetic stimulation to excite cholinergic neurons expressing ChR2. In the sampled cells, the ChR2 expression was limited to the cholinergic neurons. The direct excitation by the stimulation was further restricted to the MS by a limited spread of light from the optic fibre. The specificity of the optogenetic method due to selective expression of the opsin much improves on that of the experimental methods commonly used in the past such as electrical stimulation or local lesions or ablation of cell bodies.

Optogenetic stimulation controlled the cholinergic neurons firing with high temporal precision. However, the cholinergic release operates in slower timescales. First, the action of muscarinic receptors is slow (Thiele, 2013). Second, it is possible that the released ACh remained extracellularly following the termination of light stimulation. Nevertheless, this limited precision allowed me to dissociate the contributions of different phases on memory processes during learning. This is because the effects of the optogenetic stimulation on the ACh release were time-limited as seen in the short delay between the stimulation termination and fast return of the baseline level

multi-unit activity in the MS of urethane anaesthetised mice and in the time-limited effects on SWR incidence in sleeping mice.

Lastly, I can not exclude that the learning impairment was caused by an independent of the hippocampus change. The optic fibre was placed above the MS neurons and led to stimulation of the cholinergic neurons regardless of their axonal projections. The stimulated neurons could affect the local MS circuits and their downstream targets. MS neurons project to multiple targets, including the medial EC, prefrontal cortex and primary visual cortex (Li et al., 2018). Therefore, it is possible these structures contributed to the behavioural effects or were primarily responsible for the impairment. Additionally, the within-hippocampal effects of the cholinergic activation could extend beyond SWRs, and include changes in synaptic transmission or synaptic plasticity (Hasselmo, 2006). Either could impair the learning.

5.2.4 Evidence from one-photon calcium imaging

One-photon calcium imaging has limited sensitivity and accuracy when applied to recording neural activity. Its limitations do not invalidate the presented findings, and I discuss their possible impact.

Sensitivity of detecting neural activity

Neuronal spiking leads to fluorescent changes in the calcium reporter GCaMP6f (Chen et al., 2013). The fluorescence is visible in the soma within several milliseconds after an action potential and decays over tens of milliseconds (Chen et al., 2013). When multiple action potentials fire, the fluorescence scales non-linearly. The exact magnitude of the scaling can vary depending on the cell type and its state (Climer and Dombeck, 2021). Therefore, the action potentials can not be precisely decoded from the signal (Huang et al., 2021). Additionally, a single action potential might pass undetected (Huang et al., 2021).

The problems with the detection of individual spikes and the non-linearity of the signal affect the precision of the reported spatial and reward coding. For example, the metrics calculated from the calcium fluorescence are known to underestimate

the spatial information of place cells (Climer and Dombeck, 2021). Therefore, I draw limited conclusions from the lack of observed differences in the coding of spatial information by dCA1 and iCA1 place cells.

Accuracy of activity source identification

The imaged cells can have overlapping cell bodies because the 3-dimensional imaged volume is projected onto a 2-dimensional image. Additionally, out-of-focus fluorescence will result in blurred changes in the image. The image processing methods I used aimed to address these two issues (Giovannucci et al., 2019). First, the use of constrained non-negative matrix factorisation isolates sources of fluorescence that have overlapping ROIs (Pnevmatikakis et al., 2016). As a result, the fluorescence changes can be attributed to specific cells that can have overlapping cell bodies. Second, the background fluorescence changes are explicitly modelled and their influence excluded from the neuronal signal (Giovannucci et al., 2019).

The two computational methods minimise the errors related to the identification of fluorescence sources; however, they can not eliminate them completely. Therefore, the resulting deconvolved signal can misattribute activity between cells. Such errors should not affect the reported conclusions as the non-biased addition of the other-cell signal can only limit the specificity of a place cell or its reward coding. The limited specificity did not obscure the findings about specific cells anticipating the reward in the iCA1. Similarly, it should not obscure the evidence for the absence of a sizeable population of goal-specific cells.

Precision of cell registration

I matched the identity of cells recorded on different days to analyse how they remap after the mice learned changed reward locations. It is possible that some cells were matched incorrectly. A consequence of such error is the randomisation of the cell's activity. For example, a place field assigned to a cell on one day could have been completely different on another day. The cell registration for the dCA1 and iCA1 cells used the same algorithm, therefore any such errors would not affect their comparison.

Another type of error could be that the same cell was not identified as such. This error would only limit the number of available data used to draw the conclusions, without biasing the comparison between dCA1 and iCA1.

Brain tissue damage due to surgical procedures

To image from the CA1 pyramidal neurons, I implanted an optical lens above CA1. Implantation damaged the brain tissue above that region. Previous work has found that hippocampal activity as observed in place cell responses was not different from that measured by less invasive electrophysiological techniques (Ziv et al., 2013). Implantation of the lens above the dCA1 and iCA1 damaged different regions. However, the damage did not affect the learning or the locomotion between the two animal groups differently.

5.3 Conclusions and perspective

This thesis provides further insights into the mechanisms that support memory encoding and its later recall. For memory encoding, the results highlight the importance of the timing of cholinergic activity aligned to the animal's behavioural state. During the memory encoding at the reward location, this requires the occurrence of SWRs. Further research could confirm if the cholinergic stimulation could similarly impair learning when applied during the memory consolidation stage in sleeping animals, and whether the high cholinergic level is required during the navigational phase.

Memory of reward changes the hippocampal representations both in the dorsal and intermediate CA1. The presented results demonstrate that the activity of both encodes and anticipates the reward location. The identified encoding of reward memory persisted across multiple reward locations and over an extended time. Therefore, it could provide a time and location-invariant signal to direct the navigation. Further studies will be required to determine whether the reward-anticipatory signals in dCA1 and iCA1 have a causal role in navigation and whether they affect activity downstream of the hippocampus. The hippocampal reward-predictive signals could be important

for learning and choosing appropriate actions during reward-guided navigation as they are in reinforcement learning models (Foster et al., 2000; Sutton and Barto, 2018).

References

(2007). The nucleus accumbens as part of a basal ganglia action selection circuit. *Psychopharmacology*, 191(3):521–550.

(2017). Gamma oscillations organize top-down signalling to hypothalamus and enable food seeking. *Nature*, 542(7640):232–236.

Aigner, T. G., Walker, D. L., and Mishkin, M. (1991). Comparison of the effects of scopolamine administered before and after acquisition in a test of visual recognition memory in monkeys. *Behavioral and Neural Biology*, 55(1):61–67.

Akrami, A., Kopec, C. D., Diamond, M. E., and Brody, C. D. (2018). Posterior parietal cortex represents sensory history and mediates its effects on behaviour. *Nature*, 554(7692):368–372.

Alvarez, P. and Squire, L. R. (1994). Memory consolidation and the medial temporal lobe: a simple network model. *Proceedings of the National Academy of Sciences*, 91(15):7041–5.

Amaral, D. and Witter, M. (1989). The three-dimensional organization of the hippocampal formation: A review of anatomical data. *Neuroscience*, 31(3):571–591.

Ambrose, R. E., Pfeiffer, B. E., and Foster, D. J. (2016). Reverse replay of hippocampal place cells is uniquely modulated by changing reward. *Neuron*, 91(5):1124–1136.

Andersen, P., Blackstad, T. W., and Lömo, T. (1966). Location and identification of excitatory synapses on hippoeampal pyramidal cells. *Experimental Brain Research*, 1(3):236–248.

Andersen, P., Sandberg, S. H., Sveen, O., and Wigstrom, H. (1977). Specific long-lasting potentiation of synaptic transmission in hippocampal slices. *Nature*, 266(5604):736–737.

Annese, J., Schenker-Ahmed, N. M., Bartsch, H., Maechler, P., Sheh, C., Thomas, N., Kayano, J., Ghatan, A., Bresler, N., Frosch, M. P., Klaming, R., and Corkin, S. (2014). Postmortem examination of patient H.M.'s brain based on histological sectioning and digital 3D reconstruction. *Nature Communications*, 5(1):3122.

Arleo, A. and Gerstner, W. (2000). Spatial cognition and neuro-mimetic navigation: a model of hippocampal place cell activity. *Biological Cybernetics*, 83(3):287–299.

Atherton, L. A., Dupret, D., and Mellor, J. R. (2015). Memory trace replay: the shaping of memory consolidation by neuromodulation. *Trends in Neurosciences*, 38(9):560–570.

Atri, A., Sherman, S., Norman, K. A., Kirchhoff, B. A., Nicolas, M. M., Greicius, M. D., Cramer, S. C., Breiter, H. C., Hasselmo, M. E., and Stern, C. E. (2004). Blockade of central cholinergic receptors impairs new learning and increases proactive interference in a word paired-associate memory task. *Behavioral Neuroscience*, 118(1):223.

Auerbach, J. M. and Segal, M. (1994). A novel cholinergic induction of long-term potentiation in rat hippocampus. *Journal of Neurophysiology*, 72(4):2034–2040.

Auerbach, J. M. and Segal, M. (1996). Muscarinic receptors mediating depression and long-term potentiation in rat hippocampus. *Journal of Physiology*, 492(Pt 2):479–493.

Avi, K., David, T., S., R. B., M., A. J. J., and Dov, S. (1994). Dependence on REM Sleep of Overnight Improvement of a Perceptual Skill. *Science*, 265(5172):679–682.

Banino, A., Barry, C., Uria, B., Blundell, C., Lillicrap, T., Mirowski, P., Pritzel, A., Chadwick, M. J., Degris, T., Modayil, J., Wayne, G., Soyer, H., Viola, F., Zhang, B., Goroshin, R., Rabinowitz, N., Pascanu, R., Beattie, C., Petersen, S., Sadik, A., Gaffney, S., King, H., Kavukcuoglu, K., Hassabis, D., Hadsell, R., and Kumaran, D. (2018). Vector-based navigation using grid-like representations in artificial agents. *Nature*, 557(7705):429–433.

Bannerman, D. M., Bus, T., Taylor, A., Sanderson, D. J., Schwarz, I., Jensen, V., Hvalby, Ø., Rawlins, J. N. P., Seeburg, P. H., and Sprengel, R. (2012). Dissecting spatial knowledge from spatial choice by hippocampal NMDA receptor deletion. *Nature Neuroscience*, 15(8):1153–1159.

Bannerman, D. M., Rawlins, J. N. P., McHugh, S. B., Deacon, R. M. J., Yee, B. K., Bast, T., Zhang, W.-N., Pothuizen, H. H. J., and Feldon, J. (2004). Regional dissociations within the hippocampus—memory and anxiety. *Neuroscience & Biobehavioral Reviews*, 28(3):273–283.

Bannerman, D. M., Yee, B. K., Good, M. A., Heupel, M. J., Iversen, S. D., and Rawlins, J. N. P. (1999). Double dissociation of function within the hippocampus: A comparison of dorsal, ventral, and complete hippocampal cytotoxic lesions. *Behavioral Neuroscience*, 113(6):1170–1188.

Barry, C., Hayman, R., Burgess, N., and Jeffery, K. J. (2007). Experience-dependent rescaling of entorhinal grids. *Nature Neuroscience*, 10(6):682–684.

Bast, T., Wilson, I. A., Witter, M. P., and Morris, R. G. M. (2009). From rapid place learning to behavioral performance: A key role for the intermediate hippocampus. *PLOS Biology*, 7(4):e1000089.

Benchenane, K., Peyrache, A., Khamassi, M., Tierney, P. L., Gioanni, Y., Battaglia, F. P., and Wiener, S. I. (2010). Coherent theta oscillations and reorganization of spike timing in the hippocampal-prefrontal network upon learning. *Neuron*, 66(6):921–936.

Bi, G. Q. and Poo, M. M. (1998). Synaptic modifications in cultured hippocampal neurons: dependence on spike timing, synaptic strength, and postsynaptic cell type. *Journal of Neuroscience*, 18(24):10464–10472.

Bicanski, A. and Burgess, N. (2020). Neuronal vector coding in spatial cognition. *Nature Reviews Neuroscience*, 21(9):453–470.

Bliss, T. V. P. and Collingridge, G. L. (1993). A synaptic model of memory: long-term potentiation in the hippocampus. *Nature*, 361(6407):31–39.

Bliss, T. V. P. and Lømo, T. (1973). Long-lasting potentiation of synaptic transmission in the dentate area of the anaesthetized rabbit following stimulation of the perforant path. *Journal of Physiology*, 232(2):331–356.

Boccara, C. N., Nardin, M., Stella, F., O'Neill, J., and Csicsvari, J. (2019). The entorhinal cognitive map is attracted to goals. *Science*, 363(6434):1443–1447.

Bragin, A., Jando, G., Nadasdy, Z., Hetke, J., Wise, K., and Buzsaki, G. (1995). Gamma (40-100 Hz) oscillation in the hippocampus of the behaving rat. *Journal of Neuroscience*, 15(1):47–60.

Britt, J. P., Benaliouad, F., Mcdevitt, R. A., Stuber, G. D., Wise, R. A., and Bonci, A. (2012). Synaptic and behavioral profile of multiple glutamatergic inputs to the nucleus accumbens. *Neuron*, 76(4):790–803.

Brzosko, Z., Mierau, S. B., and Paulsen, O. (2019). Neuromodulation of spike-timing-dependent plasticity: past, present, and future. *Neuron*, 103(4):563–581.

Brzosko, Z., Zannone, S., Schultz, W., Clopath, C., and Paulsen, O. (2017). Sequential neuromodulation of Hebbian plasticity offers mechanism for effective reward-based navigation. *eLife*, 6.

Burgess, N. and O'Keefe, J. (1996). Neuronal computations underlying the firing of place cells and their role in navigation. *Hippocampus*, 6(6):749–62.

Bush, D., Barry, C., Manson, D., and Burgess, N. (2015). Using grid cells for navigation. *Neuron*, 87(3):507–520.

Butler, W. M., Hardcastle, K., and Giocomo Lisa, M. (2019). Remembered reward locations restructure entorhinal spatial maps. *Science*, 363(6434):1447–1452.

Buzsáki, G. (1986). Hippocampal sharp waves: Their origin and significance. *Brain Research*, 398(2):242–252.

Buzsáki, G. (1989). Two-stage model of memory trace formation: A role for "noisy" brain states. *Neuroscience*, 31(3):551–570.

Buzsáki, G. (2002). Theta oscillations in the hippocampus. *Neuron*, 33(3):325–340.

Buzsáki, G. (2015). Hippocampal sharp wave-ripple: A cognitive biomarker for episodic memory and planning. *Hippocampus*, 25(10):1073–1188.

Buzsáki, G., Anastassiou, C. A., and Koch, C. (2012). The origin of extracellular fields and currents — EEG, ECoG, LFP and spikes. *Nature Reviews Neuroscience*, 13(6):407–420.

Buzsaki, G., Horvath, Z., Urioste, R., Hetke, J., and Wise, K. (1992). High-frequency network oscillation in the hippocampus. *Science*, 256(5059):1025–1027.

Buzsáki, G., Lai-Wo S., L., and Vanderwolf, C. H. (1983). Cellular bases of hippocampal EEG in the behaving rat. *Brain Research Reviews*, 6(2):139–171.

Buzsáki, G. and Tingley, D. (2018). Space and time: the hippocampus as a sequence generator. *Trends in Cognitive Sciences*, 22(10):853–869.

Cacucci, F., Wills, T. J., Lever, C., Giese, K. P., and O'Keefe, J. (2007). Experience-dependent increase in CA1 place cell spatial information, but not spatial reproducibility, is dependent on the autophosphorylation of the α-Isoform of the calcium/calmodulin-dependent protein kinase II. *Journal of Neuroscience*, 27(29):7854–7859.

Cembrowski, M. S., Bachman, J. L., Wang, L., Sugino, K., Shields, B. C., and Spruston, N. (2016). Spatial gene-expression gradients underlie prominent heterogeneity of CA1 pyramidal neurons. *Neuron*, 89(2):351–368.

Cenquizca, L. A. and Swanson, L. W. (2007). Spatial organization of direct hippocampal field CA1 axonal projections to the rest of the cerebral cortex.

Chadwick, A., van Rossum, M. C. W., and Nolan, M. F. (2015). Independent theta phase coding accounts for CA1 population sequences and enables flexible remapping. *eLife*, 4:e03542.

Chen, T.-W., Wardill, T. J., Sun, Y., Pulver, S. R., Renninger, S. L., Baohan, A., Schreiter, E. R., Kerr, R. a., Orger, M. B., Jayaraman, V., Looger, L. L., Svoboda, K., and Kim, D. S. (2013). Ultrasensitive fluorescent proteins for imaging neuronal activity. *Nature*, 499(7458):295–300.

Cheng, S. and Frank, L. M. (2008). New experiences enhance coordinated neural activity in the hippocampus. *Neuron*, 57(2):303–313.

Chrobak, J. J. and Buzsaki, G. (1994). Selective activation of deep layer (V-VI) retrohippocampal cortical neurons during hippocampal sharp waves in the behaving rat. *Journal of Neuroscience*, 14(10):6160–6170.

Chrobak, J. J. and Buzsáki, G. (1996). High-frequency oscillations in the output networks of the hippocampal–entorhinal axis of the freely behaving rat. *Journal of Neuroscience*, 16(9):3056–3066.

Ciocchi, S., Passecker, J., Malagon-Vina, H., Mikus, N., and Klausberger, T. (2015). Selective information routing by ventral hippocampal CA1 projection neurons. *Science*, 348(6234):560–563.

Climer, J. R. and Dombeck, D. A. (2021). Information theoretic approaches to deciphering the neural code with functional fluorescence imaging. *eNeuro*, 8(5):ENEURO.0266–21.2021.

Colgin, L. L. (2013). Mechanisms and functions of theta rhythms. *Annual Review of Neuroscience*, 36(1):295–312.

Contreras, M., Pelc, T., Llofriu, M., Weitzenfeld, A., and Fellous, J. (2018). The ventral hippocampus is involved in multi-goal obstacle-rich spatial navigation. *Hippocampus*, 28(12):853–866.

Csicsvari, J., Hirase, H., Czurkó, A., Mamiya, A., and Buzsáki, G. (1999). Oscillatory coupling of hippocampal pyramidal cells and interneurons in the behaving rat. *Journal of Neuroscience*, 19(1):274–287.

Csicsvari, J., Jamieson, B., Wise, K. D., and Buzsáki, G. (2003). Mechanisms of gamma oscillations in the hippocampus of the behaving rat. *Neuron*, 37(2):311–322.

Csicsvari, J., O'Neill, J., Allen, K., and Senior, T. (2007). Place-selective firing contributes to the reverse-order reactivation of CA1 pyramidal cells during sharp waves in open-field exploration. *European Journal of Neuroscience*, 26(3):704–716.

Dana, H., Chen, T.-W., Hu, A., Shields, B. C., Guo, C., Looger, L. L., Kim, D. S., and Svoboda, K. (2014). Thy1-GCaMP6 transgenic mice for neuronal population imaging in vivo. *PLoS ONE*, 9(9):e108697.

Danielson, N. B., Zaremba, J. D., Kaifosh, P., Bowler, J., Ladow, M., and Losonczy, A. (2016). Sublayer-specific coding dynamics during spatial navigation and learning in hippocampal area CA1. *Neuron*, 91(3):652–665.

Davidson, T. J., Kloosterman, F., and Wilson, M. A. (2009). Hippocampal replay of extended experience. *Neuron*, 63(4):497–507.

Davis, E. A., Liu, C. M., Gianatiempo, I. H., Suarez, A. N., Cortella, A. M., Hahn, J. D., and Kanoski, S. E. (2020). Hippocampus-lateral septum circuitry mediates foraging-related spatial memory in rats. *bioRxiv*, page 2020.06.16.155721.

Denny, C. A., Kheirbek, M. A., Alba, E. L., Tanaka, K. F., Brachman, R. A., Laughman, K. B., Tomm, N. K., Turi, G. F., Losonczy, A., and Hen, R. (2014). Hippocampal memory traces are differentially modulated by experience, time, and adult neurogenesis. *Neuron*, 83(1):189–201.

Deshmukh, S. S. and Knierim, J. J. (2013). Influence of local objects on hippocampal representations: Landmark vectors and memory. *Hippocampus*, 23(4):253–267.

Diba, K. and Buzsáki, G. (2007). Forward and reverse hippocampal place-cell sequences during ripples. *Nature Neuroscience*, 10(10):1241–1242.

Dine, J., Genewsky, A., Hladky, F., Wotjak, C. T., Deussing, J. M., Zieglgänsberger, W., Chen, A., and Eder, M. (2016). Local Optogenetic Induction of Fast (20–40 Hz) Pyramidal-Interneuron Network Oscillations in the In Vitro and In Vivo CA1 Hippocampus: Modulation by CRF and Enforcement of Perirhinal Theta Activity. *Frontiers in Cellular Neuroscience*, 10.

Dolorfo, C. L. and Amaral, D. G. (1998a). Entorhinal cortex of the rat: Organization of intrinsic connections. *Journal of Comparative Neurology*, 398(1):49–82.

Dolorfo, C. L. and Amaral, D. G. (1998b). Entorhinal cortex of the rat: Topographic organization of the cells of origin of the perforant path projection to the dentate gyrus. *Journal of Comparative Neurology*, 398(1):25–48.

Dong, H.-W., Swanson, L. W., Chen, L., Fanselow, M. S., and Toga, A. W. (2009). Genomic–anatomic evidence for distinct functional domains in hippocampal field CA1. *Proceedings of the National Academy of Sciences*, 106(28):11794–11799.

Donoghue, T., Haller, M., Peterson, E. J., Varma, P., Sebastian, P., Gao, R., Noto, T., Lara, A. H., Wallis, J. D., Knight, R. T., Shestyuk, A., and Voytek, B. (2020). Parameterizing neural power spectra into periodic and aperiodic components. *Nature Neuroscience*, 23(12):1655–1665.

Dudai, Y. (2012). The restless engram: consolidations never end. *Annual review of neuroscience*, 35:227–47.

Dupret, D., O'Neill, J., Pleydell-Bouverie, B., and Csicsvari, J. (2010). The reorganization and reactivation of hippocampal maps predict spatial memory performance. *Nature Neuroscience*, 13(8):995–1002.

Duvelle, É., Grieves, R. M., Hok, V., Poucet, B., Arleo, A., Jeffery, K., and Save, E. (2019). Insensitivity of place cells to the value of spatial goals in a two-choice flexible navigation task. *Journal of Neuroscience*, 39:1578–18.

Ego-Stengel, V. and Wilson, M. A. (2010). Disruption of ripple-associated hippocampal activity during rest impairs spatial learning in the rat. *Hippocampus*, 20(1):1–10.

Eichenbaum, H. and Cohen, N. J. (2014). Can we reconcile the declarative memory and spatial navigation views on hippocampal function? *Neuron*, 83(4):764–770.

English, D. F., Peyrache, A., Stark, E., Roux, L., Vallentin, D., Long, M. A., and Buzsáki, G. (2014). Excitation and inhibition compete to control spiking during hippocampal ripples: Intracellular study in behaving mice. *Journal of Neuroscience*, 34(49):16509–16517.

Erdem, U. M. and Hasselmo, M. (2012). A goal-directed spatial navigation model using forward trajectory planning based on grid cells. *European Journal of Neuroscience*, 35(6):916–931.

Eschenko, O., Ramadan, W., Molle, M., Born, J., and Sara, S. J. (2008). Sustained increase in hippocampal sharp-wave ripple activity during slow-wave sleep after learning. *Learning & Memory*, 15(4):222–228.

Fadda, F., Cocco, S., and Stancampiano, R. (2000). Hippocampal acetylcholine release correlates with spatial learning performance in freely moving rats. *Neuroreport*, 11(10):2265–2269.

Fadel, J. R. (2011). Regulation of cortical acetylcholine release: Insights from in vivo microdialysis studies. *Behavioural Brain Research*, 221(2):527–536.

Fanselow, M. S. and Dong, H.-W. (2010). Are the dorsal and ventral hippocampus functionally distinct structures? *Neuron*, 65(1):7–19.

Fellous, J.-M. and Sejnowski, T. J. (2000). Cholinergic induction of oscillations in the hippocampal slice in the slow (0.5–2 Hz), theta (5–12 Hz), and gamma (35–70 Hz) bands. *Hippocampus*, 10(2):187–197.

Fernández-Ruiz, A., Oliva, A., Fermino de Oliveira, E., Rocha-Almeida, F., Tingley, D., and Buzsáki, G. (2019). Long-duration hippocampal sharp wave ripples improve memory. *Science*, 364(6445):1082–1086.

Fernández-Ruiz, A., Oliva, A., Nagy, G. A., Maurer, A. P., Berényi, A., and Buzsáki, G. (2017). Entorhinal-CA3 dual-input control of spike timing in the hippocampus by theta-gamma coupling. *Neuron*, 93(5):1213–1226.e5.

Fiete, I. R., Burak, Y., and Brookings, T. (2008). What grid cells convey about rat location. *Journal of Neuroscience*, 28(27):6858–6871.

Fisahn, A., Pike, F. G., Buhl, E. H., and Paulsen, O. (1998). Cholinergic induction of network oscillations at 40 Hz in the hippocampus in vitro. *Nature*, 394(6689):186–189.

Floresco, S. B. (2015). The Nucleus Accumbens: An Interface Between Cognition, Emotion, and Action. *Annual Review of Psychology*, 66(1):25–52.

Foster, D., Morris, R., and Dayan, P. (2000). A model of hippocampally dependent navigation, using the temporal difference learning rule. *Hippocampus*, 10(1):1–16.

Foster, D. J. and Wilson, M. A. (2006). Reverse replay of behavioural sequences in hippocampal place cells during the awake state. *Nature*, 440(7084):680–683.

Frank, L. M., Brown, E. N., and Wilson, M. (2000). Trajectory encoding in the hippocampus and entorhinal cortex. *Neuron*, 27(1):169–178.

Fries, P. (2015). Rhythms for cognition: Communication through coherence. *Neuron*, 88(1):220–235.

Gauthier, J. L. and Tank, D. W. (2018). A dedicated population for reward coding in the hippocampus. *Neuron*, 99(1):179–193.e7.

Gergues, M. M., Han, K. J., Choi, H. S., Brown, B., Clausing, K. J., Turner, V. S., Vainchtein, I. D., Molofsky, A. V., and Kheirbek, M. A. (2020). Circuit and molecular architecture of a ventral hippocampal network. *Nature Neuroscience*, 23(11):1444–1452.

Ghosh, K. K., Burns, L. D., Cocker, E. D., Nimmerjahn, A., Ziv, Y., Gamal, A. E., and Schnitzer, M. J. (2011). Miniaturized integration of a fluorescence microscope. *Nature Methods*, 8(10):871–878.

Giovannini, M. G., Rakovska, A., Benton, R. S., Pazzagli, M., Bianchi, L., and Pepeu, G. (2001). Effects of novelty and habituation on acetylcholine, GABA, and glutamate release from the frontal cortex and hippocampus of freely moving rats. *Neuroscience*, 106(1):43–53.

Giovannucci, A., Friedrich, J., Gunn, P., Kalfon, J., Brown, B. L., Koay, S. A., Taxidis, J., Najafi, F., Gauthier, J. L., Zhou, P., Khakh, B. S., Tank, D. W., Chklovskii, D. B., and Pnevmatikakis, E. A. (2019). CaImAn an open source tool for scalable calcium imaging data analysis. *eLife*, 8:e38173.

Girardeau, G., Benchenane, K., Wiener, S. I., Buzsáki, G., and Zugaro, M. B. (2009). Selective suppression of hippocampal ripples impairs spatial memory. *Nature Neuroscience*, 12(10):1222–1223.

Gogolák, G., Stumpf, C., Petsche, H., and S ̌terc, J. (1968). The firing pattern of septal neurons and the form of the hippocampal theta wave. *Brain Research*, 7(2):201–207.

Graves, L., Pack, A., and Abel, T. (2001). Sleep and memory: a molecular perspective. *Trends in Neurosciences*, 24(4):237–243.

Green, J. D. and Arduini, A. A. (1954). Hippocampal electrical activity in arousal. *Journal of Neurophysiology*, 17(6):533–557.

Gupta, A. S., van der Meer, M. A. A., Touretzky, D. S., and Redish, A. D. (2012). Segmentation of spatial experience by hippocampal theta sequences. *Nature Neuroscience*, 15(7):1032–1039.

Haam, J. and Yakel, J. L. (2017). Cholinergic modulation of the hippocampal region and memory function. *Journal of Neurochemistry*, 142(S2):111–121.

Hafting, T., Fyhn, M., Molden, S., Moser, M.-B., and Moser, E. I. (2005). Microstructure of a spatial map in the entorhinal cortex. *Nature*, 436(7052):801–806.

Hainmueller, T. and Bartos, M. (2018). Parallel emergence of stable and dynamic memory engrams in the hippocampus. *Nature*, 558(7709):292–296.

Harland, B., Contreras, M., Souder, M., and Fellous, J.-M. (2021). Dorsal CA1 hippocampal place cells form a multi-scale representation of megaspace. *Current Biology*, 31(10):2178–2190.e6.

Hassani, O. K., Cromwell, H. C., and Schultz, W. (2001). Influence of Expectation of Different Rewards on Behavior-Related Neuronal Activity in the Striatum. *Journal of Neurophysiology*, 85(6):2477–2489.

Hasselmo, M. E. (1999). Neuromodulation: acetylcholine and memory consolidation. *Trends in Cognitive Sciences*, 3(9):351–359.

Hasselmo, M. E. (2006). The role of acetylcholine in learning and memory. *Current Opinion in Neurobiology*, 16(6):710–715.

Hasselmo, M. E. and Fehlau, B. P. (2001). Differences in time course of ACh and GABA modulation of excitatory synaptic potentials in slices of rat hippocampus. *Journal of Neurophysiology*, 86(4):1792–1802.

Hasselmo, M. E. and Sarter, M. (2011). Modes and models of forebrain cholinergic neuromodulation of cognition. *Neuropsychopharmacology*, 36(1):52–73.

Hebb, D. O. (1949). The Organization of Behavior. *The Organization of Behavior*, 911(1):335.

Henriksen, E. J., Colgin, L. L., Barnes, C. A., Witter, M. P., Moser, M.-B., and Moser, E. I. (2010). Spatial representation along the proximodistal axis of CA1. *Neuron*, 68(1):127–137.

Hill, A. J. (1978). First occurrence of hippocampal spatial firing in a new environment. *Experimental Neurology*, 62(2):282–297.

Hok, V., Lenck-Santini, P.-P., Roux, S., Save, E., Muller, R. U., and Poucet, B. (2007). Goal-related activity in hippocampal place cells. *Journal of Neuroscience*, 27(3):472–482.

Hollerman, J. R., Tremblay, L., and Schultz, W. (1998). Influence of Reward Expectation on Behavior-Related Neuronal Activity in Primate Striatum. *Journal of Neurophysiology*, 80(2):947–963.

Hoover, W. B. and Vertes, R. P. (2007). Anatomical analysis of afferent projections to the medial prefrontal cortex in the rat. *Brain Structure and Function*, 212(2):149–179.

Huang, L., Ledochowitsch, P., Knoblich, U., Lecoq, J., Murphy, G. J., Reid, C., de Vries, S. E. J., Koch, C., Zeng, H., Buice, M. A., Waters, J., and Li, L. (2021). Relationship between simultaneously recorded spiking activity and fluorescence signal in GCaMP6 transgenic mice. *eLife*, 10:e51675.

Hunsaker, M. R. and Kesner, R. P. (2008). Dissociations across the dorsal–ventral axis of CA3 and CA1 for encoding and retrieval of contextual and auditory-cued fear. *Neurobiology of Learning and Memory*, 89(1):61–69.

Ito, R., Robbins, T. W., Pennartz, C. M., and Everitt, B. J. (2008). Functional interaction between the hippocampus and nucleus accumbens shell is necessary for the acquisition of appetitive spatial context conditioning. *Journal of Neuroscience*, 28(27):6950–6959.

Jacobson, L. and Sapolsky, R. (1991). The role of the hippocampus in feedback regulation of the hypothalamic-pituitary-adrenocortical axis. *Endocrine Reviews*, 12(2):118–134.

Jadhav, S. P., Kemere, C., German, P. W., and Frank, L. M. (2012). Awake hippocampal sharp-wave ripples support spatial memory. *Science*, 336(6087):1454–1458.

Jadhav, S. P., Rothschild, G., Roumis, D. K., and Frank, L. M. (2016). Coordinated Excitation and Inhibition of Prefrontal Ensembles during Awake Hippocampal Sharp-Wave Ripple Events. *Neuron*, 90(1):113–127.

Jarzebowski, P., Hay, Y. A., Grewe, B. F., and Paulsen, O. (2021a). Different encoding of reward location in dorsal and ventral hippocampus. *bioRxiv*, page 2021.09.07.459245.

Jarzebowski, P., Tang, C. S., Paulsen, O., and Hay, Y. A. (2021b). Impaired spatial learning and suppression of sharp wave ripples by cholinergic activation at the goal location. *eLife*, 10:e65998.

Jeffreys, H. (1961). Theory of probability (Third ed.). In *University Press, Oxford, England*.

Jezek, K., Henriksen, E. J., Treves, A., Moser, E. I., and Moser, M.-B. (2011). Theta-paced flickering between place-cell maps in the hippocampus. *Nature*, 478(7368):246–249.

Jimenez, J. C., Su, K., Goldberg, A. R., Luna, V. M., Biane, J. S., Ordek, G., Zhou, P., Ong, S. K., Wright, M. A., Zweifel, L., Paninski, L., Hen, R., and Kheirbek, M. A. (2018). Anxiety cells in a hippocampal-hypothalamic circuit. *Neuron*, 97(3):670–683.e6.

Jin, S.-W. and Lee, I. (2021). Differential encoding of place value between the dorsal and intermediate hippocampus. *Current Biology*, 31(14):3053–3072.e5.

Jing, M., Li, Y., Zeng, J., Huang, P., Skirzewski, M., Kljakic, O., Peng, W., Qian, T., Tan, K., Zou, J., Trinh, S., Wu, R., Zhang, S., Pan, S., Hires, S. A., Xu, M., Li, H., Saksida, L. M., Prado, V. F., Bussey, T. J., Prado, M. A. M., Chen, L., Cheng, H., and Li, Y. (2020). An optimized acetylcholine sensor for monitoring in vivo cholinergic activity. *Nature Methods*, 17(11):1139–1146.

Jones, M. W. and Wilson, M. A. (2005). Theta rhythms coordinate hippocampal–prefrontal interactions in a spatial memory task. *PLOS Biology*, 3(12):e402.

Joo, H. R. and Frank, L. M. (2018). The hippocampal sharp wave–ripple in memory retrieval for immediate use and consolidation. *Nature Reviews Neuroscience*, 19(12):744–757.

Joshi, A., Salib, M., Viney, T. J., Dupret, D., and Somogyi, P. (2017). Behavior-dependent activity and synaptic organization of septo-hippocampal GABAergic neurons selectively targeting the hippocampal CA3 area. *Neuron*, 96(6):1342–1357.e5.

Josselyn, S. A. and Tonegawa, S. (2020). Memory engrams: Recalling the past and imagining the future. *Science*, 367(6473):eaaw4325.

Jung, M., Wiener, S., and McNaughton, B. (1994). Comparison of spatial firing characteristics of units in dorsal and ventral hippocampus of the rat. *Journal of Neuroscience*, 14(12):7347–7356.

Jung, M. W. and McNaughton, B. L. (1993). Spatial selectivity of unit activity in the hippocampal granular layer. *Hippocampus*, 3(2):165–182.

Kaada, B. R., Rasmussen, E., and Kveim, O. (1961). Effects of hippocampal lesions on maze learning and retention in rats. *Experimental Neurology*, 3(4):333–355.

Kanoski, S. E. and Grill, H. J. (2017). Hippocampus contributions to food intake control: Mnemonic, neuroanatomical, and endocrine mechanisms. *Biological Psychiatry*, 81(9):748–756.

Karlsson, M. P. and Frank, L. M. (2008). Network dynamics underlying the formation of sparse, informative representations in the hippocampus. *Journal of Neuroscience*, 28(52):14271–14281.

Karlsson, M. P. and Frank, L. M. (2009). Awake replay of remote experiences in the hippocampus. *Nature Neuroscience*, 12(7):913–918.

Kaufman, A. M., Geiller, T., and Losonczy, A. (2020). A role for the locus coeruleus in gippocampal CA1 place cell reorganization during spatial reward learning. *Neuron*, 105(6):1018–1026.e4.

Kay, K. and Frank, L. M. (2019). Three brain states in the hippocampus and cortex. *Hippocampus*, 29(3):184–238.

Keinath, A. T., Wang, M. E., Wann, E. G., Yuan, R. K., Dudman, J. T., and Muzzio, I. A. (2014). Precise spatial coding is preserved along the longitudinal hippocampal axis. *Hippocampus*, 24(12):1533–1548.

Keysers, C., Gazzola, V., and Wagenmakers, E.-J. (2020). Using Bayes factor hypothesis testing in neuroscience to establish evidence of absence. *Nat. Neurosci.*, 23(7):788–799.

Kim, J. and Fanselow, M. (1992). Modality-specific retrograde amnesia of fear. *Science*, 256(5057):675–677.

Kimble, D. P. and Pribram, K. H. (1963). Hippocampectomy and behavior sequences. *Science*, 139(3557):824–825.

King, C., Henze, D. A., Leinekugel, X., and Buzsáki, G. (1999). Hebbian modification of a hippocampal population pattern in the rat. *Journal of Physiology*, 521(1):159–167.

Kjelstrup, K. B., Solstad, T., Brun, V. H., Hafting, T., Leutgeb, S., Witter, M. P., Moser, E. I., and Moser, M.-B. (2008). Finite scale of spatial representation in the hippocampus. *Science*, 321(5885):140–143.

Kjelstrup, K. G., Tuvnes, F. A., Steffenach, H.-A., Murison, R., Moser, E. I., and Moser, M.-B. (2002). Reduced fear expression after lesions of the ventral hippocampus. *Proceedings of the National Academy of Sciences*, 99(16):10825–10830.

Knierim, J. J. and Neunuebel, J. P. (2016). Tracking the flow of hippocampal computation: Pattern separation, pattern completion, and attractor dynamics. *Neurobiology of Learning and Memory*, 129:38–49.

Kosugi, K., Yoshida, K., Suzuki, T., Kobayashi, K., Yoshida, K., Mimura, M., and Tanaka, K. F. (2021). Activation of ventral CA1 hippocampal neurons projecting to the lateral septum during feeding. *Hippocampus*, 31(3):294–304.

Kramis, R., Vanderwolf, C. H., and Bland, B. H. (1975). Two types of hippocampal rhythmical slow activity in both the rabbit and the rat: Relations to behavior and effects of atropine, diethyl ether, urethane, and pentobarbital. *Experimental Neurology*, 49(1):58–85.

Krupic, J., Bauza, M., Burton, S., and O'Keefe, J. (2018). Local transformations of the hippocampal cognitive map. *Science*, 359(6380):1143–1146.

Kveim, O., Setekleiv, J., and Kaada, B. R. (1964). Differential effects of hippocampal lesions on maze and passive avoidance learning in rats. *Experimental Neurology*, 9(1):59–72.

Latchoumane, C. F. V., Ngo, H. V. V., Born, J., and Shin, H. S. (2017). Thalamic spindles promote memory formation during sleep through triple phase-locking of cortical, thalamic, and hippocampal rhythms. *Neuron*, 95(2):424–435.e6.

LeDoux, J. E. (2000). Emotion Circuits in the Brain. *Annual Review of Neuroscience*, 23(1):155–184.

Lee, A. K. and Wilson, M. A. (2002). Memory of sequential experience in the hippocampus during slow wave sleep. *Neuron*, 36(6):1183–1194.

Lee, J. S., Briguglio, J. J., Cohen, J. D., Romani, S., and Lee, A. K. (2020). The statistical structure of the hippocampal code for space as a function of time, context, and value. *Cell*, 183(3):620–635.e22.

LeGates, T. A., Kvarta, M. D., Tooley, J. R., Francis, T. C., Lobo, M. K., Creed, M. C., and Thompson, S. M. (2018). Reward behaviour is regulated by the strength of hippocampus–nucleus accumbens synapses. *Nature*, 564(7735):258–262.

Levey, A. I., Kitt, C. A., Simonds, W. F., Price, D. L., and Brann, M. R. (1991). Identification and localization of muscarinic acetylcholine receptor proteins in brain with subtype-specific antibodies. *Journal of Neuroscience*, 11(10):3218–3226.

Li, X., Yu, B., Sun, Q., Zhang, Y., Ren, M., Zhang, X., Li, A., Yuan, J., Madisen, L., Luo, Q., Zeng, H., Gong, H., and Qiu, Z. (2018). Generation of a whole-brain atlas for the cholinergic system and mesoscopic projectome analysis of basal forebrain cholinergic neurons. *Proceedings of the National Academy of Sciences*, 115(2):415–420.

Liu, X., Ramirez, S., Pang, P. T., Puryear, C. B., Govindarajan, A., Deisseroth, K., and Tonegawa, S. (2012). Optogenetic stimulation of a hippocampal engram activates fear memory recall. *Nature*, 484(7394):381–385.

Lorente de Nó, R. (1934). Studies on the structure of the cerebral cortex. II. Continuation of the study of the ammonic system. *Journal für Psychologie und Neurologie*.

Lubenov, E. V. and Siapas, A. G. (2009). Hippocampal theta oscillations are travelling waves. *Nature*, 459(7246):534–539.

Ma, X., Zhang, Y., Wang, L., Li, N., Barkai, E., Zhang, X., Lin, L., and Xu, J. (2020). The firing of theta state related septal cholinergic neurons disrupt hippocampal ripple oscillations via muscarinic receptors. *Journal of Neuroscience*, 40(18):3591–3603.

Madisen, L., Mao, T., Koch, H., Zhuo, J.-m., Berenyi, A., Fujisawa, S., Hsu, Y.-W. A., Garcia, A. J., Gu, X., Zanella, S., Kidney, J., Gu, H., Mao, Y., Hooks, B. M., Boyden,

E. S., Buzsáki, G., Ramirez, J. M., Jones, A. R., Svoboda, K., Han, X., Turner, E. E., and Zeng, H. (2012). A toolbox of Cre-dependent optogenetic transgenic mice for light-induced activation and silencing. *Nat. Neurosci.*, 15(5):793–802.

Madison, D. V., Lancaster, B., and Nicoll, R. A. (1987). Voltage clamp analysis of cholinergic action in the hippocampus. *Journal of Neuroscience*, 7(3):733–741.

Maguire, E. A., Burke, T., Phillips, J., and Staunton, H. (1996). Topographical disorientation following unilateral temporal lobe lesions in humans. *Neuropsychologia*, 34(10):993–1001.

Malik, R., Dougherty, K. A., Parikh, K., Byrne, C., and Johnston, D. (2016). Mapping the electrophysiological and morphological properties of CA1 pyramidal neurons along the longitudinal hippocampal axis. *Hippocampus*, 26(3):341–361.

Manseau, F., Goutagny, R., Danik, M., and Williams, S. (2008). The hippocamposeptal pathway generates rhythmic firing of GABAergic neurons in the medial septum and diagonal bands: An investigation using a complete septohippocampal preparation in vitro. *Journal of Neuroscience*, 28(15):4096–4107.

Markram, H., Lübke, J., Frotscher, M., and Sakmann, B. (1997). Regulation of synaptic efficacy by coincidence of postsynaptic APs and EPSPs. *Science*, 275(5297):213–215.

Marr, D. and Brindley, G. S. (1971). Simple memory: a theory for archicortex. *Philosophical Transactions of the Royal Society of London. B, Biological Sciences*, 262(841):23–81.

Marrosu, F., Portas, C., Mascia, M. S., Casu, M. A., Fà, M., Giagheddu, M., Imperato, A., and Gessa, G. L. (1995). Microdialysis measurement of cortical and hippocampal acetylcholine release during sleep-wake cycle in freely moving cats. *Brain Research*, 671(2):329–332.

Mathis, A., Mamidanna, P., Cury, K. M., Abe, T., Murthy, V. N., Mathis, M. W., and Bethge, M. (2018). DeepLabCut: markerless pose estimation of user-defined body parts with deep learning. *Nature Neuroscience*, 21(9):1281–1289.

Mau, W., Hasselmo, M. E., and Cai, D. J. (2020). The brain in motion: How ensemble fluidity drives memory-updating and flexibility. *eLife*, 9:e63550.

Maurer, A. P., VanRhoads, S. R., Sutherland, G. R., Lipa, P., and McNaughton, B. L. (2005). Self-motion and the origin of differential spatial scaling along the septo-temporal axis of the hippocampus. *Hippocampus*, 15(7):841–852.

McClelland, J. L., McNaughton, B. L., and O'Reilly, R. C. (1995). Why there are complementary learning systems in the hippocampus and neocortex: insights from the successes and failures of connectionist models of learning and memory. *Psychological review*, 102(3):419–457.

McNaughton, B. L., Barnes, C. A., Gerrard, J. L., Gothard, K., Jung, M. W., Knierim, J. J., Kudrimoti, H., Qin, Y., Skaggs, W. E., Suster, M., and Weaver, K. L. (1996). Deciphering the hippocampal polyglot: the hippocampus as a path integration system. *Journal of Experimental Biology*, 199(1):173–185.

McNaughton, B. L., Barnes, C. A., and O'Keefe, J. (1983). The contributions of position, direction, and velocity to single unit activity in the hippocampus of freely-moving rats. *Experimental Brain Research*, 52(1):41–49.

McNaughton, B. L., Battaglia, F. P., Jensen, O., Moser, E. I., and Moser, M.-B. (2006). Path integration and the neural basis of the 'cognitive map'. *Nature Reviews Neuroscience*, 7(8):663–678.

McNaughton, B. L., Chen, L. L., and Markus, E. J. (1991). "Dead reckoning," landmark learning, and the sense of direction: A neurophysiological and computational hypothesis. *Journal of Cognitive Neuroscience*, 3(2):190–202.

Mehta, M. R., Quirk, M. C., and Wilson, M. A. (2000). Experience-dependent asymmetric shape of hippocampal receptive fields. *Neuron*, 25(3):707–715.

Melzer, S., Michael, M., Caputi, A., Eliava, M., Fuchs, E. C., Whittington, M. A., and Monyer, H. (2012). Long-Range–Projecting GABAergic Neurons Modulate Inhibition in Hippocampus and Entorhinal Cortex. *Science*, 335(6075):1506–1510.

Mesulam, M.-M., Mufson, E., Wainer, B., and Levey, A. (1983). Central cholinergic pathways in the rat: An overview based on an alternative nomenclature (Ch1–Ch6). *Neuroscience*, 10(4):1185–1201.

Mizuseki, K., Sirota, A., Pastalkova, E., and Buzsáki, G. (2009). Theta oscillations provide temporal windows for local circuit computation in the entorhinal-hippocampal loop. *Neuron*, 64(2):267–280.

Mizuta, K., Nakai, J., Hayashi, Y., and Sato, M. (2021). Multiple coordinated cellular dynamics mediate CA1 map plasticity. *Hippocampus*, 31(3):235–243.

Morris, R. G. M., Garrud, P., Rawlins, J. N. P., and O'Keefe, J. (1982). Place navigation impaired in rats with hippocampal lesions. *Nature*, 297(5868):681–683.

Morris, R. G. M., Schenk, F., Tweedie, F., and Jarrard, L. E. (1990). Ibotenate lesions of hippocampus and/or subiculum: Dissociating components of allocentric spatial learning. *European Journal of Neuroscience*, 2(12):1016–1028.

Moser, E., Moser, M., and Andersen, P. (1993). Spatial learning impairment parallels the magnitude of dorsal hippocampal lesions, but is hardly present following ventral lesions. *Journal of Neuroscience*, 13(9):3916–3925.

Moser, M.-B. and Moser, E. I. (1998). Functional differentiation in the hippocampus. *Hippocampus*, 8(6):608–619.

Moser, M. B., Moser, E. I., Forrest, E., Andersen, P., and Morris, R. G. (1995). Spatial learning with a minislab in the dorsal hippocampus. *Proceedings of the National Academy of Sciences*, 92(21):9697–9701.

Muller, R. U. and Kubie, J. L. (1987). The effects of changes in the environment on the spatial firing of hippocampal complex-spike cells. *Journal of Neuroscience*, 7(7):1951–1968.

Nadel, L. (1968). Dorsal and ventral hippocampal lesions and behavior. *Physiology & Behavior*, 3(6):891–900.

Nadel, L. and Moscovitch, M. (1997). Memory consolidation, retrograde amnesia and the hippocampal complex. *Current Opinion in Neurobiology*, 7(2):217–227.

Newman, E. L., Gillet, S. N., Climer, J. R., and Hasselmo, M. E. (2013). Cholinergic blockade reduces theta-Gamma phase amplitude coupling and speed nodulation of theta frequency consistent with behavioral effects on encoding. *Journal of Neuroscience*, 33(50):19635–19646.

Nitz, D. and McNaughton, B. (2004). Differential modulation of CA1 and dentate gyrus interneurons during exploration of novel environments. *Journal of Neurophysiology*, 91(2):863–872.

Norimoto, H., Makino, K., Gao, M., Shikano, Y., Okamoto, K., Ishikawa, T., Sasaki, T., Hioki, H., Fujisawa, S., and Ikegaya, Y. (2018). Hippocampal ripples down-regulate synapses. *Science*, 359(6383):1524–1527.

Norman, Y., Yeagle, E. M., Khuvis, S., Harel, M., Mehta, A. D., and Malach, R. (2019). Hippocampal sharp-wave ripples linked to visual episodic recollection in humans. *Science*, 365(6454):eaax1030.

O'Keefe, J. and Conway, D. H. (1978). Hippocampal place units in the freely moving rat: Why they fire where they fire. *Experimental Brain Research*, 31(4):573–590.

O'Keefe, J. and Dostrovsky, J. (1971). The hippocampus as a spatial map. Preliminary evidence from unit activity in the freely-moving rat. *Brain Research*, 34(1):171–175.

O'Keefe, J. and Nadel, L. (1978). *The Hippocampus as a Cognitive Map*. Oxford University Press.

O'Keefe, J. and Recce, M. L. (1993). Phase relationship between hippocampal place units and the EEG theta rhythm. *Hippocampus*, 3(3):317–330.

Ólafsdóttir, H. F., Carpenter, F., and Barry, C. (2016). Coordinated grid and place cell replay during rest. *Nature Neuroscience*, 19(6):792–794.

Oliva, A., Fernández-Ruiz, A., Buzsáki, G., and Berényi, A. (2016). Role of hippocampal CA2 region in triggering sharp-wave ripples. *Neuron*, 91(6):1342–1355.

O'Neill, J., Senior, T., and Csicsvari, J. (2006). Place-selective firing of CA1 pyramidal cells during sharp wave/ripple network patterns in exploratory behavior. *Neuron*, 49(1):143–155.

Padilla-Coreano, N., Canetta, S., Mikofsky, R. M., Alway, E., Passecker, J., Myroshnychenko, M. V., Garcia-Garcia, A. L., Warren, R., Teboul, E., Blackman, D. R., Morton, M. P., Hupalo, S., Tye, K. M., Kellendonk, C., Kupferschmidt, D. A., and Gordon, J. A. (2019). Hippocampal-prefrontal theta transmission regulates avoidance behavior. *Neuron*, 104(3):601–610.e4.

Panzeri, S., Senatore, R., Montemurro, M. A., and Petersen, R. S. (2007). Correcting for the sampling bias problem in spike train information measures. *Journal of Neurophysiology*, 98(3):1064–1072.

Pastalkova, E., Itskov, V., Amarasingham, A., and Buzsaki, G. (2008). Internally generated cell assembly sequences in the rat hippocampus. *Science*, 321(5894):1322–1327.

Paulsen, O. and Sejnowski, T. J. (2000). Natural patterns of activity and long-term synaptic plasticity. *Current Opinion in Neurobiology*, 10(2):172–180.

Petsche, H., Stumpf, C., and Gogolak, G. (1962). The significance of the rabbit's septum as a relay station between the midbrain and the hippocampus I. The control of hippocampus arousal activity by the septum cells. *Electroencephalography and Clinical Neurophysiology*, 14(2):202–211.

Pfeiffer, B. E. and Foster, D. J. (2013). Hippocampal place-cell sequences depict future paths to remembered goals. *Nature*, 497(7447):74–79.

Phillips, R. G. and LeDoux, J. E. (1992). Differential contribution of amygdala and hippocampus to cued and contextual fear conditioning. *Behavioral Neuroscience*, 106(2):274–285.

Pitkänen, A., Pikkarainen, M., Nurminen, N., and Ylinen, A. (2006). Reciprocal connections between the amygdala and the hippocampal formation, perirhinal cortex, and postrhinal cortex in rat: A review. *Annals of the New York Academy of Sciences*, 911(1):369–391.

Pnevmatikakis, E. A., Soudry, D., Gao, Y., Machado, T. A., Merel, J., Pfau, D., Reardon, T., Mu, Y., Lacefield, C., Yang, W., Ahrens, M., Bruno, R., Jessell, T. M., Peterka, D. S., Yuste, R., and Paninski, L. (2016). Simultaneous denoising, deconvolution, and demixing of calcium imaging data. *Neuron*, 89(2):285–299.

Quirk, G. J., Muller, R. U., and Kubie, J. L. (1990). The firing of hippocampal place cells in the dark depends on the rat's recent experience. *Journal of Neuroscience*, 10(6):2008–2017.

Quirk, G. J., Muller, R. U., Kubie, J. L., and Ranck, J. B. (1992). The positional firing properties of medial entorhinal neurons: description and comparison with hippocampal place cells. *Journal of Neuroscience*, 12(5):1945–1963.

Ramirez, S., Liu, X., Lin, P.-A., Suh, J., Pignatelli, M., Redondo, R. L., Ryan, T. J., and Tonegawa, S. (2013). Creating a false memory in the hippocampus. *Science*, 341(6144):387–391.

Ramón Y Cajal, S. (1911). *Histologie du système nerveux de l'homme & des vertébrés: Cervelet, cerveau moyen, rétine, couche optique, corps strié, écorce cérébrale générale & régionale, grand sympathique*, volume 2. A. Maloine, Paris.

Redish, A. D. and Touretzky, D. S. (1998). The role of the hippocampus in solving the Morris water maze. *Neural computation*, 10(1):73–111.

Reijmers, L. G., Perkins, B. L., Matsuo, N., and Mayford, M. (2007). Localization of a stable neural correlate of associative memory. *Science*, 317(5842):1230–3.

Resendez, S. L., Jennings, J. H., Ung, R. L., Namboodiri, V. M. K., Zhou, Z. C., Otis, J. M., Nomura, H., McHenry, J. A., Kosyk, O., and Stuber, G. D. (2016). Visualization of cortical, subcortical and deep brain neural circuit dynamics during naturalistic mammalian behavior with head-mounted microscopes and chronically implanted lenses. *Nature Protocols*, 11(3):566–597.

Riaz, S., Schumacher, A., Sivagurunathan, S., Van Der Meer, M., and Ito, R. (2017). Ventral, but not dorsal, hippocampus inactivation impairs reward memory expression and retrieval in contexts defined by proximal cues. *Hippocampus*, 27(7):822–836.

Rich, P. D., Liaw, H.-P., and Lee, A. K. (2014). Large environments reveal the statistical structure governing hippocampal representations. *Science*, 345(6198):814–817.

Rolls, E. T. (1996). A theory of hippocampal function in memory. *Hippocampus*, 6(6):601–620.

Roux, L., Hu, B., Eichler, R., Stark, E., and Buzsáki, G. (2017). Sharp wave ripples during learning stabilize the hippocampal spatial map. *Nature Neuroscience*, 20(6):845–853.

Royer, S., Sirota, A., Patel, J., and Buzsáki, G. (2010). Distinct representations and theta dynamics in dorsal and ventral hippocampus. *Journal of Neuroscience*, 30(5):1777–1787.

Ruediger, S., Spirig, D., Donato, F., and Caroni, P. (2012). Goal-oriented searching mediated by ventral hippocampus early in trial-and-error learning. *Nature Neuroscience*, 15(11):1563–1571.

Ryan, T. J., Roy, D. S., Pignatelli, M., Arons, A., and Tonegawa, S. (2015). Engram cells retain memory under retrograde amnesia. *Science*, 348(6238):1007–1013.

Sato, M., Mizuta, K., Islam, T., Kawano, M., Sekine, Y., Takekawa, T., Gomez-Dominguez, D., Schmidt, A., Wolf, F., Kim, K., Yamakawa, H., Ohkura, M., Lee, M. G., Fukai, T., Nakai, J., and Hayashi, Y. (2020). Distinct mechanisms of over-representation of landmarks and rewards in the hippocampus. *Cell Reports*, 32(1):107864.

Schmitt, W. B., Deacon, R. M. J., Seeburg, P. H., Rawlins, J. N. P., and Bannerman, D. M. (2003). A within-subjects, within-task demonstration of intact spatial reference memory and impaired spatial working memory in glutamate receptor-A-deficient Mice. *Journal of Neuroscience*, 23(9):3953–3959.

Schoenbaum, G., Chiba, A. A., and Gallagher, M. (1998). Orbitofrontal cortex and basolateral amygdala encode expected outcomes during learning. *Nature Neuroscience*, 1(2):155–159.

Schomburg, E. W., Fernández-Ruiz, A., Mizuseki, K., Berényi, A., Anastassiou, C. A., Koch, C., and Buzsáki, G. (2014). Theta phase segregation of input-specific gamma patterns in entorhinal-hippocampal networks. *Neuron*, 84(2):470–485.

Schredl, M., Weber, B., Leins, M.-L., and Heuser, I. (2001). Donepezil-induced REM sleep augmentation enhances memory performance in elderly, healthy persons. *Experimental Gerontology*, 36(2):353–361.

Schultz, W., Dayan, P., and Montague, P. R. (1997). A neural substrate of prediction and reward. *Science*, 275(5306):1593–1599.

Schumacher, A., Vlassov, E., and Ito, R. (2016). The ventral hippocampus, but not the dorsal hippocampus is critical for learned approach-avoidance decision making. *Hippocampus*, 26(4):530–542.

Scoville, W. B. and Milner, B. (1957). Loss of recent memory after bilateral hippocampal lesions. *Journal of Neurology, Neurosurgery, and Psychiatry*, 20(1):11.

Sekeres, M. J., Winocur, G., and Moscovitch, M. (2018). The hippocampus and related neocortical structures in memory transformation. *Neuroscience Letters*, 680:39–53.

Sharp, P. E. and Green, C. (1994). Spatial correlates of firing patterns of single cells in the subiculum of the freely moving rat. *Journal of Neuroscience*, 14(4):2339–2356.

Shipton, O. A., El-Gaby, M., Apergis-Schoute, J., Deisseroth, K., Bannerman, D. M., Paulsen, O., and Kohl, M. M. (2014). Left–right dissociation of hippocampal memory processes in mice. *Proceedings of the National Academy of Sciences*, 111(42):15238–15243.

Shpokayte, M., McKissick, O., Yuan, B., Rahsepar, B., Fernandez, F. R., Ruesch, E. A., Grella, S. L., White, J. A., Liu, X. S., and Ramirez, S. (2020). Hippocampal cells multiplex positive and negative engrams. *bioRxiv*, page 2020.12.11.419887.

Siapas, A. G. and Wilson, M. A. (1998). Coordinated interactions between hippocampal ripples and cortical spindles during slow-wave sleep. *Neuron*, 21(5):1123–1128.

Singer, A. C. and Frank, L. M. (2009). Rewarded outcomes enhance reactivation of experience in the hippocampus. *Neuron*, 64(6):910–921.

Sirota, A., Csicsvari, J., Buhl, D., and Buzsaki, G. (2003). Communication between neocortex and hippocampus during sleep in rodents. *Proceedings of the National Academy of Sciences*, 100(4):2065–2069.

Smith, M. L. (1988). Recall of spatial location by the amnesic patient H.M. *Brain and Cognition*, 7(2):178–183.

Solari, N. and Hangya, B. (2018). Cholinergic modulation of spatial learning, memory and navigation. *European Journal of Neuroscience*, 48(5):2199–2230.

Sosa, M. and Giocomo, L. M. (2021). Navigating for reward. *Nature Reviews Neuroscience*, 22(8):472–487.

Spellman, T., Rigotti, M., Ahmari, S. E., Fusi, S., Gogos, J. A., and Gordon, J. A. (2015). Hippocampal–prefrontal input supports spatial encoding in working memory. *Nature*, 522(7556):309–314.

Squire, L. R. (2004). Memory systems of the brain: A brief history and current perspective. *Neurobiology of Learning and Memory*, 82(3):171–177.

Stachenfeld, K. L., Botvinick, M. M., and Gershman, S. J. (2017). The hippocampus as a predictive map. *Nature Neuroscience*, 20(11):1643–1653.

Staresina, B. P., Bergmann, T. O., Bonnefond, M., Van Der Meij, R., Jensen, O., Deuker, L., Elger, C. E., Axmacher, N., and Fell, J. (2015). Hierarchical nesting of slow oscillations, spindles and ripples in the human hippocampus during sleep. *Nature Neuroscience*, 18(11):1679–1686.

Strange, B. A., Witter, M. P., Lein, E. S., and Moser, E. I. (2014). Functional organization of the hippocampal longitudinal axis. *Nature Reviews Neuroscience*, 15(10):655–669.

Sullivan, D., Csicsvari, J., Mizuseki, K., Montgomery, S., Diba, K., and Buzsáki, G. (2011). Relationships between hippocampal sharp waves, ripples, and fast gamma oscillation: Influence of dentate and entorhinal cortical activity. *Journal of Neuroscience*, 31(23):8605–8616.

Sutton, R. S. and Barto, A. G. (2018). *Reinforcement learning: an introduction*. The MIT Press, second edition.

Swanson, L. and Cowan, W. (1975). Hippocampo-hypothalamic connections: origin in subicular cortex, not ammon's horn. *Science*, 189(4199):303–304.

Swanson, L. W., Wyss, J. M., and Cowan, W. M. (1978). An autoradiographic study of the organization of intrahippocampal association pathways in the rat. *Journal of Comparative Neurology*, 181(4):681–715.

Tanaka, K. Z., Pevzner, A., Hamidi, A. B., Nakazawa, Y., Graham, J., and Wiltgen, B. J. (2014). Cortical representations are reinstated by the hippocampus during memory retrieval. *Neuron*, 84(2):347–354.

Tang, Y., Mishkin, M., and Aigner, T. G. (1997). Effects of muscarinic blockade in perirhinal cortex during visual recognition. *Proceedings of the National Academy of Sciences*, 94(23):12667–12669.

Taube, J., Muller, R., and Ranck, J. (1990). Head-direction cells recorded from the postsubiculum in freely moving rats. I. Description and quantitative analysis. *Journal of Neuroscience*, 10(2):420–435.

Taube, J. S. (2007). The head direction signal: Origins and sensory-motor integration. *Annual Review of Neuroscience*, 30(1):181–207.

Thiele, A. (2013). Muscarinic Signaling in the Brain. *Annual Review of Neuroscience*, 36(1):271–294.

Thompson, C. L., Pathak, S. D., Jeromin, A., Ng, L. L., MacPherson, C. R., Mortrud, M. T., Cusick, A., Riley, Z. L., Sunkin, S. M., Bernard, A., Puchalski, R. B., Gage, F. H., Jones, A. R., Bajic, V. B., Hawrylycz, M. J., and Lein, E. S. (2008). Genomic anatomy of the hippocampus. *Neuron*, 60(6):1010–1021.

Tonegawa, S., Liu, X., Ramirez, S., and Redondo, R. (2015). Memory engram cells have come of age. *Neuron*, 87(5):918–931.

Tóth, K., Freund, T. F., and Miles, R. (1997). Disinhibition of rat hippocampal pyramidal cells by GABAergic afferents from the septum. *Journal of Physiology*, 500(2):463–474.

Tremblay, L. and Schultz, W. (1999). Relative reward preference in primate orbitofrontal cortex. *Nature*, 398(6729):704–708.

Treves, A. and Panzeri, S. (1995). The upward bias in neasures of information derived from limited data samples. *Neural Computation*, 7(2):399–407.

Trouche, S., Koren, V., Doig, N. M., Ellender, T. J., El-Gaby, M., Lopes-dos Santos, V., Reeve, H. M., Perestenko, P. V., Garas, F. N., Magill, P. J., Sharott, A., and Dupret, D. (2019). A hippocampus-accumbens tripartite neuronal motif guides appetitive memory in space. *Cell*, 176(6):1393–1406.e16.

Tulving, E. (1972). Episodic and semantic memory. In Tulving, E. and Donaldson, W., editors, *Organization of memory*, pages 381–403. Academic Press.

Turi, G. F., Li, W.-K., Chavlis, S., Pandi, I., O'Hare, J., Priestley, J. B., Grosmark, A. D., Liao, Z., Ladow, M., Zhang, J. F., Zemelman, B. V., Poirazi, P., and Losonczy, A. (2019). Vasoactive intestinal polypeptide-expressing interneurons in the hippocampus support goal-oriented spatial learning. *Neuron*, 101(6):1150–1165.e8.

van der Meer, M. A. A. and Redish, A. D. (2011). Theta phase precession in rat ventral striatum links place and reward information. *Journal of Neuroscience*, 31(8):2843–2854.

Vandecasteele, M., Varga, V., Berényi, A., Papp, E., Barthó, P., Venance, L., Freund, T. F., and Buzsáki, G. (2014). Optogenetic activation of septal cholinergic neurons suppresses sharp wave ripples and enhances theta oscillations in the hippocampus. *Proceedings of the National Academy of Sciences*, 111(37):13535–13540.

Vanderwolf, C. (1969). Hippocampal electrical activity and voluntary movement in the rat. *Electroencephalography and Clinical Neurophysiology*, 26(4):407–418.

Vann, S. D., Aggleton, J. P., and Maguire, E. A. (2009). What does the retrosplenial cortex do? *Nature Reviews Neuroscience*, 10(11):792–802.

W. E. Skaggs, B. L. McNaughton, K. M. Gothard, E. J. M. (1993). An Information-Theoretic Approach to Deciphering the Hippocampal Code. *Proceedings of the IEEE*, (1990):1030—-1037.

Wagenmakers, E.-J. (2007). A practical solution to the pervasive problems of p values. *Psychonomic Bulletin & Review*, 14(5):779–804.

Whittington, J. C., Muller, T. H., Mark, S., Chen, G., Barry, C., Burgess, N., and Behrens, T. E. (2020). The Tolman-Eichenbaum machine: Unifying space and relational memory through generalization in the hippocampal formation. *Cell*, 183(5):1249–1263.e23.

Wilson, M. and McNaughton, B. (1993). Dynamics of the hippocampal ensemble code for space. *Science*, 261(5124):1055–1058.

Winocur, G. (1990). Anterograde and retrograde amnesia in rats with dorsal hippocampal or dorsomedial thalamic lesions. *Behavioural Brain Research*, 38(2):145–154.

Witter, M. P. and Amaral, D. G. (2004). Hippocampal formation. In *The Rat Nervous System*, pages 635–704. Elsevier Inc.

Wood, E. R., Dudchenko, P. A., Robitsek, R., and Eichenbaum, H. (2000). Hippocampal neurons encode information about different types of memory episodes occurring in the same location. *Neuron*, 27(3):623–633.

Xu, C., Krabbe, S., Gründemann, J., Botta, P., Fadok, J. P., Osakada, F., Saur, D., Grewe, B. F., Schnitzer, M. J., Callaway, E. M., and Lüthi, A. (2016). Distinct hippocampal pathways mediate dissociable roles of context in memory retrieval. *Cell*, 167(4):961–972.e16.

Yan-You Huang, P. V., Nguyen, T. A., and Kandel, E. R. (1996). Long-lasting forms of synaptic potentiation in the mammalian hippocampus. *Learning & Memory*, 3(2-3):74–85.

Yoder, R. M. and Pang, K. C. (2005). Involvement of GABAergic and cholinergic medial septal neurons in hippocampal theta rhythm. *Hippocampus*, 15(3):381–392.

Yoshida, K., Drew, M. R., Mimura, M., and Tanaka, K. F. (2019). Serotonin-mediated inhibition of ventral hippocampus is required for sustained goal-directed behavior. *Nature Neuroscience*, 22(5):770–777.

Zaremba, J. D., Diamantopoulou, A., Danielson, N. B., Grosmark, A. D., Kaifosh, P. W., Bowler, J. C., Liao, Z., Sparks, F. T., Gogos, J. A., and Losonczy, A. (2017). Impaired hippocampal place cell dynamics in a mouse model of the 22q11.2 deletion. *Nature Neuroscience*, 20(11):1612–1623.

Zhou, Y., Zhu, H., Liu, Z., Chen, X., Su, X., Ma, C., Tian, Z., Huang, B., Yan, E., Liu, X., and Ma, L. (2019). A ventral CA1 to nucleus accumbens core engram circuit mediates conditioned place preference for cocaine. *Nature Neuroscience*, 22(12):1986–1999.

Ziv, Y., Burns, L. D., Cocker, E. D., Hamel, E. O., Ghosh, K. K., Kitch, L. J., Gamal, A. E., and Schnitzer, M. J. (2013). Long-term dynamics of CA1 hippocampal place codes. *Nature Neuroscience*, 16(3):264–266.

Zola-Morgan, S. M. and Squire, L. R. (1990). The primate hippocampal formation: Evidence for a time-limited role in memory storage. *Science*, 250(4978):288–290.